TOPOLOGICAL CONFIGURATIONS OF CORONAL MAGNETIC FIELDS AND CURRENT SHEETS

Timothy N. Bungey

A Thesis Submitted for the Degree of PhD
at the
University of St Andrews

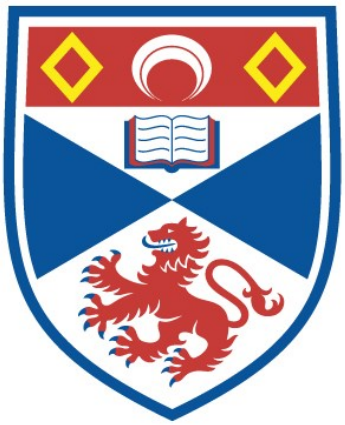

1996

Topological Configurations Of Coronal Magnetic Fields And Current Sheets

Timothy N. Bungey

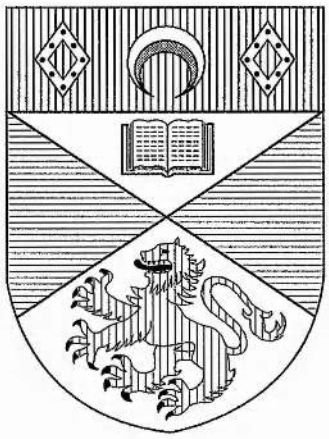

Thesis submitted for the degree of Doctor of Philosophy
of the University of St. Andrews on 21st November 1995

Abstract

The question of topology in the coronal magnetic field is addressed in this thesis. Magnetic reconnection, which plays a major role in many of the fascinating phenomena seen in the solar atmosphere, is likely to occur at the boundaries between different topological regions of the magnetic field. By modelling the coronal field using discrete sources of flux, to represent the concentrations seen at the photospheric surface, we study the varying topological structures present in the field. We generate a criterion for determining the presence of null points above the photospheric surface and establish that any separatrix surfaces present in the field are due to the presence of either null points, or regions where the field tangentially grazes the surface. We follow the evolution of these separatrix surfaces and, in particular, determine the existence of a well-defined separator field line in the absence of coronal null points. Finally, we look locally at the configuration of the magnetic field in the region surrounding a straight current sheet. We derive an analytical expression to describe the topology of both potential and constant-current force-free fields in the neighbourhood of a sheet, and in so doing generalise the previously known expressions.

Declaration

1. I, Timothy Nicholas Bungey, hereby certify that this thesis, which is approximately 30,000 words in length, has been written by me, that it is a record of work carried out by me and that it has not been submitted in any previous application for a higher degree.

   date ...15./1./96... signature of candidate ...

2. I was admitted as a research student in October 1992 and as a candidate for the degree of Ph.D. in October 1993; the higher study for which this is a record was carried out in the University of St. Andrews between 1992 and 1995.

   date ..15./1./96.... signature of candidate .. ...

3. I hereby certify that the candidate has fulfilled the conditions of the Resolution and Regulations appropriate to the Degree of Ph.D. in the University of St. Andrews and that the candidate is qualified to submit this thesis in application for that degree.

   date ..15./1./96... signature of supervisor ... .

Copyright

4. In submitting this thesis to the University of St. Andrews I understand that I am giving permission for it to be made available for use in accordance with the regulations of the University Library for the time being in force, subject to any copyright vested in the work not being affected thereby. I also understand that the title and abstract will be published, and that a copy of the work may be made and supplied to any bona fide library or research worker.

date ..15/1/96..signature of candidate .. ..

Acknowledgements

I would like to thank all my friends and colleagues who have helped to make my time in St. Andrews so enjoyable and rewarding. Particular thanks must go to my supervisor, Prof. Eric Priest, for his continual support and encouragement over the last three years. It is his endless enthusiasm for the subject which has kept me going. Further thanks must also go to all the members of the Solar Group whose help and knowledge has proved invaluable, particularly where computers are concerned.

My mother and father have been a constant source of support and encouragement throughtout my extended student days and their tolerance will long be remembered.

Finally, a special mention must go to Fiona, for keeping me sane, and to Nick, Ian and Graham for their constant provision of entertainment and philosophical enlightenment.

Contents

Chapter 1

Introduction

1.1 Introduction

As our closest and most easily observable star, the Sun is naturally an ideal starting point for any study of stellar behaviour. Of all the billions of stars in the universe, our Sun is not unusual: a standard G2-type star in the middle of its life and with an average temperature and size for stars in its class. Yet it provides us with an almost ideal testing ground for theories of stellar activity and cosmical plasma processes in general. Indeed the study of solar processes are particularly justified in their own right due to the profound effects that solar activity has on the Earth's environment. For example, the disturbance of the Earth's magnetic field by solar emissions and changes in the solar wind, and maybe more importantly, the effect on the Earth's climate of variations in the solar radiation. It is both the importance of understanding these processes that effect us, together with the diverse nature of the phenomena observed on the Sun, that help make solar theory such a fascinating area of modern research.

Within the one guise of solar theory there exist many, very different questions and areas of research. These range from Helioseismology, which uses wave techniques to try and explore the structuring of the solar interior and explain the observed '5-minute' oscillations of the solar surface, to the study of the well publicised 11-year cycle for solar activity, traditionally monitored by the abundance of sunspots. Over the years the study of solar eclipses, which permit the observer a rare view of the surrounding solar atmosphere, and more recently the study of X-ray and H-α images of the Sun, have also

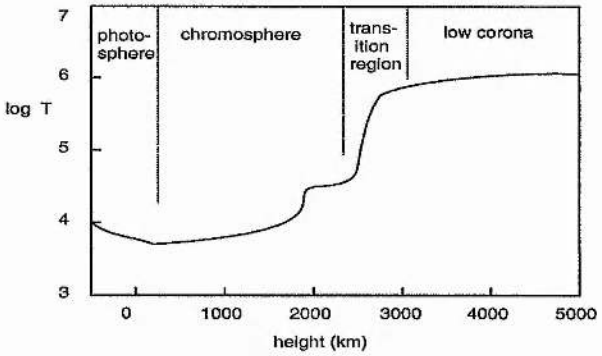

Figure 1.1: Variation of plasma temperature with distance from the solar surface (Athay 1976).

revealed the existence of many fascinating structures and dynamical events above the visible surface of the Sun, or photosphere. These include solar prominences, which are seen as large, cool, dense regions in the solar atmosphere, and the rapid release of large amounts of energy and the ejection of plasma which are associated with solar flares and coronal mass ejections. Perhaps one of the most fascinating and widely studied problems in solar theory, however, is that of the heating of the outer solar atmosphere known as the corona.

Whilst one might intuitively expect that as you move outwards from the surface of a hot radiating body the temperature of the plasma would steadily decrease, it seems that this is not the case when it comes to the solar atmosphere. It has been found, rather, that whilst the temperature decreases down to a minimum of around 4300 K in the photosphere, it then proceeds to rise again. This rise is gradual at first through the lower regions of the surrounding chromosphere but then the temperature increases dramatically through a narrow transition region to give values of several million degrees in the lower solar corona, at about 3000km above the photospheric surface. From here the temperature gradually decreases again as we move out into the interplanetary medium and solar wind (see Figure 1.1).

It has gradually been recognised over the course of this century that the majority of the features observed on or above the solar surface are in some way related to the presence of a magnetic field, and the heating of the corona it would seem is no exception to this. Indeed, at present, the coronal magnetic field is the key for the only plausible explanations for the large amounts of energy present at such heights above the surface.

Brief discussions of the origins and nature of this atmospheric magnetic field together with its modelling and the various methods for its possible heating of the solar corona are given in the following sections. This chapter will then conclude with an outline of the work contained in the remainder of the thesis.

1.2 The Magnetic Field of the Solar Atmosphere

The magnetic field that threads the solar corona and is attributed with all the interesting structures seen above the photosphere has its origins beneath the solar surface. Beneath the photosphere, which has a thickness of just a few hundred kilometres, lies the convection zone and at the base of this region lies a thin layer known as the 'overshoot' layer, separating the convection zone from the radiative solar interior. It is thought that, concentrated within this region, dynamo mechanisms are responsible for the generation of the solar magnetic field (e.g. Gilman et al 1989).

Fibrils of magnetic flux generated in the thin overshoot layer can become unstable and are able to rise up through the convection zone due to buoyancy effects and protrude through the photosphere into the solar atmosphere. The rise of these flux tubes through the convection zone has been studied by many authors and it is found that the rise time, which may be of the order of months, and the latitude at which the flux tubes emerge through the photosphere depends on the strength of the magnetic field and the amount of flux contained in the tubes. Those flux tubes with a stronger field and larger flux are found to rise faster and appear at lower latitudes with the majority of flux tubes emerging at latitudes between 10° and 30° (see e.g. Moreno-Insertis 1986, Choudhuri 1989, D'Silva & Choudhuri 1992).

These findings are in good agreement with observations of the photospheric magnetic field. Magnetogram images of the solar surface show that the magnetic flux is locally gathered into discrete elements or flux tubes. These flux tubes may have field strengths of approximately 1-2 kG and radii of 200-300 km, with these radii rising to the order of 1000 km for active region fields. Large granular convection cells in the convection zone sweep the individual flux tubes to the cell boundaries where they concentrate, and large active region sunspots are thought to form in this way as more and more like-polarity flux concentrations are swept together. These sunspots are typically found to be

located in bands up to 30 degrees North or South of the equatorial plane and traditionally their abundance has been a measure of the varying level of solar activity. A further observational fact that may also be explained by this buoyant rise of flux tubes through the convection zone is the asymmetry in sunspot size and strength between the preceeding and following edges of active regions (Fan et al 1993). Typically it is found that spots at the preceeding edge of an active region are larger and longer lived than those of opposite polarity at the trailing edge where they are seen to be more fragmented.

Within the convection zone and the photosphere the gas pressure of the plasma is of the same order of magnitude as the magnetic pressure and the flux tubes are restricted to radii of a few hundred kilometres. However, both the plasma density and pressure decrease very rapidly with height above the solar surface. The magnetic pressure forces soon dominate, therefore, and the rising flux tubes expand rapidly as they emerge into the solar atmosphere (Figure 1.2). This expansion will generally continue until separate flux tubes press against one another and virtually the whole volume contains magnetic lines of force.

The global structure of the coronal magnetic field then consists of two distinct types of field structure. The first, coronal holes, are regions where the coronal field is open, with the field lines being dragged out into the interplanetary medium by the solar wind. Typically, coronal holes exist above the polar regions and above various large unipolar flux regions; they are large, long-lived structures, lasting for the order of months at a time. Coronal loops, in contrast, are closed magnetic structures covering roughly 80% of the solar surface. They take the form of magnetic loops and may vary greatly in size, field strength and temperature, from the small emerging loop structures of ephemeral regions covering the majority of the solar disc and associated with X-ray bright points, to the large-scale loop structures both within active regions and inter-connecting different active regions. It is the loop structures which are of geatest interest in studies of coronal energy release, since these closed field loops are able to confine the coronal plasma and store energy above the solar surface.

1.3 Modelling the Coronal Magnetic Field

Much of the information gleaned about the temperature, plasma motions and magnetic field of the solar atmosphere comes from the study of spectral absorption lines. In particular, it is the study of Zeeman splitting effects on these absorbtion lines which gives rise to measurements of the magnetic field strength. Whilst this technique may be applied with a great deal of success in the photosphere and lower chromosphere, it does not seem possible, unfortunately, to find suitable spectral lines in the upper chromosphere and corona to allow any direct measurements of the magnetic field in these regoins. It has, therefore, been necessary to try and model the coronal magnetic field in some way. To this end, many attempts have been made to generate a magnetic field in the corona by extrapolating the field structures measured in the photosphere (e.g. Sakurai 1981, McClymont & Mikic 1994, Roumeliotis 1995).

In order to perform such extrapolations of the photospheric boundary data some assumptions necessarily have to be made about the nature of the coronal field. In general, the usual assumption is that the field is force-free,

$$\mathbf{J} = \nabla \times \mathbf{B} = \alpha \mathbf{B}, \tag{1.1}$$

implying that the current ($\mathbf{J}$) is parallel to the magnetic field ($\mathbf{B}$). This assumption is made on the basis that the magnetic Lorentz force ($\mathbf{J} \times \mathbf{B}$) dominates any other forces such as pressure and gravity, and this is certainly true for active-region coronal plasma, as already mentioned. One difficulty, however, of such an extrapolation problem is that α, as given in Eq.(1.1), is in general a function of space (as are $\mathbf{J}$ and $\mathbf{B}$), and thus the problem is non-linear. This makes any analytical solutions against which to test the accuracy of an extrapolation procedure very hard to find, although a few do exist (Low & Lou 1990).

By making the further assumption that α in Eq.(1.1) is a constant, the non-linearity of the problem is avoided and much analytical theory can be applied to the extrapolation process. However, further problems still arise due to the mathematical problem of extrapolation being ill-posed, and also through the need to restrict the extent of such constant-α fields in order to avoid an unphysical periodicity inherent in the solutions. A final difficulty, common to all extrapolation attempts, comes from the fact that observational measurements have an ambiguity of 180° in the direction of the horizontal magnetic

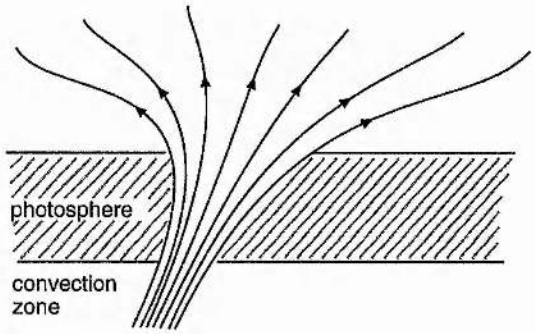

Figure 1.2: Schematic view of a rising flux tube expanding as it emerges through the photospheric surface.

field components. The ambiguous field vectors, therefore, have to be estimated and any errors in this estimation will lead to meaningless and misleading results. This ambiguity is particularly difficult to resolve in highly sheared regions of the field, although various techniques have been proposed in order to aid this process (e.g. Gary & Démoulin 1995).

An alternative approach to the modeling of the coronal field which avoids all the analytical and computational problems described above is the use of discrete magnetic flux sources. As described in Section 1.2, the confined flux tubes emerging through the photosphere expand rapidly as the plasma pressure decreases (Figure 1.2), and it is convenient to model the discrete photospheric concentrations of emerging flux tubes using either point sources or dipoles, located close to the photospheric surface. One advantage of this approach is that it is then easy to describe the field analytically using either the potential or linear force-free expressions for point sources or dipoles (Démoulin & Priest 1992). By altering the number, location and relative strengths of these flux concentrations it is then possible to build model fields which match well the observed photospheric fields. Several studies of this kind have been carried out using both point sources (Démoulin Henoux & Mandrini 1992, 1994, Démoulin et al 1993) and dipoles (Mandrini et al 1991, Démoulin Henoux & Mandrini 1992, Lau 1993). These studies have found good agreements between observed regions of coronal energy release and the regions of magnetic interest predicted by these models.

The relative merits of using either point sources or dipoles have also been studied (Démoulin Henoux & Mandrini 1992, 1994). Whilst the use of dipolar flux sources appears favourable in terms of satisfying observational effects such as the magnetic knots

of opposite polarity seen in abundance around the edges of large sunspots, it is found that, as far as locating the main topological areas of interest is concerned, there is little to choose between the use of sources or dipoles. Indeed, the use of dipoles often tends to introduce extra magnetic structures which are of little observational significance and may be confusing. Similarly, a linear force-free model which allows the presence of electric currents would seem more realistic than a potential field model which is current-free. Potential models are, however, mathematically much simpler and the differences found between the two models in locating the magnetic regions of interest are often small. Furthermore, any linear force-free models suffer from the same problem as described above of having an unphysical periodicity in their solutions and so they need to be truncated at some finite distance. Thus, potential models using magnetic point sources to model the discrete photospheric flux concentrations, despite their simplicity, give a good first approximation to the coronal field of an active region.

1.4 Heating of the Solar Atmosphere

We have seen from Figure 1.1 that the coronal plasma has a very high temperature on the order of 10^6 K, and, without an energy input, this temperature would fall away significantly due to conduction and radiative cooling effects over a time scale of order $\sim 10^4$ s. Thus, in order to maintain its high temperature, there needs to be an almost continual supply of energy to the atmospheric plasma. This energy is believed to originate as dynamic energy due to continual plasma motions in the photosphere and convection zone which is then transported into the solar atmosphere by some mechanism. Initially, the belief was that the motions in the convection zone merely generate sound waves which steepen to form shock waves as they propogate upwards. These shock waves could then, in turn, heat the plasma. It has since been realised, however, that whilst such acoustic wave mechanisms may heat the lower chromospheric regions it is very unlikely that they will contain sufficient energy to be an effective heating source at coronal heights (Athay & White 1977).

The now generally accepted view is that the magnetic field provides a suitable alternative to acoustic waves as a mechanism for the transportation of the photospheric energy into the coronal plasma. One feature of the coronal magnetic field which is important to

such a mechanism is the fact that the solar plasma is very highly conductive. This means that the magnetic lines of force do not slip through the plasma but are effectively 'frozen-in', thus being convected with any motions of the plasma. Also, as already mentioned, the corona is a low-beta plasma, meaning that magnetic pressure forces dominate over any plasma pressures. Combined with the frozen-in condition, this suggests that coronal field lines are free to move in response to magnetic pressures and drag the plasma with them. In contrast, the plasma-beta of the photosphere and convection zone is greater than unity and plasma motions in these regions drag the magnetic field along. These changes in order of magnitude of the plasma-beta on passing from photosphere to corona give rise to the important effect of 'line-tying'. This means that, whilst magnetic field lines are free to move in the corona, their footpoints in the photosphere remain effectively fixed. In this way, motions of the photospheric plasma transfer energy into the coronal magnetic field which cannot then be transferred back and is effectively trapped in the corona by the line-tying effect. Furthermore, line-tying effects may also modify the stability of the coronal field (e.g. Velli & Hood 1989).

The processes by which energy trapped in the coronal field is released can now be broadly divided into two categories. This division is based on the ratio of the characteristic timescale, τ_v, of the photospheric flows which drive the magnetic footpoints, to the Alfvén transit time, τ_a, which is the time it takes for an Alfvén wave to propagate along the magnetic structure. If the driving flow is fast compared to the Alfvén transit time, $\tau_v \ll \tau_a$, MHD waves will propagate along the field lines. This case is probably most applicable to quiet region coronal loops which are generally longer and have an Alfvén time in the range 10-1000 s. For a detailed description of the various wave types and their properties see Roberts (1985).

Of the possible MHD wave modes it seems that only the Alfvén waves themselves are likely to propagate effectively into the corona (e.g. Hollweg 1979, Leroy 1981). There exist a number of different mechanisms by which the energy carried by these Alfvén waves may then be transferred to the coronal plasma. These may include resisitive dissipation, (although dissipation timescales may be too long for effective heating unless the field is inhomogeneous), resonant absorption and phase mixing (Heyvaerts & Priest 1983). A great deal of work has been done on understanding these various processes and a good

review is given by Browning (1991).

The second category of energy transfer mechanisms occur if the driving flow is slow compared to the Alfvén time, $\tau_v \gg \tau_a$, and this regime is more applicable to active region loops. In this scenario the magnetic field will essentially evolve through a series of quasi-static equilibria, with the particular equilibrium state at any moment being determined by the positions of the magnetic footpoints. These equilibrium states will be force-free since the plasma-beta is small. The photospheric energy is thus stored as currents in the distorted magnetic field in excess of the lowest energy state which is the potential (current-free) field.

As the footpoints continue to move, the field becomes more and more stressed and the currents will build up. Simple Ohmic dissipation of these stored currents would then provide a source of heating. The Ohmic dissipation time for the plasma, however, is given by

$$t_d = \frac{L^2}{\eta}, \tag{1.2}$$

where η is the resistivity and L is a typical loop lengthscale. With the corona being highly conductive the resistivity is very small, typically $\eta \sim 10^{-6}$ km^2 s^{-1}, and for a typical loop length $L \sim 1000$ km, this gives a dissipation time of $t_d \sim 10^{12}$ s. This is much too slow to account for the required energy input timescale of $\sim 10^4$ s, and in order to produce effective timescales the typical width of a dissipation region needs to be up to four orders of magnitude smaller, approximately 100 m.

It is believed, therfore, that the excess energy stored in the magnetic field will dissipate rapidly in localised regions where the field changes over small distances, rather than throughout the entire volume of a loop. These localised dissipation regions are known as current sheets since the current density, given by $\mathbf{J} = \nabla \times \mathbf{B}$, is enhanced as the length scales decrease. Within these current sheets the effects of resistivity are enhanced allowing magnetic field lines to reconnect and alter their topology to produce a lower energy configuration, hence dissipating the currents. The theory of magnetic reconnection in current sheets and the rate at which it may proceed has been well studied in simplified two-dimensional geometries (Sweet 1958, Parker 1958, Petschek 1964, Priest & Forbes 1986, Biskamp 1986, Priest & Lee 1990), although the study of fully three-dimensional reconnection is still in its infancy (Schindler et al 1988, Lau & Finn 1990, Priest & Titov

1995, Priest & Démoulin 1995).

One major ongoing debate concerning this current dissipation mechanism is related to the formation and location of current sheets. Parker (1972) has proposed that if the footpoints of a smooth equilibrium field are moved in a continuous, random manner, the field will eventually reach a state where it can no longer achieve a smooth equilibrium due to the imposition of the frozen-in condition. Some discontinuities (tangential) must therefore spontaneously arise in the field, at which locations the field changes over an infinitesimally small scale. Magnetic reconnection (or topological dissipation) can then occur at these very thin current sheets. This, however, is only in the limiting case of an ideal plasma and realistically dissipation will start before the currents become infinite. Furthermore, the basic idea of discontinuities forming due to a lack of equilibrium resulting from continuous boundary motions has been contested by several authors (e.g. Van Ballegooijen 1985, Zweibel & Li 1987). As an alternative Van Ballegooijen (1986) has proposed that, as the footpoints of neighbouring field lines are continuously intertwined, currents build up and a cascade of energies to smaller scales takes place. As the scales decrease, dissipation occurs, but no infinite current regions or tangential disconuities are generated.

A feature of both the proposed models is that they start with fields having an initially uniform footpoint distribution. The photospheric flux, however, is generally clustered into discrete concentrations. The discrete flux tubes emerging and expanding into the corona are likely to carry differing degrees of twist and will be topologically distinct from one another. Thus a natural site for the formation of current sheets would appear to be at the boundaries between neighbouring regions of distinct flux. As the footpoints are shuffled around and topologically distinct field lines are forced together tangential discontinuities will naturally be expected at these boundaries.

Current sheets have also been shown to form due to the collapse of two-dimensional X-type neutral points (Green 1965, Syrovatskii 1971), and recent numerical studies have shown the formation of localised thin current structures in fields with three-dimensional null points (Galsgaard & Nordlund 1996). The key criterion in all these cases of current sheet formation is the presence within the magnetic field of separatrix surfaces, being surfaces which separate the field into topologically distinct regions. Such separatrix surfaces

will arise due to the presence of either null points or flux originating from distinct sources.

The above theoretical picture of rapid dissipation of stored electric currents in reconnecting current sheets is also associated with solar flares. Indeed, the rapid release of large amounts of energy seen in flares can realistically only be achieved by this mechanism. It has been suggested, furthermore, that the same general reconnection model which has been developed to explain solar flares, may be responsible for the general heating of the corona via many smaller scale events, or 'nanoflares' (e.g. Parker 1988, Cargill 1993).

1.5 Outline of Thesis

In Section 1.3 we have discussed how the magnetic field of a coronal active region may be modelled to a good first approximation using simple potential sources of magnetic flux. It has also been described, in Section 1.4, how the process of magnetic reconnection, which appears the most likely candidate for explaining both the heating of active regions and the more dynamic energy release necessary for solar flares, requires the presence of regions in which the field changes over small distances. Such small length scales are most likely to be found at the boundaries between topologically distinct flux regions, and it is these which we are interested in locating in any active region model. Before complicated models using large numbers of sources are studied, it is important to understand the basic topological elements of the field and how they change and interact with one another. It is this subject which we address in Chapter 2 using simple fields produced by just two, three and four photospheric potential sources, and studying the evolution and interaction of the separatrix surfaces which determine the topology of the field.

In Chapter 3 we go on to look at a more realistic coronal model in which the discrete sources are located a finite distance below the photospheric boundary. We discuss how the topological skeleton of the field now consists of separatrix surfaces formed by field lines which tangentially graze the photosphere, together with the separatrix surfaces due to only those nulls lying on or above the photospheric plane. A simple criterion is also given for determining those nulls which lie above the photosphere. Furthermore, we establish the existence of a well-defined separator field line, at the mutual intersection of distinct topological regions, in the absence of any coronal null points. The work contained in this chapter has been written up in Bungey et al (1995).

The question of the local field configuration in the vicinity of a current sheet is then considered in Chapter 4. Previously, the classical topological picture of a two-dimensional, potential magnetic field containing a current sheet had been described analytically by Green (1965) and Syrovatskii (1971). We develop a more general analytical expression (Bungey & Priest 1995) describing the local configuration of a current sheet, in both potential and constant-current force-free fields, and encompassing the previous potential solutions as special cases.

The contents of this thesis are finally summarised in Chapter 5, together with a brief discussion of some unanswered questions and suggestions for future study.

Chapter 2

3D Topology of Interacting Magnetic Sources

2.1 Introduction

In order to model the effect on the overlying corona of the discrete concentrations of magnetic flux seen at the photospheric surface we use simple point sources or sinks of magnetic flux placed on the photospheric plane itself. We then study the coronal magnetic field generated by these point sources. Our main interest here is to understand the complex topology of such a field as a preliminary to studying energy release via magnetic reconnection, whether this be as a source of general heating for the coronal plasma or as a source of the more dynamic energy release associated with solar flares.

As already discussed in Chapter 1.4, the release of magnetic energy by reconnection of magnetic field lines necessarily requires the presence of large gradients in the magnetic field (or discontinuities if the plasma is assumed to be ideal). Thus when studying the topology of the coronal field we are interested in locating regions where possible discontinuities in the field may occur as a result of ideal plasma motions. These regions will often tend to be at separatrices, the boundaries between regions of differing magnetic connectivity. In our model, the vertical component of the field vanishes everywhere on the photospheric plane, except at the magnetic sources themselves. This means that the only possibilities for separating the coronal volume into regions of distinct magnetic connectivity are the separatrix surfaces associated with the presence of 3D null points in the field.

In two dimensions, the separatrix field lines passing through an X-type magnetic neutral point separate the plane into regions of differing connectivity. In three dimensions the field lines threading a null point in general form two classes, namely an isolated field line, or spine, and a surface of field lines, or fan. It is the fans which represent separatrix surfaces that separate the volume into topologically distinct regions. A brief review of magnetic fields in the vicinity of 3D null points is given in the next section. Sections 3, 4, and 5 then go on to study the null points, separatrix surfaces, and associated magnetic topology of the fields generated by combinations of 2, 3, and 4 sources of magnetic flux, respectively.

2.2 Three-Dimensional Magnetic Null Points

Recall that the field near a magnetic null point at $\mathbf{r}_N$ is given to the first order by $\mathbf{B}(\mathbf{r}) \simeq [(\mathbf{r} - \mathbf{r}_N) \cdot \nabla]\mathbf{B}(\mathbf{r}_N)$. This may be written in matrix form as

$$\mathbf{B}(\mathbf{r}) \simeq (\mathbf{r} - \mathbf{r}_N)\mathcal{B}, \tag{2.1}$$

where $\mathcal{B}$ is the 3×3 matrix of derivatives,

$$\mathcal{B} = \begin{pmatrix} \frac{\partial B_x}{\partial x} & \frac{\partial B_y}{\partial x} & \frac{\partial B_z}{\partial x} \\ \frac{\partial B_x}{\partial y} & \frac{\partial B_y}{\partial y} & \frac{\partial B_z}{\partial y} \\ \frac{\partial B_x}{\partial z} & \frac{\partial B_y}{\partial z} & \frac{\partial B_z}{\partial z} \end{pmatrix}. \tag{2.2}$$

Since $\nabla \cdot \mathbf{B} = 0$ this matrix has zero trace

$$\mathrm{tr}(\mathcal{B}) \equiv \sum_{j=1}^{3} \frac{\partial B_j}{\partial x_j} = 0, \tag{2.3}$$

which then requires that the three eigenvalues of the matrix sum to zero ($\lambda_1 + \lambda_2 + \lambda_3 = 0$). Also, by definition, the eigenvalues of $\mathcal{B}$ satisfy

$$\det(\mathcal{B} - \lambda\mathcal{I}) = 0, \tag{2.4}$$

where $\mathcal{I}$ is the unit matrix. Expanding this equation and taking into account Eq.(2.3), we obtain

$$\lambda^3 - \frac{1}{2}\,\mathrm{tr}(\mathcal{B}^2)\,\lambda - \det(\mathcal{B}) = 0, \tag{2.5}$$

which is valid for an arbitrary magnetic null point.

This may be significantly simplified when all the sources lie in the photospheric $z = 0$ plane. Thus

$$B_z|_{z=0} = 0$$

and so

$$\nabla_h B_z|_{z=0} = 0, \tag{2.6}$$

where the subscript $_h$ represents the horizontal component. However, at any null point of a potential (or indeed linear force-free) field we must have

$$\nabla \times \mathbf{B}|_{\mathbf{r}=\mathbf{r}_N} = 0 \tag{2.7}$$

and so

$$\left(\frac{\partial \mathbf{B}_h}{\partial z} - \nabla_h B_z\right)\Big|_{\mathbf{r}=\mathbf{r}_N} = 0. \tag{2.8}$$

Thus, if the null point lies in the photospheric plane $z = 0$, Eqs.(2.6) and (2.8), imply that

$$\frac{\partial \mathbf{B}_h}{\partial z}\Big|_{\mathbf{r}=\mathbf{r}_N} = 0. \tag{2.9}$$

This means that the matrix $\mathcal{B}$ has the following structure

$$\mathcal{B} = \begin{pmatrix} b_{11} & b_{12} & 0 \\ b_{21} & b_{22} & 0 \\ 0 & 0 & b_{33} \end{pmatrix}, \tag{2.10}$$

where the matrix of the horizontal field gradients is

$$\begin{pmatrix} b_{11} & b_{12} \\ b_{21} & b_{22} \end{pmatrix} \equiv \mathcal{B}_h = \nabla_h \mathbf{B}_h(\mathbf{r}_N) \tag{2.11}$$

and

$$b_{33} = \frac{\partial B_z}{\partial z}. \tag{2.12}$$

Due to Eq.(2.7) the matrix $\mathcal{B}_h$ in Eq.(2.11) is symmetric, i.e. $b_{12} = b_{21}$ or

$$\mathcal{B}_h = \mathcal{B}_h^T. \tag{2.13}$$

After some straightforward algebra and making use of Eqs.(2.3) and (2.10)-(2.13) it is now possible to show that

$$\mathrm{tr}(\mathcal{B}^2) = 2\left[b_{33}^2 - \det(\mathcal{B}_h)\right], \tag{2.14}$$

$$\det(\mathcal{B}) = b_{33}\det(\mathcal{B}_h). \tag{2.15}$$

This enables us to factorize Eq.(2.5) in the form

$$(\lambda - b_{33})[\lambda^2 + b_{33}\,\lambda + \det(\mathcal{B}_{\rm h})] = 0\,, \tag{2.16}$$

from which explicit expressions for the eigenvalues follow, namely

$$\begin{aligned} \lambda_{1,2} &= -\frac{b_{33}}{2} \pm \sqrt{D}\,, \\ \lambda_3 &= b_{33}\,. \end{aligned} \tag{2.17}$$

Here, due to the fact that $\mathcal{B}_{\rm h}$ is symmetric, the discriminant

$$D = \frac{b_{33}^2}{4} - \det(\mathcal{B}_{\rm h}) \tag{2.18}$$

is always non-negative. This can be verified directly from Eqs.(2.3) and (2.13), by rewriting Eq.(2.18) as

$$D = \frac{1}{4}\,{\rm tr}(\mathcal{B}_{\rm h})^2 - \det(\mathcal{B}_{\rm h}) = \frac{1}{4}(b_{11} - b_{22})^2 + b_{12}^2\,. \tag{2.19}$$

Thus all three eigenvalues of the null point matrix $\mathcal{B}$ of Eq.(2.2) are real and are given by Eq.(2.17). Also, from their structure we must have either one positive and two negative eigenvalues, or alternatively one negative and two positive eigenvalues. These two cases give rise to nulls of positive and negative type, respectively, following the notation of Priest & Titov (1995). From the three eigenvalues we may also find the three corresponding eigenvectors

$$\begin{aligned} \mathbf{h}_1 &= (b_{12}\,, \lambda_1 - b_{11}\,, 0) \\ \mathbf{h}_2 &= (\lambda_2 - b_{22}\,, b_{21}\,, 0) \\ \mathbf{h}_3 &= (0\,, 0\,, 1), \end{aligned} \tag{2.20}$$

and due to the symmetry of $\mathcal{B}_{\rm h}$ it is easy to show that these eigenvectors are orthogonal.

In both the above cases the eigenvectors corresponding to the two eigenvalues of the same sign define a plane in the vicinity of the null point and all field lines either leaving or entering the null (in the cases of positive and negative nulls, respectively) lie in this plane close to the null and fan out away from the null to form the so-called '*fan surface*'. The eigenvector corresponding to the remaining eigenvalue of opposite sign forms a curve known as the '*spine curve*' in the notation of Priest & Titov (Lau & Finn (1990) referred to the fan and spine as the Σ-surface and γ-line, respectively). This spine

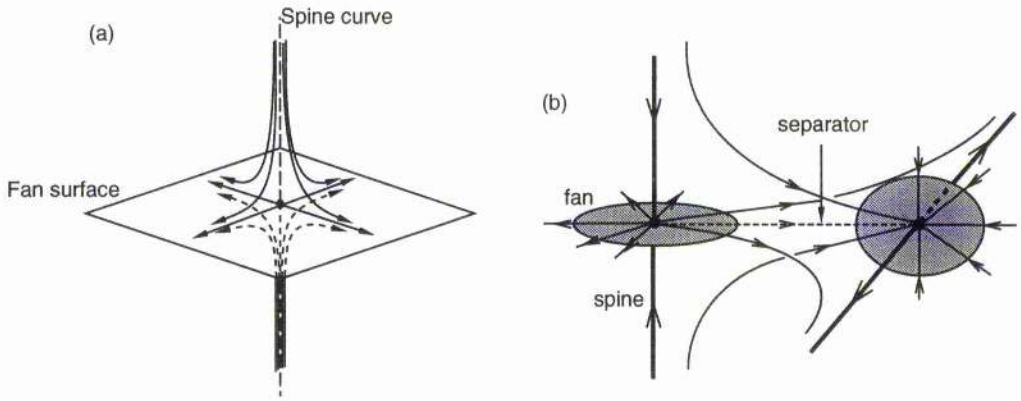

Figure 2.1: (a) General 3D null point configuration, with the spine curve intersecting the fan surface normally at the null point. The null shown in this case is of positive type in the notation of Priest & Titov (1995). (b) Two or more fan surfaces may intersect one another with the extent of each fan surface being limited by the spine of the other null. The spine curves are shown as the thick lines and the fan surfaces are shaded in the region of the nulls. A separator field line, which lies at the intersection of the two surfaces, is also shown as the dashed field line.

curve is perpendicular to the fan surface in the case of potential or force-free fields (see e.g. Parnell et al 1995 for a comprehensive classification of null points). An example of such a configuration is shown in Figure 2.1a, and Figure 2.1b gives gives an example of how different fan surfaces may interact with one another.

We shall now study more closely the fan surfaces emanating from the 3D null points and forming the separatrix surfaces which separate the coronal field into regions of distinct magnetic connectivity.

2.3 Two Unbalanced Sources of Opposite Polarity

Let us define a system of spherical coordinates (r, θ, ϕ) as shown in Figure 2.2, where θ represents the inclination to the x-axis and ϕ is the inclination of the plane through the x-axis with the xz-plane. The relation to the Cartesian frame is thus given by

$$\begin{aligned} x &= r\cos\theta \\ y &= r\sin\theta\sin\phi \\ z &= r\sin\theta\cos\phi. \end{aligned} \tag{2.21}$$

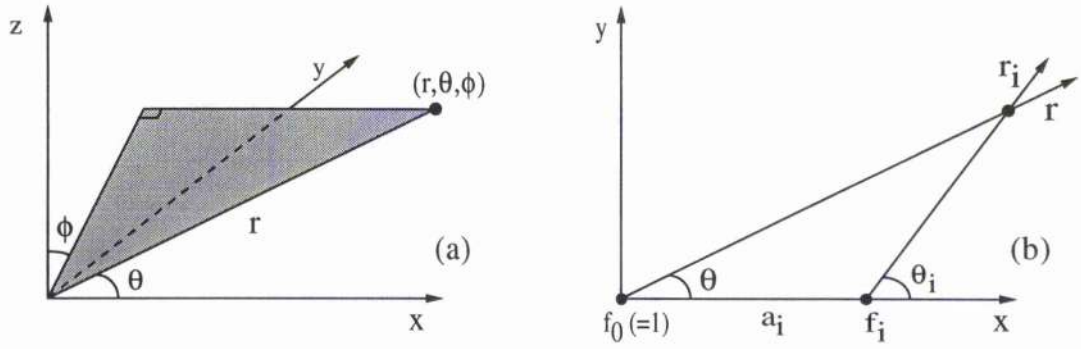

Figure 2.2: (a) The spherical coordinate system $(r\,,\theta\,,\phi)$ to be used, and (b) the directional vectors in the plane $\phi = \pi/2$ for a source f_i located at a distance a_i along the x-axis.

The magnetic field of a unit point source at the origin is given by

$$\mathbf{B}(r\,,\theta\,,\phi\,) = \frac{\hat{\mathbf{r}}}{r^2}. \tag{2.22}$$

We may write this field in terms of a curl as

$$\mathbf{B}(r\,,\theta\,,\phi\,) = \nabla \times \left(\frac{F\hat{\phi}}{r\sin\theta} \right), \tag{2.23}$$

where $F = -\cos\theta$. Thus we have automatically ensured that $\nabla \cdot \mathbf{B} = 0$ (except at the isolated source itself) and also the condition $\mathbf{B} \cdot \nabla F = 0$, which implies that $\mathbf{B}$ is normal to ∇F and hence lies along surfaces of constant F. Indeed we may rewrite Eq.(2.23) in terms of Euler potentials in the form

$$\mathbf{B} = \nabla \times (F\nabla G) = \nabla F \times \nabla G\,, \tag{2.24}$$

where $G = \phi$, which also then implies $\mathbf{B} \cdot \nabla G = 0$ so that field lines lie in surfaces of constant G. Thus the magnetic field lines are, as expected, determined by the intersections of surfaces $\phi =$ constant and $\theta =$ constant.

If we now consider a source located at a distance a along the x-axis (Figure 2.2b), the field is given by

$$\mathbf{B} = \nabla \times \left(\frac{-\cos\theta_i\,\hat{\phi}_i}{r_i\,\sin\theta_i} \right). \tag{2.25}$$

However, using the coordinate system defined above and with this displaced source lying on the x-axis we have both $\hat{\phi}_\mathbf{i} = \hat{\phi}$ and also $r_i\,\sin\theta_i = r\,\sin\theta\,$. Thus the magnetic field of

this displaced source becomes

$$\mathbf{B} = \nabla \times \left(\frac{-\cos\theta_i \, \hat{\phi}}{r \sin\theta} \right). \tag{2.26}$$

This is in an equivalent form to Eq.(2.23), with the field lines now lying in surfaces of $-\cos\theta_i = \text{constant}$.

Consider next the magnetic field generated by two discrete, unbalanced magnetic sources. Without loss of generality we can set one source at the origin, with strength $f_0 = 1$, and the other at a distance a_1 along the x-axis and with strength $f_1 = -\epsilon_1 f_0$, where $\epsilon_1 > 0$ (Figure 2.2b). This field is given by

$$\mathbf{B} = \frac{\hat{\mathbf{r}}}{r^2} - \frac{\epsilon_1 \hat{\mathbf{r}}_1}{r_1^2}, \tag{2.27}$$

or in terms of the notation of Eqs.(2.23) and (2.26)

$$\mathbf{B} = \nabla \times \left(\frac{-\cos\theta + \epsilon_1 \cos\theta_1}{r \sin\theta} \hat{\phi} \right). \tag{2.28}$$

This is again of the same form as Eq.(2.23), where now $F = \epsilon_1 \cos\theta_1 - \cos\theta$, and thus the field lines are simply defined by the intersections of the surfaces $\phi = \text{constant}$ and $\epsilon_1 \cos\theta_1 - \cos\theta = \text{constant}$.

The magnetic field due to these two unbalanced sources produces a null point on the x-axis at a point x_N given by (from Eq.(2.27))

$$\frac{1}{x_N^2} - \frac{\epsilon_1}{(x_N - a_1)^2} = 0,$$

so that

$$x_N = \frac{a_1}{(1 - \sqrt{\epsilon_1})}. \tag{2.29}$$

Thus when $0 < \epsilon_1 < 1$ this null point will lie at a point on the x-axis beyond the source at a_1 (Figure 2.3a).

As mentioned in the previous section, the fan surface for this null point will form a separatrix surface in the coronal volume above the source plane. In any plane $\phi = \text{constant}$ the separatrix field line may easily be found. At the null point itself we have $\theta = \theta_1 = 0$ and hence $\epsilon_1 \cos\theta_1 - \cos\theta = \epsilon_1 - 1$. The separatrix field line in any plane $\phi = \text{constant}$ is thus given by

$$\epsilon_1 \cos\theta_1 - \cos\theta = \epsilon_1 - 1. \tag{2.30}$$

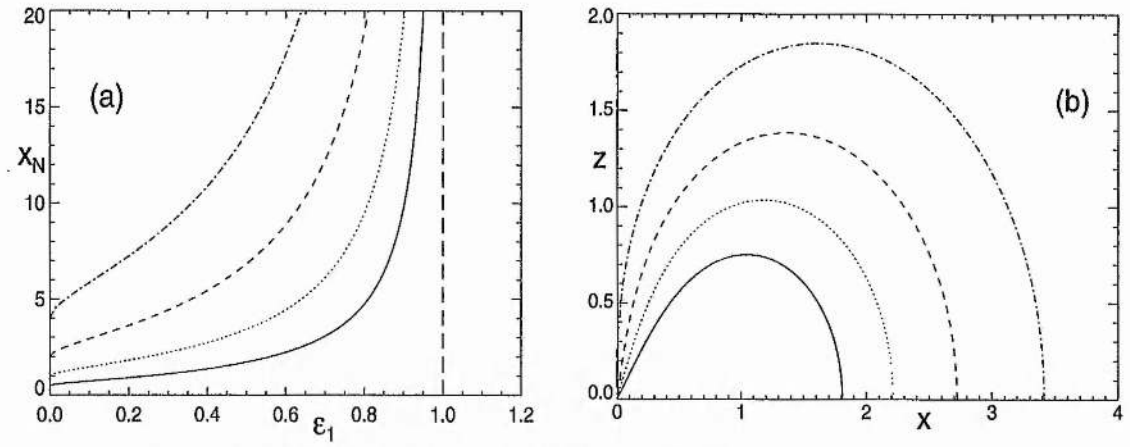

Figure 2.3: (a) Null point position x_N against source strength ϵ_1 for source separations of $a_1 = 0.5$, 1, 2, and 4 given by the solid, dotted, dashed, and dot-dashed curves, respectively. The null point is seen to diverge to infinity as $\epsilon_1 \to 1$. (b) The shape of the separatrix field line plotted in the plane $\phi = 0$ for a fixed value of a_1 and values of $\epsilon_1 = 0.2$, 0.3, 0.4, and 0.5 given by the solid, dotted, dashed and dot-dashed curves, respectively.

Where this separatrix field line meets the stronger of the two sources, located at the origin here, we also have $\theta_1 = \pi$ and thus, from Eq.(2.30)

$$\cos\theta_0 = 2\epsilon_1 - 1\,, \tag{2.31}$$

where θ_0 is the angle at which the separatrix field line meets the source. It is worth noting that this angle is independent of the source separation and depends merely on the strength ratio ϵ_1 of the two sources. The variation of the null point position, x_N, with source strength ratio is plotted in Figure 2.3a, with the shape of the corresponding separatrix field lines shown in Figure 2.3b for differing values of ϵ_1. A cross-sectional view of the general field structure, along with a three-dimensional view of a selection of field lines emanating from the null point and forming the coronal separatrix surface are given in Figures 2.4a and 2.4b, respectively.

So, for this basic field of two unbalanced sources of opposite polarity, the skeleton of the magnetic field topology is relatively simple and consists of a null point, a spine curve, and a separatrix fan surface (Figure 2.4). The separatrix fan surface passes through one source and the null point, while the spine curve starts at the other source, passes through the null and ends at infinity. As already discussed in Section 2.2, the eigenvectors of the field in the vicinity of the null point are orthogonal and given by Eq.(2.20). For

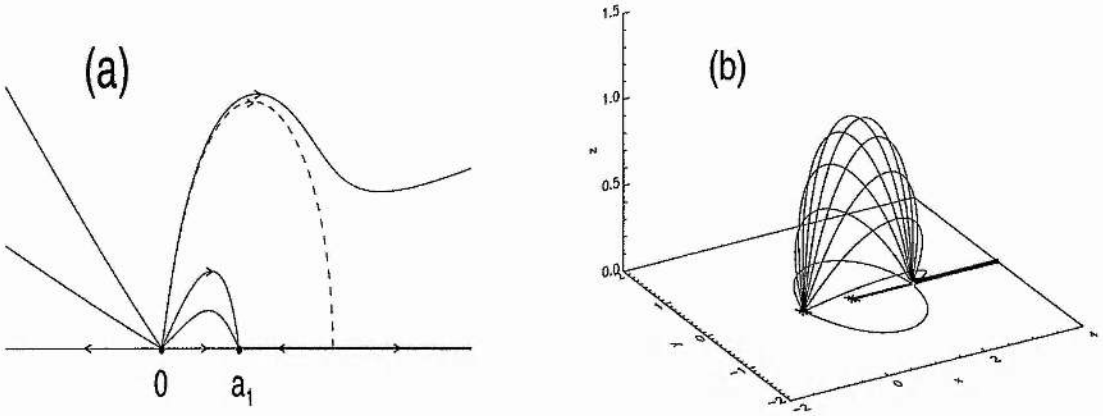

Figure 2.4: (a) Cross-section of the basic field structure showing field lines both inside and outside of the closed separatrix surface (dashed curve) in the plane $\phi = 0$. (b) Field lines forming the fan surface and hence the coronal separatrix surface of a photospheric null. The spine is shown as a thicker field line.

this two-source field, with the sources located on the x-axis, it is easy to show that $b_{12} = \partial B_x/\partial y = 0$ for a null on the x-axis. Thus the three eigenvectors of Eq.(2.20) are seen to lie along the Cartesian $\hat{\mathbf{y}}$-, $\hat{\mathbf{x}}$- and $\hat{\mathbf{z}}$-directions, respectively. Also, by evaluating b_{33} and D for this two-source arrangement, it is possible to show that the eigenvector lying along the $\hat{\mathbf{x}}$-direction corresponds to the eigenvalue of opposite sign and hence is the spine curve.

Thus the spine curve of the null point lies along the line of the sources, connecting flux from the weaker source to the null point. The fan surface intersects the source plane perpendicularly at the null and closes over the weaker of the two sources, connecting the null point to the stronger source. The coronal field is separated into just two topologically distinct regions: those field lines inside the closed fan surface join the two sources, whilst those outside connect the stronger source to a flux source at infinity (Figure 2.4a). The overall topology of this field remains unaltered by variations in the source separation or strength ratio.

2.4 Three-Source Fields

Let us now add a third source of magnetic flux to the field produced by the two already studied. What we shall find is that for unbalanced sources the skeleton of the field

usually consists of two null points together with their fan separatrix surfaces and spines curves. The spines join the nulls either to one of the sources or to infinity and thus they effectively join the nulls to sources of the same polarity. In general the two separatrix fan surfaces may either be nested or independent and may either meet at one source or remain completely distinct depending on the positions and the strengths of the sources. In a few special cases, however, we may find the coalescence of the null points and either the birth of a null curve or the formation of additional nulls.

2.4.1 Colinear Sources

If this third source is also placed along the x-axis (or the line $\theta = 0$) at a distance a_2, say, the magnetic field is now described by

$$\mathbf{B} = \frac{\hat{\mathbf{r}}}{r^2} - \frac{\epsilon_1 \hat{\mathbf{r}}_1}{r_1^2} - \frac{\epsilon_2 \hat{\mathbf{r}}_2}{r_2^2}\,, \tag{2.32}$$

where the strengths of the sources at a_1 and a_2 are given by $f_1 = -\epsilon_1 f_0$ and $f_2 = -\epsilon_2 f_0$, respectively, and as before we have taken $f_0 = 1$ for simplicity. We shall also assume that both ϵ_1 and $\epsilon_2 > 0$. Generalising Eq.(2.23) we may write the field of this colinear case as

$$\mathbf{B} = \nabla \times \left(\frac{-\cos\theta + \epsilon_1 \cos\theta_1 + \epsilon_2 \cos\theta_2}{r \sin\theta}\, \hat{\phi} \right), \tag{2.33}$$

and thus field lines are now given by the intersections of planes $\phi =$ constant and

$$-\cos\theta + \epsilon_1 \cos\theta_1 + \epsilon_2 \cos\theta_2 = \text{constant}. \tag{2.34}$$

(i) The Case $a_2 > a_1 > 0$ (Opposite-Polarity Source to One Side)

Suppose now we initially look at the case $a_2 > a_1 > 0$. Then all field lines emanating from the source at the origin satisfy

$$-\cos\theta + \epsilon_1 \cos\theta_1 + \epsilon_2 \cos\theta_2 = -\cos\theta_0 - \epsilon_1 - \epsilon_2\,, \tag{2.35}$$

where θ_0 is the angle at which the field line leaves the source.

This field will contain null points along the x-axis at positions $x_{\rm N}$ given by

$$\frac{1}{x_{\rm N}^2} - \frac{\epsilon_1}{(x_{\rm N} - a_1)^2} - \frac{\epsilon_2}{(x_{\rm N} - a_2)^2} = 0, \tag{2.36}$$

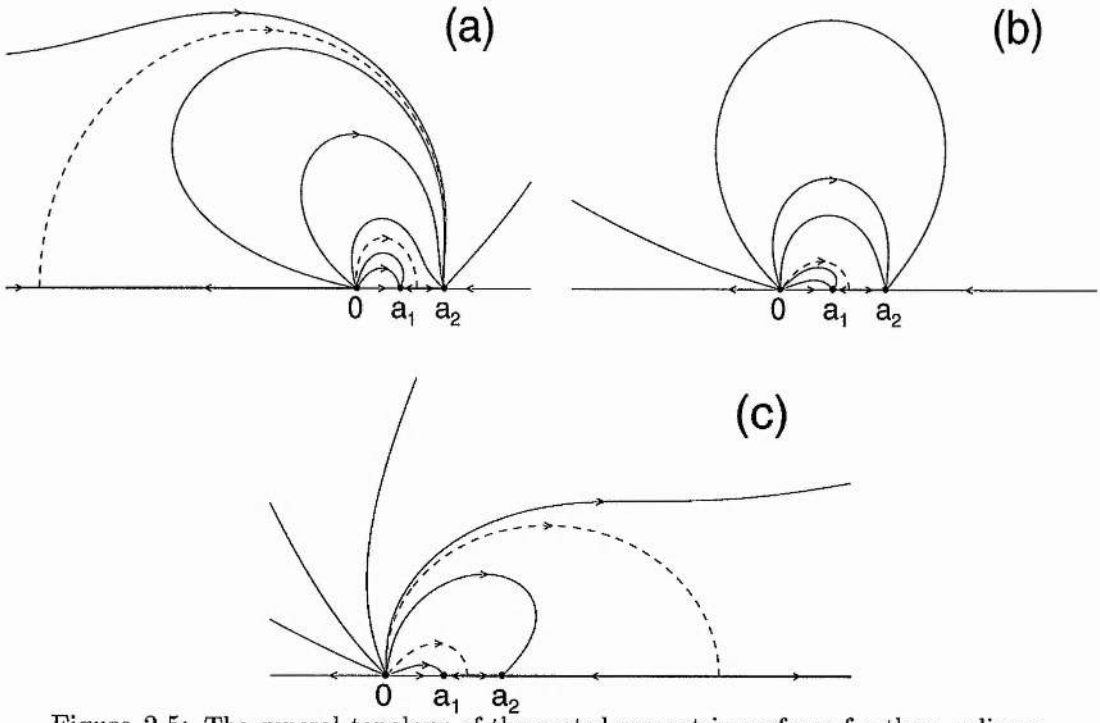

Figure 2.5: The general topology of the nested separatrix surfaces for three colinear sources when $a_2 > a_1 > 0$ seen in cross-section in the plane $\phi = 0$. The exterior null changes sides as the net flux changes from (a) negative to (b) zero (when the outer separatrix surface expands to infinity) to (c) positive. The spines are denoted by the thick lines and the separatrices by dashed curves.

which may easily be rearranged to give a quartic in $x_{\rm N}$,

$$x_{\rm N}^4(1-\epsilon_1-\epsilon_2) - 2x_{\rm N}^3\{a_1(1-\epsilon_2)+a_2(1-\epsilon_1)\} + x_{\rm N}^2\{a_1^2(1-\epsilon_2)+a_2^2(1-\epsilon_1)+4a_1a_2\} - 2x_{\rm N}\,a_1a_2(a_1+a_2)+a_1^2a_2^2 = 0. \tag{2.37}$$

In general this equation will have two real and two complex roots. For the case $a_2 > a_1 > 0$ one of the real roots will lie in the region $a_1 \leq x_{\rm N} \leq a_2$, whilst the other will lie in either $x_{\rm N} < 0$ or $a_2 < x_{\rm N}$, corresponding to the total (net) flux being negative or positive, respectively. Examples of the general magnetic structure showing the separatrix field lines emanating from the distinct null points for both these cases are given in Figures 2.5a and 2.5c, respectively, with Figure 2.5b showing the special case of flux balance (i.e. zero net flux).

The angle, θ_0, at which the separatrix field lines (of the permanent internal null) leave

the origin, is given by (from Eq.(2.35))

$$\begin{aligned} -\cos\theta_0 - \epsilon_1 - \epsilon_2 &= -1 + \epsilon_1 - \epsilon_2\,, \\ \text{i.e.} \qquad \cos\theta_0 &= 1 - 2\epsilon_1. \end{aligned} \tag{2.38}$$

This angle is independent of the source separations (a_1 and a_2) and depends only on the relative strengths of the sources at a_1 and the origin, varying from 0 to π as ϵ_1 increases from 0 to 1.

In general then for this colinear source arrangement the topological skeleton consists of two null points, which produce distinct separatrix surfaces nested inside one another and separating the coronal volume into three regions of differing magnetic connectivity. These nested separatrix surfaces are either completely detached from one another or meet in a single point at the source of opposite polarity (at the origin in this case), depending on the whether the net flux is negative or positive (see Figure 2.5).

(ii) The Case $a_2 < 0$, $0 < a_1$ (Opposite-Polarity Source in the Middle)

The second possible colinear source configuration occurs when $a_2 < 0$ and $a_1 > 0$, so that the opposite-polarity source (positive, say) now lies between the two like-polarity concentrations. In the general case this field will also contain two null points along the line of the sources, given again by the real roots of Eq.(2.37). An example of such a field when the net flux is positive (i.e. $\epsilon_1 + \epsilon_2 < 1$) is given in Figure 2.6a.

For this configuration with positive net flux we have again two distinct nulls producing distinct separatrix surfaces and separating the coronal volume into three topologically different regions. Unlike the previous configuration, however, the coronal surfaces are no longer nested inside one another.

An interesting situation arises for this arrangement as the net flux changes from positive to negative. When the net flux decreases to zero the null corresponding to the stronger of the two like-polarity sources migrates out to infinity (Figure 2.6b). As the flux then becomes negative we again have two real roots of the quartic Eq.(2.37), but these now both lie in the same region, either $x_N < a_2$ or $a_1 < x_N$, corresponding to $\epsilon_2 < \epsilon_1$ or $\epsilon_2 > \epsilon_1$, respectively (Figure 2.6c). The overall topology has now altered slightly with the separatrix surfaces produced by these null points being nested as in Figure 2.5a, but with

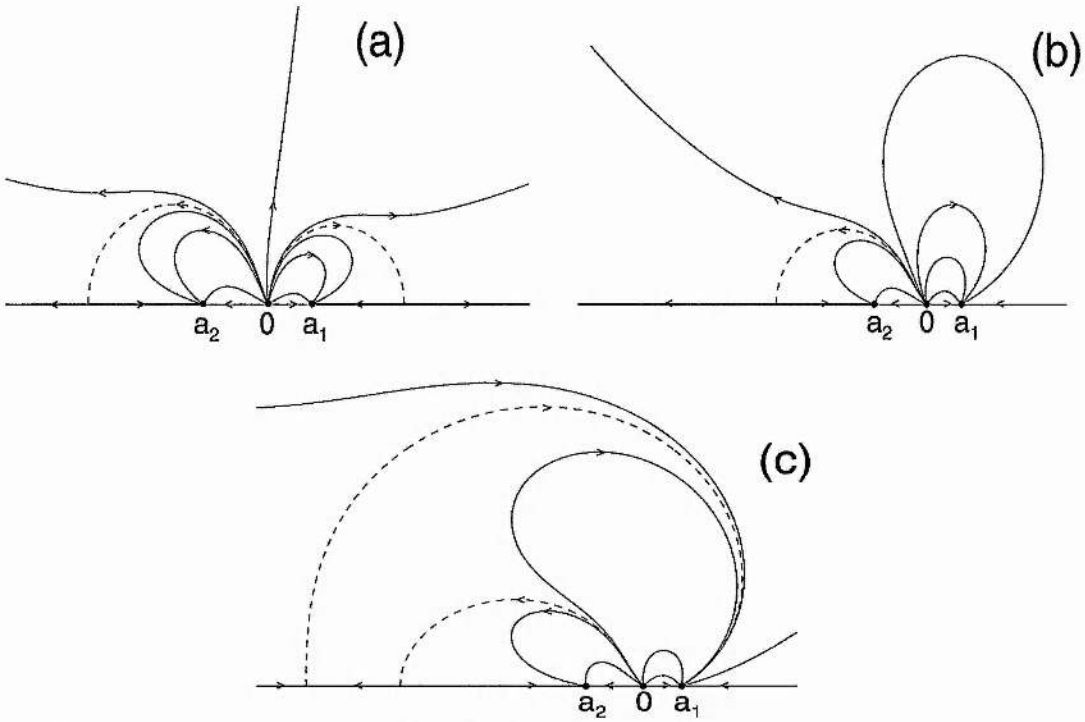

Figure 2.6: The general topology of the colinear case when $a_2 < 0$ and $a_1 > 0$. (a) The net flux is positive and the two nulls lie on opposite sides of the central source, in the regions $x_N < a_2$ and $a_1 < x_N$, and produce distinct separatrix surfaces. (b) As the net flux decreases to zero one null migrates to infinity, reappearing on the same portion of the x-axis as the other when the flux becomes negative. (c) The nulls are now connected by a common spine and the fan surfaces are nested.

the nulls now directly connected to one another by a common spine curve lying along the x-axis.

The configuration described above and shown in Figure 2.6c is for a small negative net flux. If, however, this negative net flux is allowed to become stronger, the two nulls migrate towards each other and eventually coalesce; the point of coalescence may be found by studying more closely the eigenvalues of the null point field described in Section 2.2.

A bifurcation point, where nulls coalesce, occurs whenever one of the eigenvalues of the field vanishes. Similarly, degenerate cases may also be found when two of the eigenvalues become equal (see e.g. Lau & Finn 1990). To study then the coalescence of the two nulls in the above three-source configuration we look for the vanishing of one or more of these

eigenvalues.

Consider the third eigenvalue given by $\lambda_3 = b_{33} = \partial B_z/\partial z$, which we may calculate by writing the field in terms of $\mathbf{B}(x\,,y\,,z\,)$. Using Eq.(2.3) we have

$$\lambda_3 = \frac{\partial B_z}{\partial z} = -\left(\frac{\partial B_x}{\partial x} + \frac{\partial B_y}{\partial y}\right), \tag{2.39}$$

where

$$B_x = \sum_{i=1}^{3} \frac{\epsilon_i (x - x_i)}{R_i^3}, \quad B_y = \sum_{i=1}^{3} \frac{\epsilon_i (y - y_i)}{R_i^3},$$
$$R_i = \left[(x - x_i)^2 + (y - y_i)^2\right]^{\frac{1}{2}} \tag{2.40}$$

for sources lying in the plane $z = 0$. Thus we find

$$\lambda_3 = \sum_{i=1}^{3} \left\{ -2\frac{\epsilon_i}{R_i^3} + 3\frac{\epsilon_i \left[(x - x_i)^2 + (y - y_i))^2\right]}{R_i^5} \right\} \quad = \sum_{i=1}^{3} \frac{\epsilon_i}{R_i^3}, \tag{2.41}$$

and hence for $\lambda_3 = 0$ we require simply

$$\frac{1}{R_0^3} - \frac{\epsilon_1}{R_1^3} - \frac{\epsilon_2}{R_2^3} = 0.$$

However, since the three sources and the nulls being studied are all located on the x-axis we have $y = y_i = 0$, and so this reduces to

$$\frac{1}{x^3} - \frac{\epsilon_1}{(x - a_1)^3} - \frac{\epsilon_2}{(x - a_2)^3} = 0. \tag{2.42}$$

We may now also make use of the fact that we are studying a null point of the field. Thus, replacing x_N by x in Eq.(2.36), we also have the condition

$$\frac{1}{x^2} - \frac{\epsilon_1}{(x - a_1)^2} - \frac{\epsilon_2}{(x - a_2)^2} = 0, \tag{2.43}$$

and, after eliminating ϵ_2, Eqs.(2.42) and (2.43) give a cubic in x

$$x^3[\epsilon_1(a_2 - a_1) - a_2] + 3x^2 a_1 a_2 - 3x a_1^2 a_2 + a_1^3 a_2 = 0. \tag{2.44}$$

This cubic will in general have one real and two complex roots, with the real root giving the value of x, in terms of the parameters a_1 , a_2, and ϵ_1, for which the eigenvalue λ_3 vanishes. Furthermore, it is also possible to show that under this same condition, Eq.(2.44), the discriminant D given by Eq.(2.19) vanishes. Thus, at the point given by the real root

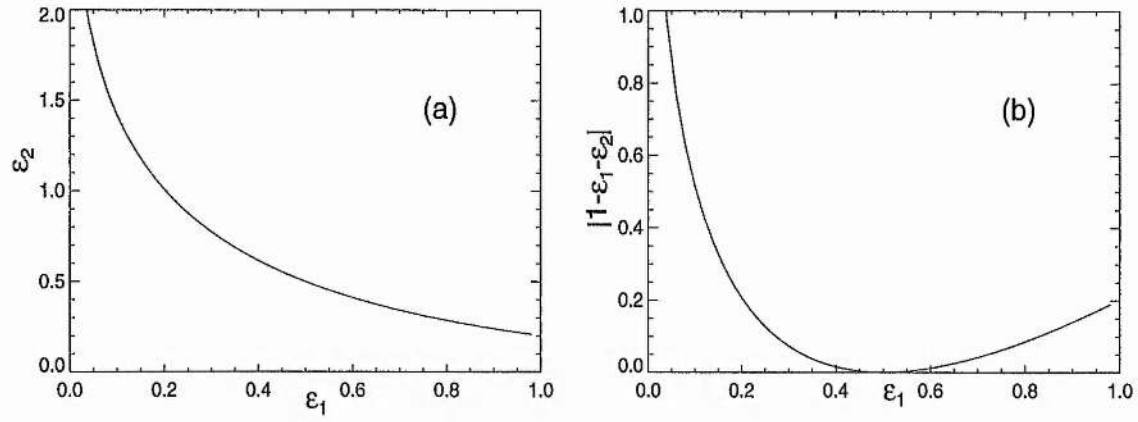

Figure 2.7: (a) The critical value of ϵ_2 against ϵ_1 for null point coalescence in the symmetric case $a_2 = -a_1$. (b) The size of the net flux $|1 - \epsilon_1 - \epsilon_2|$ at coalescence as a function of ϵ_1, with $\epsilon_1 = \epsilon_2 = 1/2$ corresponding to the balanced state.

of Eq.(2.44) all three eigenvalues become identically zero and the two nulls coalesce. If we specify the source separations (a_1 , a_2) and the relative strength of one of the sources (ϵ_1), we are therefore able to find the position at which the two nulls coalesce. Then by substituting into Eq.(2.43) we may also find the corresponding source strength (ϵ_2) required for coalescence.

As an example let us consider the particular case when $a_2 = -a_1$. Then Eq.(2.44) reduces to

$$x^3(1 - 2\epsilon_1) - 3x^2 a_1 + 3x a_1^2 - a_1^3 = 0, \tag{2.45}$$

and the real root of this cubic is given by

$$\begin{aligned} x &= T^{\frac{1}{3}} + \frac{2a_1^2\epsilon_1}{(2\epsilon_1 - 1)^2 T^{\frac{1}{3}}} - \frac{a_1}{(2\epsilon_1 - 1)}, \\ \text{where} \quad T &= \frac{-2\epsilon_1 a_1^3}{(2\epsilon_1 - 1)^3}. \end{aligned} \tag{2.46}$$

Also, from Eq.(2.43) we have

$$\epsilon_2 = (x + a_1)^2 \left[\frac{1}{x^2} - \frac{\epsilon_1}{(x - a_1)^2}\right], \tag{2.47}$$

and by substituting for x from Eq.(2.46) we may obtain an expression for ϵ_2 in terms of ϵ_1, and a_1. This relationship is plotted in Figure 2.7a, and it is interesting to note that this relationship is identical for all values of a_1. Also plotted in Figure 2.7b is the corresponding net flux value $|1 - \epsilon_1 - \epsilon_2|$ at coalescence as a function of ϵ_1. It is seen from

this plot that the coalescence occurs for only a small net flux, i.e. with a small imbalance in the positive and negative fluxes.

A plot of the magnetic field at this moment of coalescence is given in Figures 2.8a and 2.8c for this symmetric case and it can be seen that the two nested separatrix surfaces now meet at the degenerate null point.

As the size of the net flux $|1-\epsilon_1-\epsilon_2|$ increases beyond the coalescence value plotted in Figure 2.7b, the quartic of Eq.(2.37) no longer has any real roots and hence we no longer find any null points along the x-axis. This is due to the degenerate null of Figures 2.8a and 2.8c bifurcating to form a *null line*, which may be regarded as being made up of an infinite number of adjacent null points and forms a semi-circular arc in a plane $\theta = \pi/2$. It is the intersection of two separatrix surfaces (dashed curves in Figure 2.8b) whose field lines are shown in a vertical and horizontal plane in Figure 2.8d. These surfaces split the coronal field into four topologically distinct regions of magnetic connectivity. The null line is likely to be a favoured site for magnetic reconnection since it is at the intersection of all four of these topological regions (Figure 2.8d).

(iii) Balanced Flux Cases

In the preceeding two sections we have examined a model coronal field generated by three unbalanced sources of magnetic flux. For these unbalanced cases there is an overall non-zero net flux which it is assumed will connect to a more distant source concentration. It is worth noting, however, how the topological skeleton of the fields described in the previous sections varies in the special case of balanced sources, i.e. with zero net flux.

Under these balanced flux conditions we have simply $1 = \epsilon_1 + \epsilon_2$ and hence Eq.(2.37) reduces now to a cubic in x_N. This cubic has just one real root which lies in the region $a_1 < x_N < a_2$ for the case of $a_2 > a_1 > 0$ of Section 2.4.1(i). The other previous real root exterior to this region has migrated to infinity in the limit $\epsilon_1 + \epsilon_2 \rightarrow 1$. Thus we are left with just one null point and hence one separatrix surface, with the previously external surface disappearing to infinity along with the null.

Similarly, for the case $a_2 < 0\,, a_1 > 0$, we are left with just one null lying either in the region $x_N < a_2$ or $a_1 < x_N$ (corresponding to $\epsilon_2 < \epsilon_1$ or $\epsilon_2 > \epsilon_1$, respectively). Again, this behaviour corresponds to one of the nulls migrating to infinity in the limit $\epsilon_1 + \epsilon_2 \rightarrow 1$.

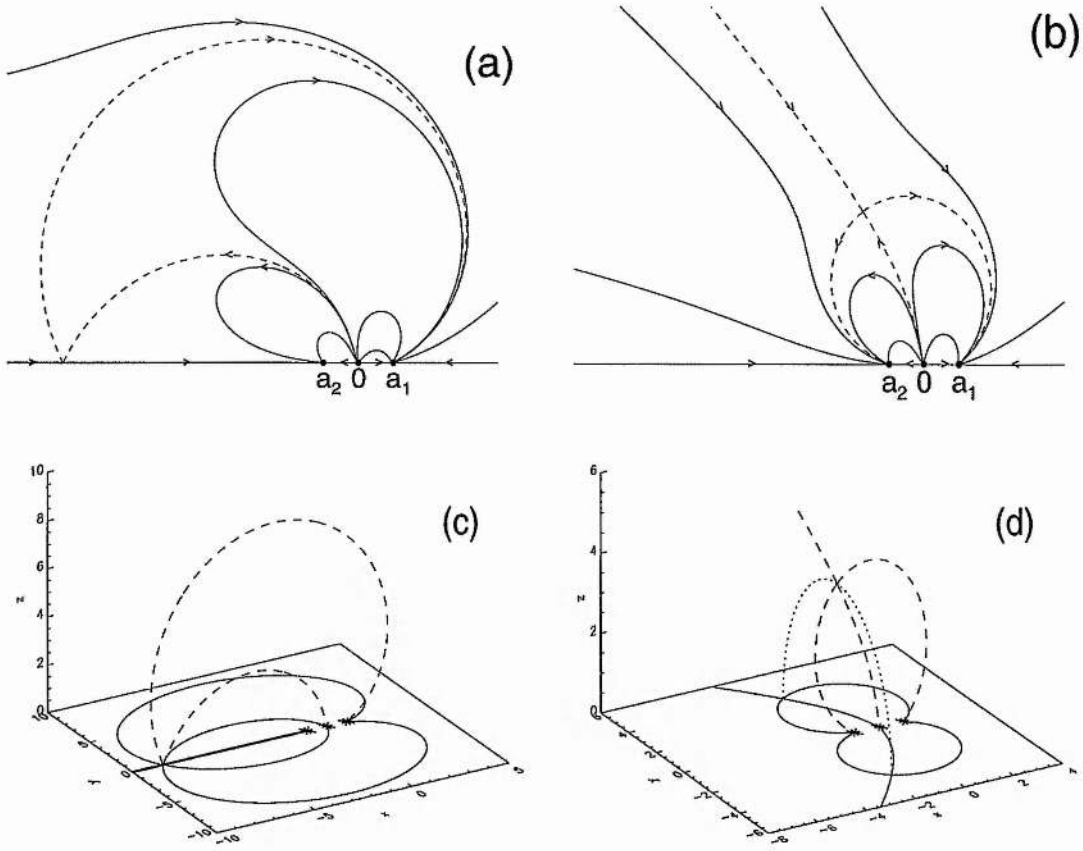

Figure 2.8: The degenerate null point at the moment of coalescence (or bifurcation) is shown in (a) in a cross-section through the plane $\phi = 0$ and in (c) in a general 3D view. The two separatrix surfaces meet at the null and their intersections with the planes $\phi = -\pi/2$, 0, and $\pi/2$ are drawn in (c). Similar views are given in (b) and (d) after the bifurcation of the null and the separatrices now intersect one another at a null line (the dotted curve in (d)).

Also, with now only one null point present in this balanced flux case, we no longer see the coalescence and bifurcation described in Section 2.4.1(ii). The topology of both source configurations is then reduced simply to that of one null point and one separatrix surface and hence just two regions of differing connectivity.

2.4.2 Non-Colinear Sources

Thus far in this section we have only considered the special case of a colinear three-source field. We now ask how the topological features will change, if at all, when this colinearity is destroyed.

(i) General Field Evolution

In order to study this case we shall start by fixing a source of strength $\epsilon_0 = 1$ at the origin as in the previous section. We shall also then fix, without loss of generality, a source of strength $-\epsilon_1$ at the position $a_1 = 1$ on the positive x-axis. The remaining source, of strength $-\epsilon_2$, will be initially placed at $x = -a_2$ on the negative x-axis, where $|a_2| \geq 1$, and then be rotated around the origin from its initial position at $\theta = \pi$ through to $\theta = 0$, corresponding to the point $x = a_2$ on the positive x-axis. This motion should generate, without loss of generality, all possible source arrangements and hence all possible topological configurations.

Unfortunately, in breaking the colinearity of the sources we are no longer able to express the field in the form of Eq.(2.23) and hence find an analytical expression for the separatrix field lines. We shall therefore revert to a standard Cartesian coordinate system for the remainder of this section, with the photosphere being given by the plane $z = 0$.

Following the procedure described above, we initially have the two like-polarity sources, ϵ_1 and ϵ_2, located on either side of the opposite-polarity source at the origin. This situation is then just as described in Section 2.4.1(ii), with two nulls lying outside the soures, one of which migrates to infinity as the net flux decreases to zero, and which merge and bifurcate to form a null line as the flux becomes sufficiently negative. Suppose we now start with a positive net flux, so that the two distinct nulls and their fan surfaces are on opposite parts of the x-axis, and we move the source ϵ_2 away from the axis. As this source moves smoothly in an arc around the origin the topological structure of the field

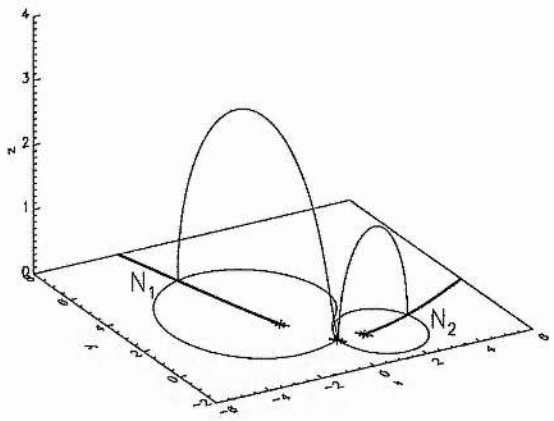

Figure 2.9: General topology for non-colinear sources with net positive flux. The two nulls N_1 and N_2 produce distinct fan surfaces.

will also evolve smoothly.

In Cartesian form the field in the $z = 0$ plane is given by Eq.(2.40) and for null points of the field we require $B_x = B_y = 0$. This, however, is not straightforward to solve analytically when we no longer have $y_2 = y_1 = 0$. There will though, in general, still exist two null points in the photospheric plane producing distinct separatrix surfaces. As the source rotates, so will the corresponding null, and the null previously on the positive x-axis also becomes displaced. A general configuration is shown in Figure 2.9, with the overall topology being unchanged from that of the initial case (e.g. compare with Figure 2.6a), and the skeleton consisting of two null points, N_1 and N_2, two spines and two distinct fan surfaces.

With continuing rotation the two distinct separatrix surfaces become increasingly pressed together and distorted at one side until at some critical point the spine curve of the null originally on the positive x-axis intersects the fan surface of the other null. At this point the smaller separatrix surface becomes engulfed by the larger one and the topology changes to one with nested surfaces. This configuration then tends to that of Section 2.4.1(i), as in Figure 2.5b, as the moving source continues towards the x-axis. The topology of the field is shown just prior to capture in Figures 2.10a and 2.10b, with Figure 2.10b giving a plan view of the photospheric field lines, showing the spine curves (thick curves) and separatrices (dashed curves). Similar plots are given at the moment of transition (Figures 2.10c and 2.10d) and just after the nesting of the two surfaces (Figures

2.10e and 2.10f).

Throughout this evolution the basic topological features have remained unaltered, consisting of two magnetic null fan surfaces separating the volume into three distinct regions, with the most interesting feature being the change from independent to nested fan surfaces. Around this point in the evolution the magnetic surfaces, although never intersecting, become pressed very close together. In general, high current densities and coronal heating events tend to be produced at separatrix surfaces in the magnetic field and so in such a region where two separatrices are pressed close together any heating is likely to be enhanced.

In general, this evolution is very similar to that of the colinear case already studied, with the overall topology, despite changing from independent to nested surfaces, remaining the same. However, for the colinear case of Section 2.4.1(ii) we also found that the basic topological structure of the field does change quite dramatically at the bifurcation point given by Eq.(2.44) when the nulls coalesce and a null line is born. We may now ask whether a similar moment of basic topological change can be found for the non-colinear case.

(ii) Null Point Coalescence

We may anticipate that, as in Section 2.4.1(ii), any major topological changes will be associated with the bifurcation or coalescence of a null point, and it is this which we shall now seek for the non-colinear field. The field in the photospheric plane is given by Eq.(2.40) along with the z-component

$$B_z = z\left\{\frac{1}{[x^2+y^2+z^2]^{\frac{3}{2}}} - \frac{\epsilon_1}{[(x-x_1)^2+(y-y_1)^2+z^2]^{\frac{3}{2}}} - \frac{\epsilon_1}{[(x-x_1)^2+(y-y_1)^2+z^2]^{\frac{3}{2}}}\right\}, \tag{2.48}$$

which will naturally vanish in the plane $z=0$. Now recall from Section 2.4.1(ii) that in order to find a bifurcation point we require one of the eigenvalues (λ) of the null point field to vanish. We shall therefore start our search, as in Section 2.4.1(ii), by supposing that

$$\lambda_3 = \frac{\partial B_z}{\partial z} = 0.$$

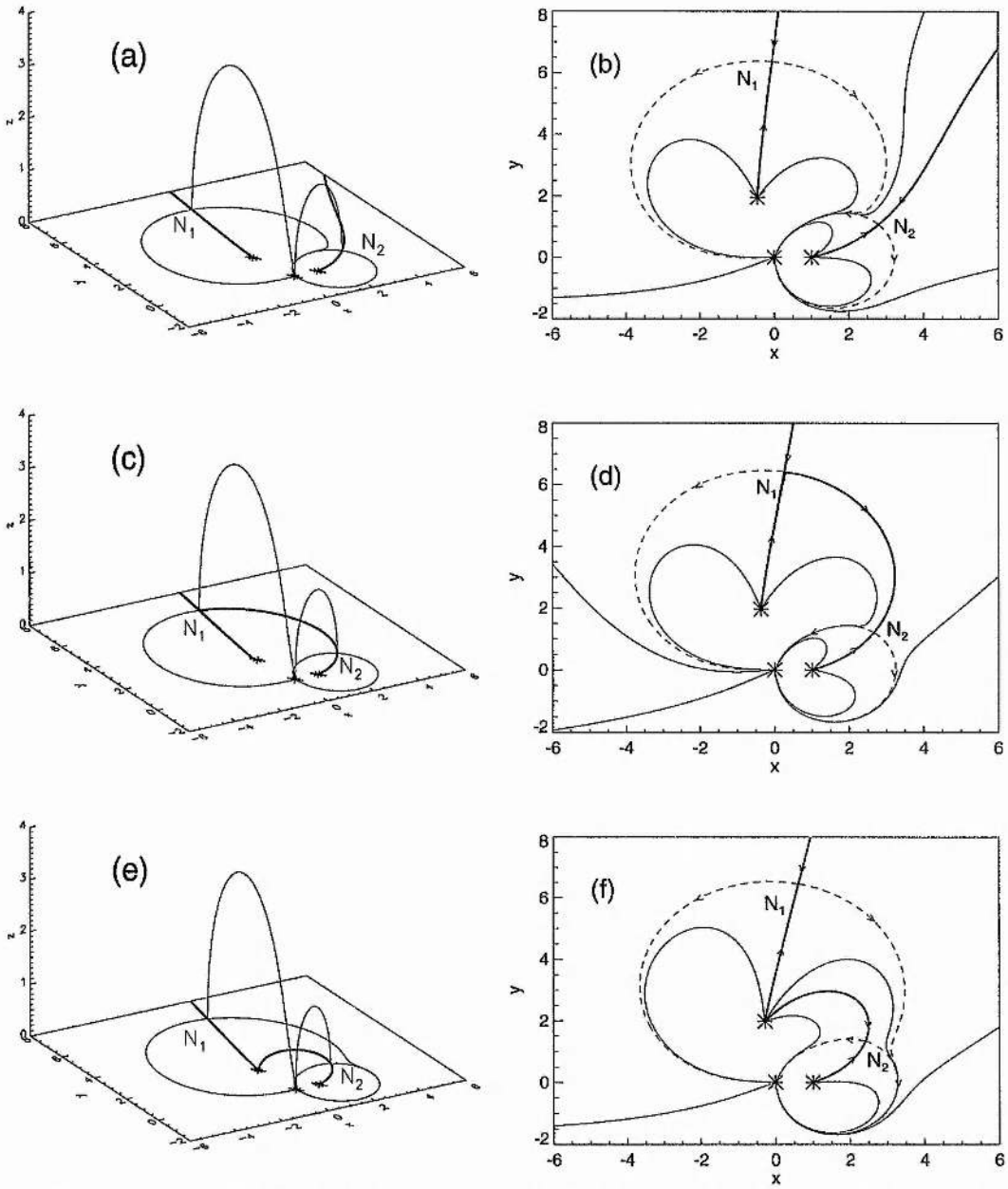

Figure 2.10: (a) The independent separatrix surfaces approach one another; they meet at some critical point in (c) and become nested (e). Corresponding plan views of photospheric field lines are given in (b), (d) and (f) to illustrate the different connectivity regions.

From Eq.(2.48) we have

$$\lambda_3 = \frac{\partial B_z}{\partial z}\,|_{z=0} = \frac{1}{[x^2+y^2]^{\frac{3}{2}}} - \frac{\epsilon_1}{[(x-x_1)^2+(y-y_1)^2]^{\frac{3}{2}}} - \frac{\epsilon_2}{[(x-x_2)^2+(y-y_2)^2]^{\frac{3}{2}}}, \quad (2.49)$$

and by setting this to zero and multiplying by y we obtain

$$\frac{y}{[x^2+y^2]^{\frac{3}{2}}} - \frac{y\epsilon_1}{[(x-x_1)^2+(y-y_1)^2]^{\frac{3}{2}}} = \frac{y\epsilon_2}{[(x-x_2)^2+(y-y_2)^2]^{\frac{3}{2}}}. \quad (2.50)$$

However, for a null point we must also satisfy $B_y = 0$, and from Eq.(2.40) this gives

$$\frac{y}{[x^2+y^2]^{\frac{3}{2}}} - \frac{(y-y_1)\epsilon_1}{[(x-x_1)^2+(y-y_1)^2]^{\frac{3}{2}}} = \frac{(y-y_2)\epsilon_2}{[(x-x_2)^2+(y-y_2)^2]^{\frac{3}{2}}}. \quad (2.51)$$

For the source arrangement under consideration we also have $y_1 = 0$ and the left-hand side of Eq.(2.51) is equal to that of Eq.(2.50). Thus we find

$$\frac{y\epsilon_2}{[(x-x_2)^2+(y-y_2)^2]^{\frac{3}{2}}} = \frac{(y-y_2)\epsilon_2}{[(x-x_2)^2+(y-y_2)^2]^{\frac{3}{2}}},$$

which simply implies that $y_2 = 0$. This means that for a null to be degenerate with $\lambda_3 = 0$ we require $y_2 = 0$ and hence the sources to be colinear, as already discussed in the previous section.

For a bifurcation point in the non-colinear field we must then consider instead $\lambda_1 = 0$, say, and this requires from Eq.(2.17)

$$D = \frac{b_{33}^2}{4} = \frac{1}{4}\left(\frac{\partial B_z}{\partial z}\right)^2. \quad (2.52)$$

Making use of Eqs.(2.3) and (2.19) this implies

$$\left(\frac{\partial B_x}{\partial x} - \frac{\partial B_y}{\partial y}\right)^2 + 4\left(\frac{\partial B_x}{\partial y}\right)^2 = \left(\frac{\partial B_x}{\partial x} + \frac{\partial B_y}{\partial y}\right)^2,$$

which may be rearranged to give the condition

$$\left(\frac{\partial B_x}{\partial y}\right)^2 = \frac{\partial B_x}{\partial x}\frac{\partial B_y}{\partial y}. \quad (2.53)$$

The three individual expressions in Eq.(2.53) may all be derived from Eq.(2.40), and after some straightforward algebra we obtain

$$-2\left(\frac{1}{R_0^3} - \frac{\epsilon_1}{R_1^3} - \frac{\epsilon_2}{R_2^3}\right)^2 + 9\left\{-\frac{\epsilon_1}{R_0^5 R_1^5}[x(y-y_1) - y(x-x_1)]^2 - \right. \quad (2.54)$$
$$\left. \frac{\epsilon_2}{R_0^5 R_2^5}[x(y-y_2) - y(x-x_2)]^2 + \frac{\epsilon_1\epsilon_2}{R_1^5 R_2^5}[(x-x_1)(y-y_2) - (x-x_2)(y-y_1)]^2\right\} = 0,$$

where R_i (for $i = 0 \rightarrow 2$) is given by Eq.(2.40) with $x_0 = y_0 = 0$.

This condition for bifurcation is, however, too hard to solve analytically for the general case, even with $y_1 = 0$, but some progress may be made if we consider a special symmetric source arrangement. Suppose that the sources $-\epsilon_1$ and $-\epsilon_2$ are equal in strength, i.e. $\epsilon_1 = \epsilon_2$, and that they are placed symmetrically about the x-axis such that $x_1 = x_2$ and $y_1 = -y_2$. Under this symmetric arrangement we may now expect that any bifurcation or coalescence of nulls will take place on the line of symmetry, i.e. the x-axis. Thus we may set $y = 0$ in Eq.(2.54), so that

$$R_0 = x\,, \quad R_1 = R_2 = \left[(x - x_1)^2 + y_1^2\right]^{\frac{1}{2}}, \tag{2.55}$$

and Eq.(2.54) reduces to

$$-2\left(\frac{1}{x^3} - \frac{2\epsilon_1}{R_1^3}\right)^2 + 9\left\{-\frac{\epsilon_1}{x^5 R_1^5}\left[2x^2 y_1^2\right] - \frac{\epsilon_1^2}{R_1^{10}}\left[4y_1^2(x - x_1)^2\right]\right\} = 0. \tag{2.56}$$

Since we are considering a null-point field we must, of course, also satisfy $B_x = B_y = 0$. Clearly for this symmetric source arrangement $B_y = 0$ will automatically be satisfied at all points on the x-axis and hence we just require, from Eq.(2.40)

$$B_x = \frac{1}{x^2} - \frac{2\epsilon_1(x - x_1)}{R_1^3} = 0. \tag{2.57}$$

Equations (2.56) and (2.57) determine the null point position (x) and the value of ϵ_1 for null-point coalescence as functions of x_1 and y_1, with R_1 given by Eq.(2.55). After eliminating R_1, Eq.(2.56) may be written as a quartic in x, namely,

$$\begin{aligned} -2x^4x_1^2 \;&+\; x^3(8x_1^3 + 4x_1y_1^2) - x^2(12x_1^4 + 22x_1^2y_1^2 + 9y_1^4) \\ &+\; x(8x_1^5 + 17x_1^3y_1^2 + 9x_1y_1^4) - (2x_1^6 + 4x_1^4y_1^2 + 2x_1^2y_1^4) = 0, \end{aligned} \tag{2.58}$$

which has four real roots given by

$$x = \frac{3y_1^2 + 2x_1^2 \pm T}{2x_1}, \quad \frac{3y_1^2 + 4x_1^2 \pm T}{4x_1}, \tag{2.59}$$

where

$$T = \sqrt{9y_1^4 + 8x_1^2y_1^2}.$$

Just as in Section 2.4.1(ii), we may now substitute these real values of x from Eq.(2.59) along with Eq.(2.55) into Eq.(2.57) to give a value for the relative source strength ϵ_1

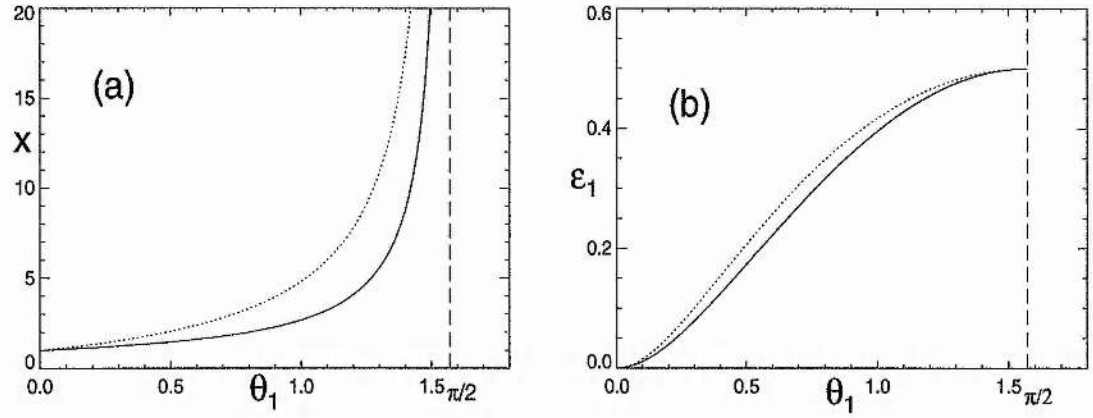

Figure 2.11: Variations with angular position (θ_1) of the sources of (a) the positions of the bifurcation points, x_{initial} (solid) and x_{final} (dashed), and (b) the critical values of ϵ_1 for bifurcation.

($= \epsilon_2$). We then find that two of the roots in Eq.(2.59), namely those with "$-T$", lead to negative values for ϵ_1 and so may be discarded since we have stipulated at the beginning of this section that both ϵ_1 and ϵ_2 be positive. Thus we are left with two real roots, given by the "$+T$" solutions of Eq.(2.59), which give two values of ϵ_1 ($= \epsilon_2$) for which the eigenvalue λ_1 vanishes for this non-colinear, symmetric field.

Let us now follow the evolution of such a field in order to study the bifurcation and the associated topological changes. We keep the source of strength $f_0 = 1$ fixed at the origin as before and place the equal-strength sources, $\epsilon_1 = \epsilon_2$, at positions (x_1, y_1) and $(x_1, -y_1)$, or in polar coordinates at (r_1, θ_1) and $(r_1, -\theta_1)$, respectively. Thus, by writing $x_1 = r_1 \cos\theta_1$ and $y_1 = r_1 \sin\theta_1$ in Eq.(2.59), we find that bifurcation occurs on the x-axis at positions

$$\begin{aligned} x_{\text{initial}} &= r_1 \left[\frac{4 - \sin^2\theta_1 + \sin\theta_1 \sqrt{\sin^2\theta_1 + 8}}{4\cos\theta_1} \right] \\ x_{\text{final}} &= r_1 \left[\frac{\sin^2\theta_1 + 2 + \sin\theta_1 \sqrt{\sin^2\theta_1 + 8}}{2\cos\theta_1} \right] . \end{aligned} \tag{2.60}$$

Without loss of generality we may now fix $r_1 = 1$ and simply study the evolution of this field as we vary θ_1. From Eq.(2.60) we plot the relationship between x and θ_1 at bifurcation, as shown in Figure 2.11a, and by substituting for x from Eq.(2.60) into Eq.(2.57) we may also find and plot the relation between ϵ_1 and θ_1 at bifurcation, Figure 2.11b. In both figures the solid curve corresponds to x_{initial} and the dotted to x_{final}. In order to study the nature of this bifurcation we shall fix ϵ_1 at some value $\epsilon_1 < 0.5$, which is

seen to be the upper limit of both curves in Figure 2.11b and corresponds to zero net flux, and simply vary θ_1. For a fixed value of ϵ_1 we may now define two critical values of θ_1, $\theta_{1_{\text{initial}}}$ and $\theta_{1_{\text{final}}}$, given by the relevant values of θ_1 from Figure 2.11b and corresponding to x_{initial} and x_{final}, respectively.

Starting from $\theta_1 = \pi/2$ we have all three sources colinear and the field is that of Section 2.4.1(ii) (see Figure 2.6a), with two distinct, closed fan surfaces. As θ_1 decreases, this field evolves as described earlier in this section, with the distinct separatrix surfaces gradually becoming more and more pressed together in the vicinity of the positive x-axis and the two null points (N_1 and N_2) approaching one another. A plot of the field topology is given in Figure 2.12a and can be seen to be very similar to that of Figure 2.10a, except that now the field is symmetric. This smooth evolution will continue until θ_1 reaches the first critical value $\theta_{1_{\text{initial}}}$, at which point a degenerate null (N) appears on the x-axis at $x = x_{\text{initial}}$. The topology at this moment of degenerate null appearance is shown in Figure 2.12b.

With a further decrease of θ_1, so that θ_1 now lies between the two curves of Figure 2.11b, i.e. $\theta_{1_{\text{final}}} < \theta_1 < \theta_{1_{\text{initial}}}$, the newly formed null bifurcates to give two nulls (N_3 and N_4) which diverge from each other along the axis of symmetry as θ_1 continues to decrease. Thus, for values of θ_1 in this range, the three-source magnetic field now contains four null points and the topological structure of this field is as shown in Figure 2.12c. The two new nulls produced along the x-axis have different orientations: the inner of the two (N_3) has its spine curve connected to each of the two symmetric sources and its fan surface in a vertical plane along the the x-axis; the outer null (N_4) has its spine in the vertical plane through the x-axis and its fan surface in the horizontal xy-plane. The fan of (N_3) extends to the spine of (N_4) whilst the fan of (N_4) extends in the $z = 0$ plane to the spines of the other three nulls (see Figures 2.12c and 2.13c).

Whilst this topological reconstruction has been taking place along the x-axis, the two original nulls (N_1 and N_2) have been gradually migrating inwards towards the positive x-axis from either side. As θ_1 continues to decrease so the migration continues and, when the second critical value is reached, $\theta_1 = \theta_{1_{\text{final}}}$, these two nulls coalesce on the x-axis, together with the outer of the two new nulls (N_4) at a point given by x_{final} of Eq.(2.60) and Figure 2.11a. With any futher decrease of θ_1 below this second critical value the field

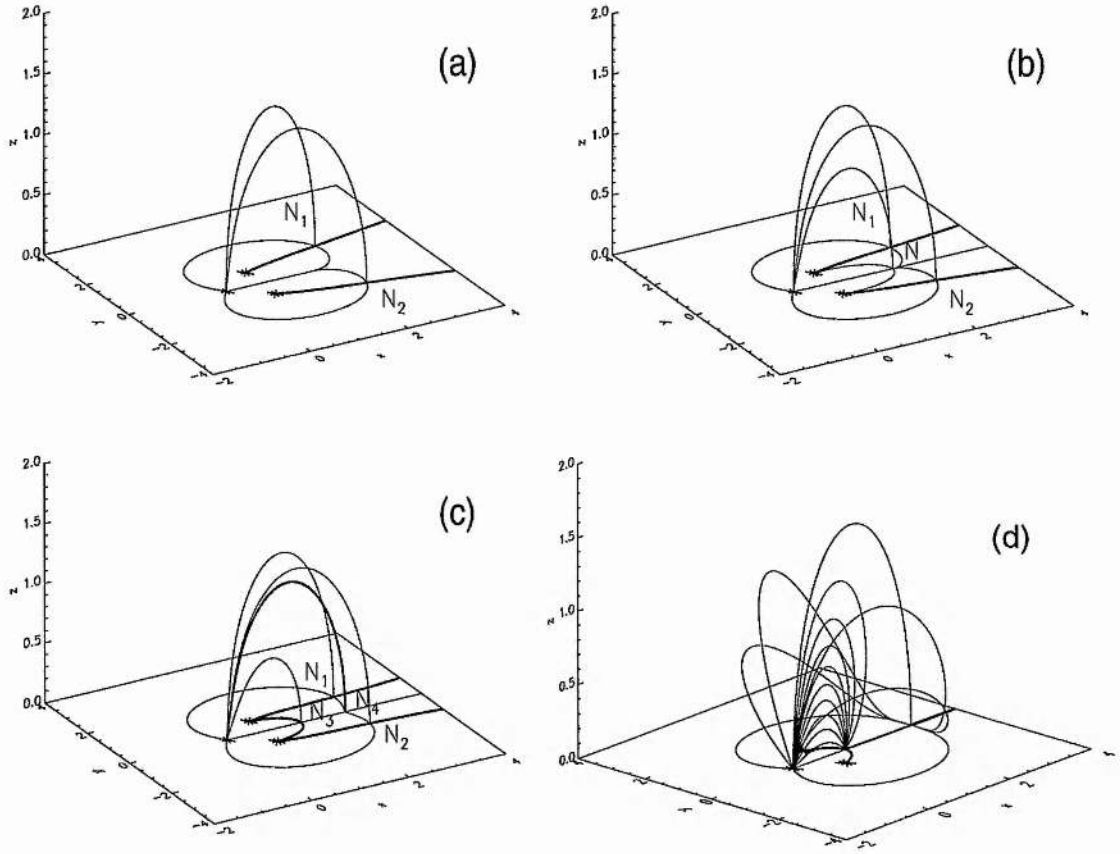

Figure 2.12: Evolution of a symmetric field with two nulls N_1 and N_2 from (a) independent fan surfaces for $\theta_1 < \theta_{1_{\text{initial}}}$, through (b), the birth of a degenerate null point N on the x-axis for $\theta_1 = \theta_{1_{\text{initial}}}$, to (c) the bifurcation of this degenerate null to give two extra nulls (N_3 and N_4) when $\theta_{1_{\text{final}}} < \theta_1 < \theta_{1\text{initial}}$. (d) Finally, after the coalesence of the three nulls (N_1, N_2 and N_4) the configuration returns to a two-null field when $\theta_1 < \theta_{1_{\text{final}}}$.

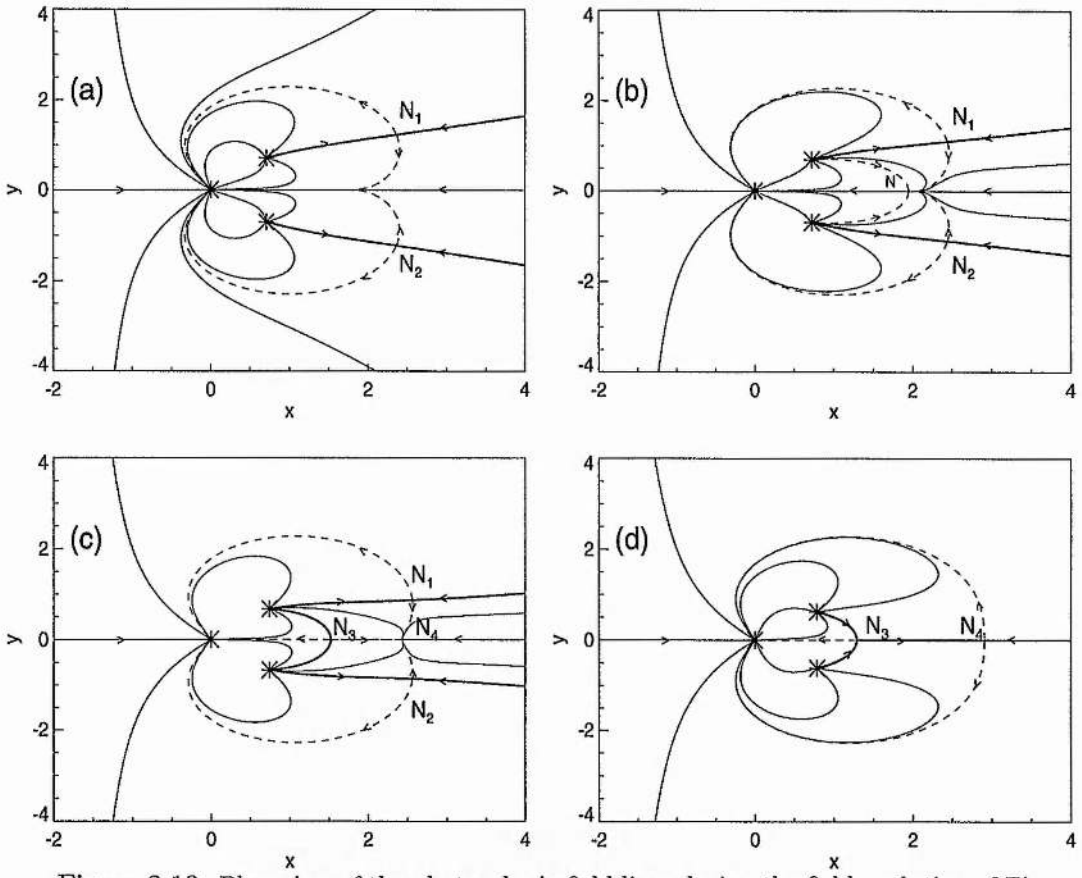

Figure 2.13: Plan view of the photospheric field lines during the field evolution of Figure 2.12. The spine curves (thick) and the separatrices (dashed) are shown to illustrate the changing topological regions.

now possesses just two magnetic null points, both lying on the symmetry axis. The final field configuration following the coalesence of the three nulls is shown in Figure 2.12d, with a selection of field lines shown in the two fan surfaces. The fan surface of the inner null still lies in a vertical plane above the x-axis, whilst that of the resulting outer null now intersects the x-axis and the photospheric plane normally and closes over to the source at the origin, much as in the case of the colinear arrangements studied in Section 2.4.1. A plan view of the photospheric field lines during the same evolution is shown in Figures 2.13a-d to illustrate more clearly the different connectivity regions present during the reconstruction of the field.

Although having no direct bearing on the overall topological skeleton of the field it is interesting to note briefly here the variation of the local field structure around the null points. For example, the null of Section 2.4.1 (Figure 2.4b) is a standard potential, radial

null, whilst the resulting outer null described above, despite still being potential of course, is clearly seen from Figure 2.12d to be an improper radial null with the major fan axis being in the vertical direction (see Parnell et al, 1995).

The above bifurcation and coalescence study was carried out by fixing the relative symmetric source strength (ϵ_1) and varying the position of the sources, θ_1. It is also possible of course to follow exactly the same field reorganisation by keeping the sources fixed and simply varying the strength. The range of parameters for which the field contains four null points corresponds for both scenarios to the region between the two curves of Figure 2.11b. Also, whilst the above study looked at a symmetric field arrangement, the same topological changes may still be found if a small degree of asymmetry is introduced (e.g. by having ϵ_1 slightly larger than ϵ_2 or $|\theta_1|$ slightly larger than $|\theta_2|$ etc.). The symmetric case, however, gives the optimal configuration for this field restructuring, having the largest parameter range for which the four null points are present. If the asymmetry becomes too large then the bifurcation and coalescence described above does not occur and the field merely evolves from independent to nested fan surfaces as described in Section 2.4.2(i). Finally, in the case of balanced flux we have $\epsilon_1 = \epsilon_2 = 0.5$ for the symmetric field, and from Figure 2.11b, bifurcation and coalescence occur at the same moment for $\theta_1 = \frac{\pi}{2}$. This is now seen from Figure 2.11a to take place at an infinite distance from the sources.

2.5 Balanced Four-Source Fields

Let us now go on to study the topological structure of coronal fields generated by four magnetic flux concentrations. In general, the variety of possible source arrangements in this case is rather large and an exhaustive study of all possible configurations does not seem worthwhile. Thus in this section we shall restrict ourselves to studying just a few specific source arrangements which are of particular interest. We shall first make the assumption that the total flux is balanced, i.e. zero net flux, and then go on to study two specific source arrangements.

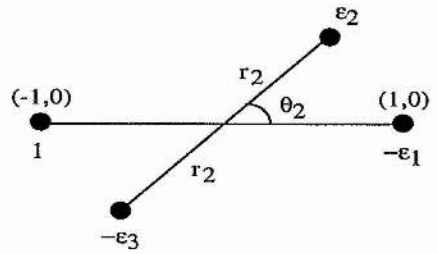

Figure 2.14: General centro-symmetric four-source arrangement considered in this section.

2.5.1 Emerging Flux Break-Out

In addition to the flux balance assumption let us now also assume a centro-symmetric source arrangement, centred on the origin. Thus we shall position the opposite polarity source pair, $\epsilon_0(=1)$ and $-\epsilon_1$, on the x-axis at $x = -1$ and $x = 1$, respectively, with the remaining opposite polarity pair, ϵ_2 and $-\epsilon_3$, at positions $(r_2\,, \theta_2)$, $(r_2\,, \theta_2 + \pi)$, respectively, where $0 < r < 1$ (see Figure 2.14).

The condition for flux balance in this case is simply

$$1 - \epsilon_1 + \epsilon_2 - \epsilon_3 = 0, \tag{2.61}$$

and this particular configuration is of general interest in the modelling of solar coronal magnetic fields and has been studied previously by several authors (e.g. Baum & Bratenthal 1980, Gorbachev & Somov 1988). The two external sources, ϵ_0 and $-\epsilon_1$, along the x-axis may represent an existing bipolar region of the coronal field and by allowing the internal sources, ϵ_2 and $-\epsilon_3$, to increase in strength this arrangement may be useful in modelling the emergence of a new bipolar region into an overlying field.

An emerging bipolar flux scenario is widely accepted as an integral part of the dynamic evolution of photospheric active regions and has been observed for many years (e.g. Zirin 1972). Moreover, this form of field evolution may be of particular interest in the future study of prominence formation, with recent observations suggesting the formation of many coronal structures may be due to newly emerging flux interacting with an overlying field, in contrast to previously considered models involving the shearing and twisting of the existing field.

For the sake of simplicity let us study the further special case of centro-symmetric

source strengths as well as positions. Thus we shall set $\epsilon_1 = -\epsilon_0 = -1$ and $\epsilon_3 = -\epsilon_2$. Now let us consider initially the case $\theta = 0$, so that all four sources are colinear along the x-axis with alternating polarity. This case is therefore equivalent to an internal bipolar region emerging antiparallel to an existing one. The magnetic field along the x-axis, in the central region between the internal sources is simply given by

$$B_r = \frac{1}{(r+1)^2} + \frac{1}{(r-1)^2} - \frac{\epsilon_2}{(r+r_2)^2} - \frac{\epsilon_2}{(r-r_2)^2},$$

and hence any nulls along this region of the x-axis are located at the roots of

$$r^6(1-\epsilon_2) + r^4(1-2r_2^2-\epsilon_2 r_2^2+2\epsilon_2) + r^2(r_2^4-2r_2^2-\epsilon_2+2\epsilon_2 r_2^2) + r_2^2(r_2^2-\epsilon_2) = 0. \quad (2.62)$$

This cubic in r^2 will have one real root, corresponding to two nulls symmetrically located either side of the origin. Clearly, when $\epsilon_2 = 0$ the field is just that of the external bipole and contains no separatrix surfaces. With an increase of ϵ_2 from zero, however, the two nulls described above will appear and their fan surfaces now divide the coronal volume into three regions of distinct connectivity . A cross-sectional view of this field configuration is shown in Figure 2.15a.

With increasing ϵ_2, i.e. a growing in strength of the internal bipole, the two nulls migrate inwards along the x-axis, meeting at the origin when $\epsilon_2 = r_2^2$. By studying the third eigenvector, $\lambda_3 = \partial B_z/\partial z$ of the localised null point field, as in Section 2.4.1(ii), it can be shown that $\partial B_z/\partial z \equiv 0$ for $r = 0$, and thus the nulls coalesce at the origin as shown in Figure 2.15b. Just as described for the colinear three source field of Section 2.4.1(ii), a null line is formed and arches out of the photospheric plane into the coronal field as ϵ_2 increases beyond the critical value of $\epsilon_2 = r_2^2$. With the birth of this null line the coronal volume is now split into four distinct regions of field line connectivity rather than the previous three, with the null line being at the intersection of all four regions. A cross-sectional view of this field for $\epsilon_2 > r_2^2$ is shown in Figure 2.15c.

The null line which is born at this coalesence will form a semi-circular arc normal to the x-axis whose maximum height we may determine. In terms of the vertical height (z) the field in the x-direction, evaluated on the z-axis, is given by

$$B_x(0,\,0,\,z) = \frac{2}{(1+z^2)^{\frac{3}{2}}} - \frac{2\epsilon_2 r_2}{(r_2^2+z^2)^{\frac{3}{2}}},$$

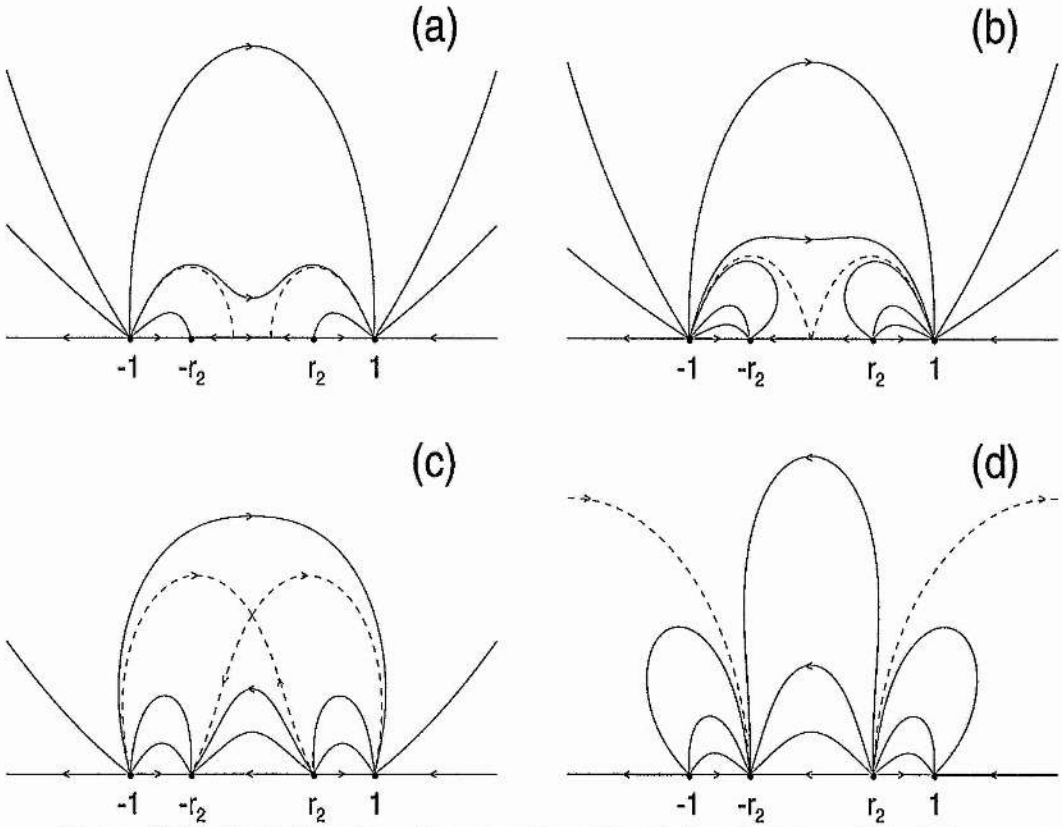

Figure 2.15: Evolution of a colinear, antiparallel field as the internal bipole increases in strength. (a) Initially there are two distinct nulls, together with their fan surfaces, which then (b) coalesce at the origin, and (c) form a null line. (d) Following the rise of the null line the internal flux erupts through the external field forming two new, distinct nulls exterior to the active region.

and so the height of the null point on the z-axis is simply

$$z = \left[\frac{(\epsilon_2 r_2)^{\frac{2}{3}} - r_2^2}{1 - (\epsilon_2 r_2)^{\frac{2}{3}}}\right]^{\frac{1}{2}}. \tag{2.63}$$

We see from Eq.(2.63) that $\epsilon_2 = r_2^2$ is the critical value for formation of the null line and as ϵ_2 increases so the height of this null line will increase. We may also see from Eq.(2.63) that as $\epsilon_2 \to 1/r_2$, the height of the null line will approach infinity. A plot of the rise of the null line with internal bipole strength is given by the solid curve of Figure 2.16a.

It can be seen from this curve that following a quick rise in its initial stages the upward velocity of the null line steadies slightly before accelerating rapidly to infinity as the internal bipole strength continues to increase. This rapid asymptotic rise of the null line signifies the emerging bipolar field 'breaking through' the overlying coronal field at

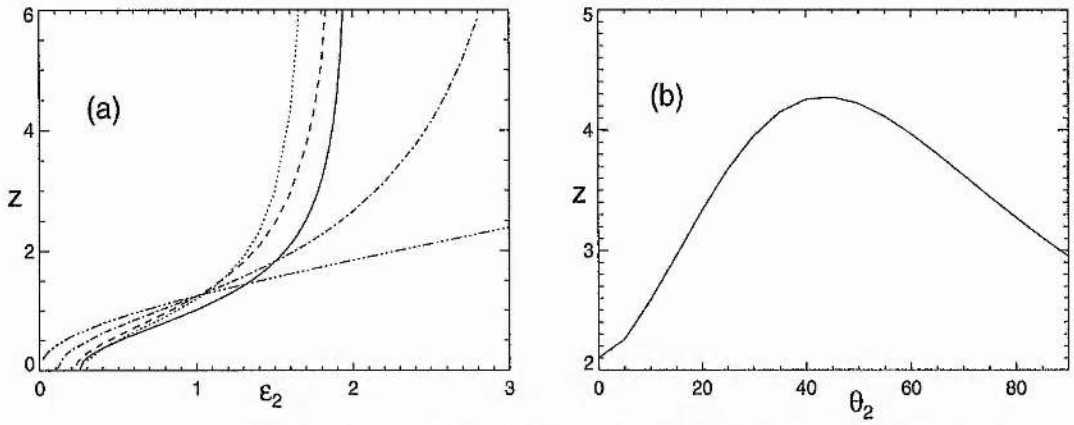

Figure 2.16: (a) The rise with internal bipole strength of the null line (solid curve) and separator field lines (dotted, dashed, dot-dashed and dot-dot-dot-dashed curves) for values of $\theta_2 = 0$, $\pi/4$, $\pi/2$, $3\pi/4$, and π, respectively. (b) Height of the separator against internal angle, θ_2, for a fixed value of $\epsilon_2 = 1.6$, showing a maximum separator height at an angle of $\theta_2 \simeq \pi/4$.

this critical limit. Following this breakthrough of the internal field, two nulls appear along the outer regions of the x-axis (i.e. on $x < -1$ and $x > 1$) and their fan surfaces close over the external sources leaving the coronal volume once again with just three regions of magnetic connectivity. The final state is shown in cross-section in Figure 2.15d.

The case considered above is a special case with the internal bipole emerging anti-parallel to the existing field. Let us, therefore, now study a similar evolution with the internal bipole emerging at some arbitrary angle, θ_2, to the x-axis. With the sources now non-colinear we no longer have null points of the magnetic field located on the x-axis, and although the field will still contain two null points in the photospheric plane it is no longer possible to find their locations analytically. We may still, however, follow the evolution of the field numerically, and we find that this evolution is very similar to that of the colinear case above ($\theta_2 = 0$).

Initially, for small ϵ_2, the coronal field is divided into three distinct connectivity regions by the independent fan surfaces of the two photospheric nulls, which close over the individual flux concentrations of the emerging field. As ϵ_2 increases, these fan surfaces expand and for a critical value of ϵ_2, which will depend on θ_2, they will meet at the origin in this centro-symmetric case. The moment of meeting of the independent fan surfaces is equivalent to the moment of null coalescence in the previous colinear case, except that it

is the fan surfaces alone which meet rather than the nulls themselves.

Any further increase of ϵ_2 sees the formation of a *separator* field line which arches out of the photospheric plane and connects the two null points. This separator field line lies in both fan surfaces and represents their mutual intersection. It is the equivalent of the null line in the colinear case. Also, with the birth of this separator, the coronal volume is now split into four topologically distinct regions rather than just three. The separator lies at the intersection of all four regions and for this reason is often regarded as a favoured site for coronal reconnection.

It is maybe worth noting here a fundamental difference between this evolution and that of the three source field of Section 2.4.2(i). For the four source case the distinct separatrix surfaces physically intersect one another in the separator field line, and the topological structure of the field is altered. In the case of the three source field, however, the separatrix surfaces, despite becoming pressed very close together, never intersect one another, except at the moment of nesting, at which point the spine curve of one null lies in the fan surface of the other.

As the internal bipole strength increases beyond the birth of the separator we may follow the separator height just as for the null line in the colinear case. This separator rise is plotted alongside the null line rise in figure 2.16a for various angles of θ_2. It can be seen from these curves that, just as in the colinear case, $\theta_2 = 0$, given by the solid curve, the rise becomes very rapid as ϵ_2 approaches some asymptotic limit. This limit again corresponds to the flux of the emerging bipolar region bursting through the existing coronal field.

The separator rise is shown in Figure 2.16a for angles of $\theta_2 = \pi/4$, $\pi/2$, $3\pi/4$, and π, and it can be seen that for the angles $\theta_2 = \pi/4$ (dotted) and $\pi/2$ (dashed), the asymptotic rise of the separator occurs for a smaller value of ϵ_2 than the anti-parallel, colinear case $\theta_2 = 0$. Also shown, in Figure 2.16b, is a plot of separator height against internal bipole angle, θ_2, for a fixed value of $\epsilon_2 = 1.6$. This shows that an internal bipole angle of $\theta_2 \simeq \pi/4$ leads to a maximum height of the separator and we may expect that the emerging bipolar flux breaks through the overlying coronal field with greatest ease for this value of the internal angle.

Following the breakthrough of the newly emerged flux the coronal field is again re-

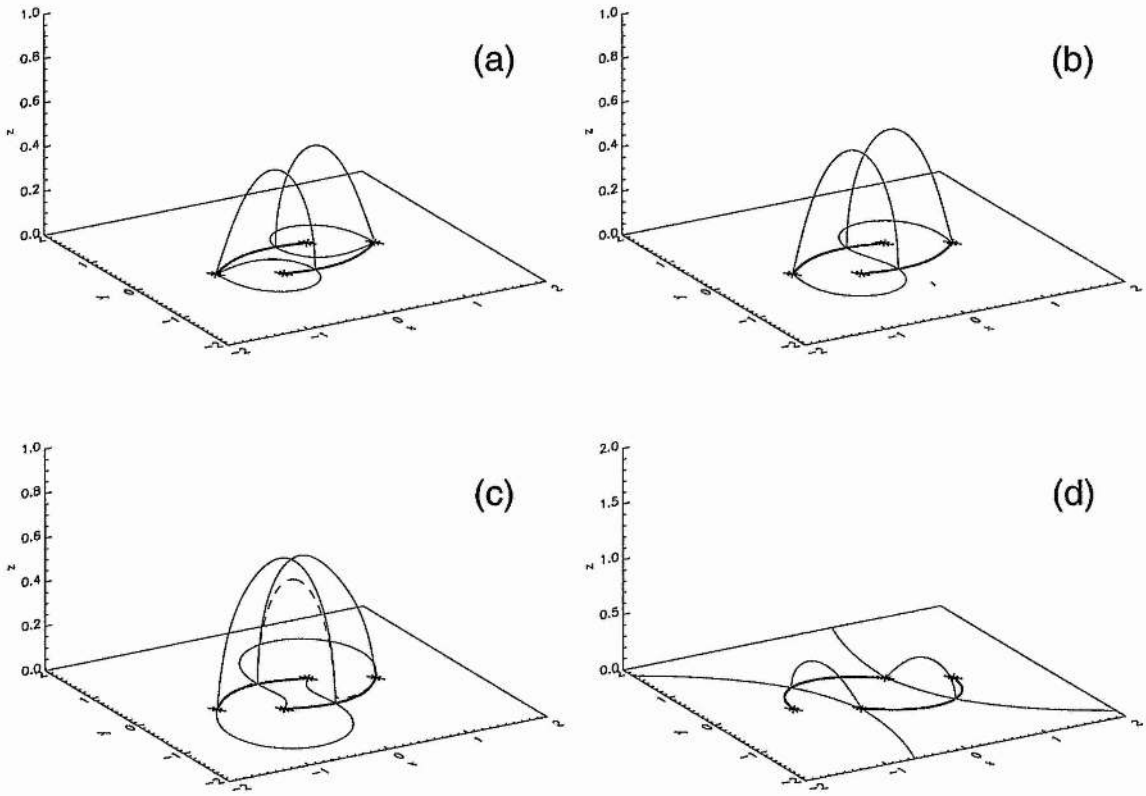

Figure 2.17: General flux break-out of an emerging bipolar region. (a) The independent fan surfaces grow and (b) meet in the photospheric plane. (c) A separator field line (dashed) rises as the internal bipole strength increases until (d) the internal field breaks through the existing field and the outer sources are no longer connected to one another.

turned to three distinct connectivity regions, with the fan surfaces of the two nulls no longer intersecting one another and now closing over the external sources. This general evolution pattern is displayed in Figure 2.17a-d. Starting from an initially weak bipolar field producing producing two distinct separatrix surfaces in (a), and progressing through the meeting of the surfaces in (b), the rise of the separator, (c), and the resultant field following the breakthrough of the internal flux in (d). In all cases the spine curve of each null is seen to connect to the like polarity sources of the internal and external flux regions, with the fan surfaces initially closing over the internal sources and finally closing over the outer. A plan view of the same evolution is also shown in Figure 2.18a-d, showing the spine curves and photospheric fan field lines. A few further photospheric field lines are also shown to highlight the differing connectivity regions.

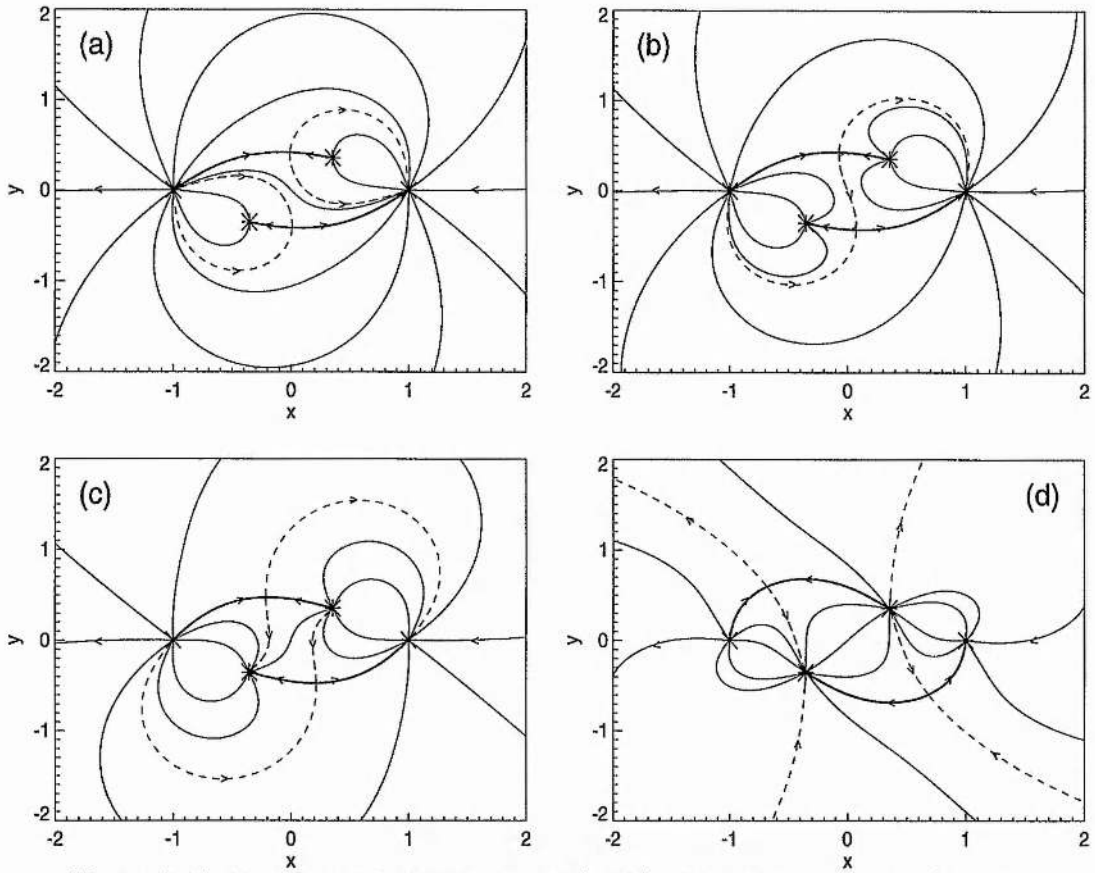

Figure 2.18: The photospheric spine curves (thick) and separatrices (dashed) are shown in plan view during the emerging flux break-out of Figure 2.17 to illustrate the changing connectivity.

The solid curve in Figure 2.16a, corresponding to the rise height of the null line in the anti-parallel case $\theta_2 = 0$, is very similar to that of Syrovatskii (1982) who studied a similar evolution of an internal dipolar region emerging inside an existing bipolar field, generated by finite size sources. The rapid rise of the resulting null line, and the reconnection between the emerging and existing fields that is assumed to take place at its location, maybe related to rapidly rising loops that are observed with energy sources at their summits. We have shown here, by the curves of Figure 2.16a, that this general scenario of accelerated flux breakthrough is not just limited to the colinear case. Indeed, the process is enhanced for non-colinear sources, with the optimal internal angle being $\theta_2 \simeq \pi/4$.

The one anomaly of Figure 2.16a is the curve corresponding to $\theta_2 = \pi$. In this case the internal flux emerges parallel to the existing field. It is found for this configuration

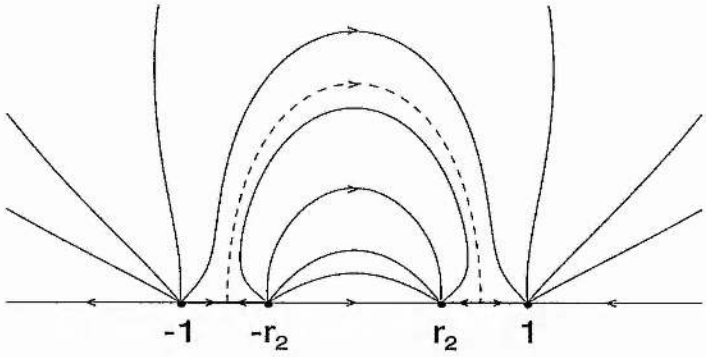

Figure 2.19: Cross-sectional view of the parallel internal field topology, with the emerging flux confined beneath a common fan surface.

that the two nulls, lying along the x-axis, share the same fan surface, and the coronal volume is thus divided into just two distinct regions. The emerging flux can never break through the overlying field in this case, remaining confined beneath it for all values of ϵ_2, and the rise of the common fan surface is seen from Figure 2.16a to be steady. A general cross-sectional view of this field topology is shown in Figure 2.19.

2.5.2 Separating Flux Break-Up

In this section we shall briefly examine one further four-source configuration in an attempt to model a specific form of magnetic evolution. Zhang (1994) has studied a feature termed " Incorporation of magnetic flux of the same polarity " in which two distinct concentrations of flux, having the same polarity split through an intervening region of opposing polarity and merge together. A correlation is reported between major X-ray flares and sites of this magnetic incorporation with a sufficiently strong field. This form of magnetic incorporation is briefly modelled as the break-up of the separating flux, using four magnetic sources. For simplicity we shall retain in this model our basic assumption of flux balance, together with a centro-symmetric source positioning (see Figure 2.20).

In order to model the break-up of the separating flux we shall start with the sources ϵ_2 and ϵ_3 both located at the origin. i.e. $r_2 = 0$. Thus we initially have a colinear, balanced, three-source configuration with alternating polarity (see Sections 2.4.1(ii) and 2.4.1(iii)). We shall then move the central sources, ϵ_2 and ϵ_3, apart along the y-axis, in order to represent the splitting of the intervening flux, and study the change in field structure as

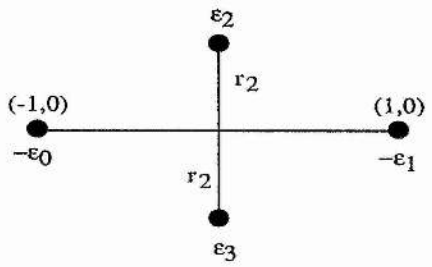

Figure 2.20: General centro-symmetric source positioning for the separating flux break-up model.

r_2 increases (see Figure 2.20).

For simplicity let us assume that the central flux splits equally, i.e. set $\epsilon_2 = \epsilon_3 = 1$. Flux balance is now simply given by $\epsilon_0 + \epsilon_1 = 2$, and any magnetic null points must lie on the x-axis corresponding to the real roots of

$$B_x = \frac{-\epsilon_0}{(r+1)^2} - \frac{\epsilon_1}{(r-1)^2} + \frac{2r}{(r^2+r_2^2)^{\frac{3}{2}}} = 0\,. \tag{2.64}$$

In general there will be two nulls, one lying in the central region, close to the origin, and the other lying in either $r < -1$ or $r > 1$, depending on whether $\epsilon_1 > \epsilon_0$ or $\epsilon_1 < \epsilon_0$, respectively. If we look for degeneracy of the nulls by studying $\lambda_3 \equiv \partial B_z/\partial z = 0$ we also require

$$\frac{-\epsilon_0}{(r+1)^3} - \frac{\epsilon_1}{(r-1)^3} + \frac{2}{(r^2+r_2^2)^{\frac{3}{2}}} = 0, \tag{2.65}$$

and, by eliminating r_2 between Eqs.(2.64) and (2.65) together with the flux balance condition, we obtain

$$r^3 - 3r^2\left(\frac{\epsilon_0 - \epsilon_1}{2}\right) + 3r - \left(\frac{\epsilon_0 - \epsilon_1}{2}\right) = 0. \tag{2.66}$$

The one real root of this cubic in r will give the position of the null, located near the origin, at the point of degeneracy. This point is found to be

$$r = \frac{1}{2}(\epsilon_0 - \epsilon_1) + (-\epsilon_0\epsilon_1)^{\frac{1}{3}}\left[(-\epsilon_0)^{\frac{1}{3}} + (\epsilon_1)^{\frac{1}{3}}\right], \tag{2.67}$$

and by substituting this into Eq.(2.65) the value of r_2 required for the null to become degenerate is given by

$$r_{2_d} = \left[\left(\frac{2(r^2-1)^3}{\epsilon_0(r-1)^3 - \epsilon_1(r+1)^3}\right)^{\frac{2}{3}} - r^2\right]^{\frac{1}{2}}. \tag{2.68}$$

Just as has already been seen in the previous sections, this moment of null-point degeneracy will correspond to the moment of major topological field reconstruction.

If we now look initially at the simplest case of a purely symmetric field, by setting $\epsilon_0 = \epsilon_1 = 1$, we find from Eqs.(2.67) and (2.68) just one null point, situated at the origin, and becoming degenerate for $r_{2_d} = 1$. Thus, as may be expected for this symmetric case, the topological features of the field change when the central sources (ϵ_2 and ϵ_3) become further from the origin than the fixed pair (ϵ_0 and ϵ_1). The evolution is shown in Figure 2.21(a-f), with Figures (a), (c) and (e) giving a general view of the field together with the photospheric polarity inversion line (IL) and (b), (d) and (f) showing field lines in the xz-plane only.

We see from the IL in Figure 2.21a, shown as a dashed curve, that the sources ϵ_0 and ϵ_1 are initially separated by the central flux, and the null at the origin is of positive type (Priest & Titov 1995) with its fan surface in the xz-plane. As r_2 increases, the null point becomes more and more improper (see Parnell et al 1995) and the fan surface closes up along the z-axis until, at the moment of degeneracy ($r_2 = r_{2_d} = 1$) the IL is seen to meet at the origin (Figures 2.21c and d). The fan surface has now completely closed up onto the z-axis and a vertical null line is formed. In plan view this field would just have the structure of an X-type neutral point with separatrix field lines lying along the x- and y-axes.

With continuing outward motion of the sources ϵ_2 and ϵ_3 the IL is seen to change orientation (Figure 2.21e) with the moving sources now separated by the flux from the stationary pair. The null line then vanishes and the fan surface of an improper null appears once again. The null point has, however, changed from positive to negative type and the fan surface now lies in the yz-plane rather than the xz-plane. With the null line formation and subsequent change in separatrix surface orientation occurring at the same moment as the change in connectivity of the IL, this structural change is identified as the moment of break-up of the separating flux.

A similar evolution is also found if we remove the symmetry along the x-axis. For example, Figures 2.22a-f show the evolution of a similar field, but with $\epsilon_0 = 1.5$ and $\epsilon_1 = 0.5$ giving an asymmetry in the fixed source strengths. We now find two nulls on the x-axis, given by the roots of Eq.(2.64), and for a value of $r_2 < r_{2_d}$ the general topology

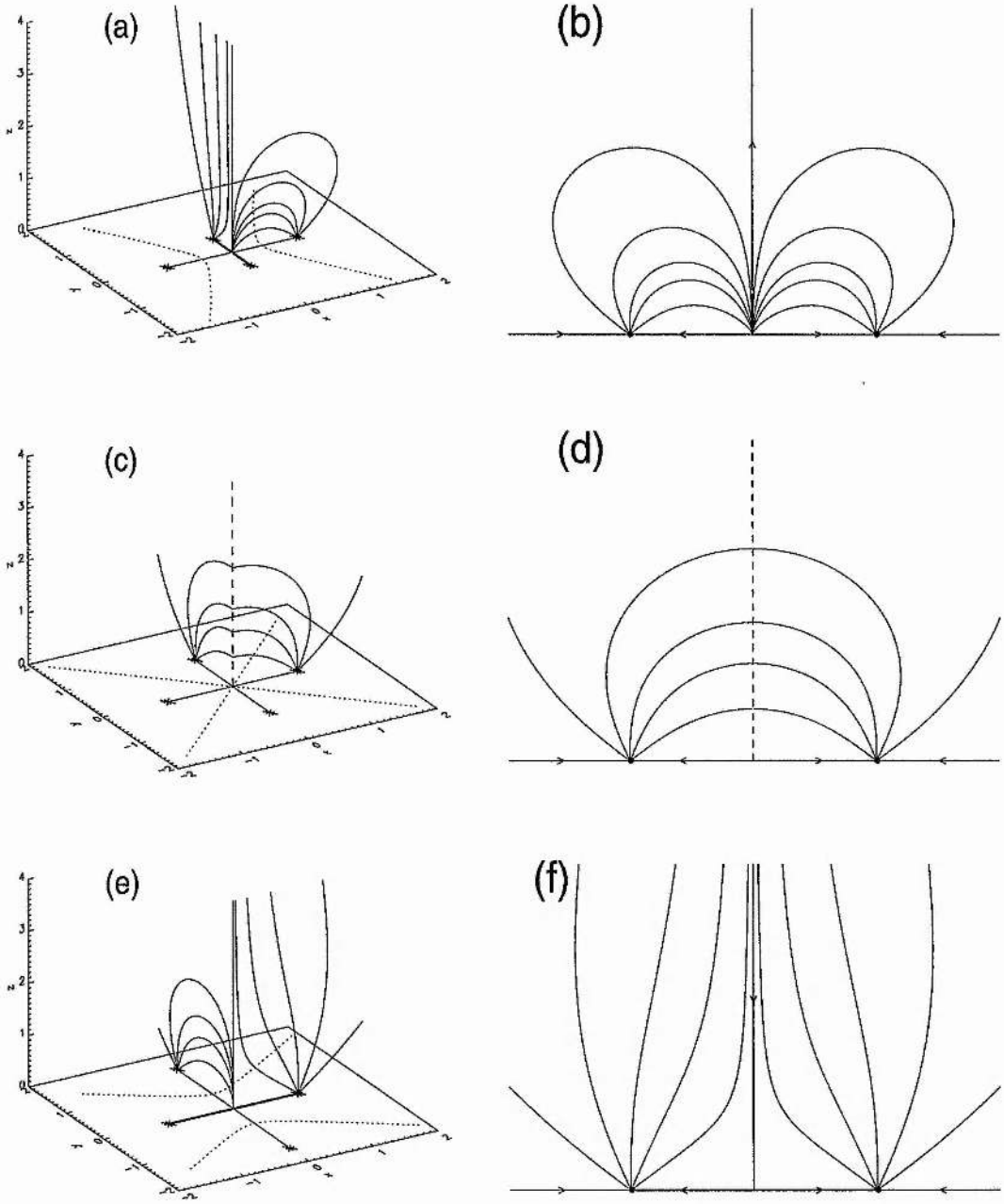

Figure 2.21: Break-up of separating flux in a purely symmetric field. (a) and (b) A null of positive type with a fan in the xz-plane evolves into a null line, (c) and (d), along the z-axis when $r_2 = r_{2_d}$. This null line collapses (e) and (f) to form a negative null at the origin with a fan in the yz-plane as the break-up of the separating flux occurs. In (a), (c) and (e) field lines are only drawn along the positive portions of the x- and y-axes for clarity.

is shown in Figure 2.22a and b. The central null is seen to have a fan surface in the xz-plane, with the fan surface of the outer null being normal to the x-axis and closing over the weaker source, ϵ_1. Thus the two fan surfaces intersect in a common field line, or separator, which connects the two null points and is shown as the dashed curve in Figure 2.22b. The sources ϵ_0 and ϵ_1 are again seen from the IL to be initially separated by the central flux.

As r_2 increases towards the critical value r_{2_d}, given by Eq.(2.68), the fan surfaces are seen to close up along the separator field line as the nulls become more and more improper in nature. The field just prior to degeneracy is shown in Figure 2.22c and d to demonstrate this improper nature of the nulls, and although only field lines in the fan surface of the internal null are shown in these figures, a similar behaviour is simultaneously exhibited at the outer null. When r_2 reaches the critical value ($r_2 = r_{2_d}$) the field vanishes all along the separator and hence it becomes a null line. This is just as for the previous symmetric case, although now the null line is of finite length, beginning and ending at the photospheric plane.

Once again, at this moment of degeneracy of the internal null, the IL changes form and the sources ϵ_2 and ϵ_3 now become separated as the break-up takes place. Figures 2.22e and f show the resulting field following the break-up. Just as found in the symmetric case, the nulls have changed both their type and their orientation. The internal null has evolved from positive to negative type, with its fan surface switching from the xz-plane to being normal to the x-axis, and vice versa for the outer null.

Throughout this evolution the coronal volume has remained split into four connectivity regions by the two intersecting fan surfaces, with the separator lying at the intersection of these four regions. The changing of nulls leads to a reversal of the magnetic field direction along the separator as the break-up of the separating flux takes place. The flares found by Zhang (1994), and related to incorporating magnetic fields, appear to be located at the centre of the flux break-up site. It is therefore possible that magnetic reconnection occurring in the region of the separator field line during this separating flux break-up will provide the required flare energy.

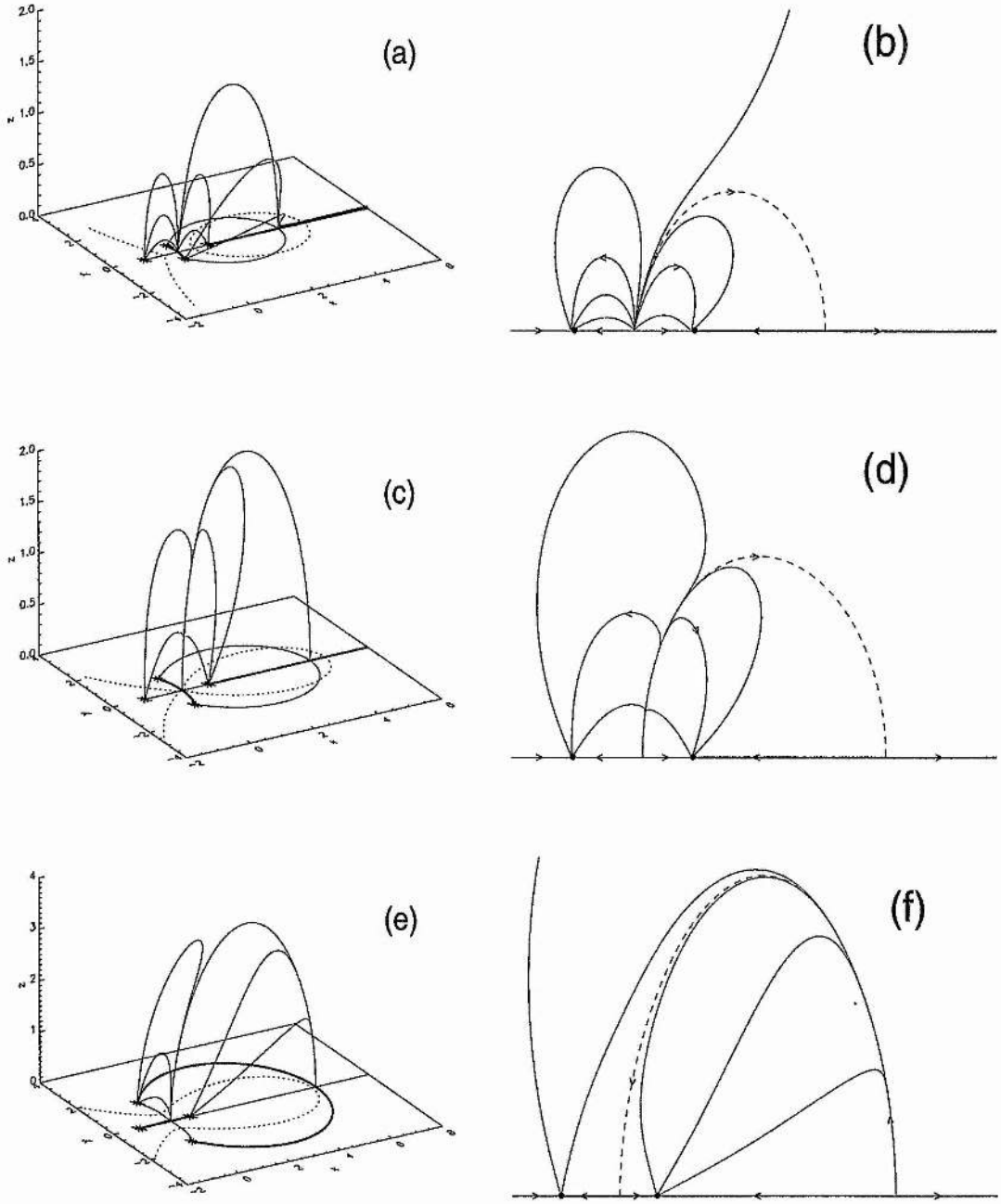

Figure 2.22: Break-up of the separating flux in an asymmetric field. (a) and (b) A positive central null is connected to a negative outer null by a separator field line (dashed in (b)). The fan surfaces close up along the separator , (c) and (d), as r_2 approaches r_{2_d} and after a becoming a null line in the limit $r_2 = r_{2_d}$ the field along the separator reverses as the break-up takes place and the nulls switch type, (e) and (f).

2.6 Summary and Discussion

The magnetic field of the solar corona has as its sources many discrete magnetic flux elements of high intensity in the photosphere, clustering especially around the edges of supergranule cells. These sources are continually moving and causing the coronal field to evolve slowly through a series of highly complex equilibria. The skeleton of this coronal field consists of three-dimensional null points and a network of spine curves and separatrix fan surfaces, which are the most important features for understanding the topology of the complex field. In this chapter we have studied the skeletons that are produced by two, three and four flux sources with a view to uncovering some of the general properties and building blocks of a complex three-dimensional field generated by magnetic sources.

For two unbalanced sources, the skeleton consists simply of a null point, a spine curve (which starts at the weaker source, passes through the null and ends at infinity), and a separatrix fan surface which passes through the stronger source and the null point and separates the coronal volume into two regions of distinct magnetic connectivity.

The overall behaviour of the three-source fields is more involved. Whether the source arrangement is linear or not, the general skeleton of the magnetic field generated by the three flux concentrations usually consists of two null points and two distinct fan surfaces. These fan surfaces may be either independent or nested (one inside the other) depending on the relative source strengths and positions. In following the evolution of the field due to the varying of either the strengths or positions of the sources, the field will generally restructure itself smoothly from an independent to a nested configuration, or vice-versa. During this, the fan surfaces remain distinct although they may become increasingly pressed together during the evolution. In the course of switching from independent to nested surfaces the spine of one null intersects the fan of the other and thus directly connects the two nulls by a field line in the photospheric plane. Throughout this evolution the coronal volume remains split into three regions of distinct connectivity.

There are just two exceptions to this basic picture and in these cases the field undergoes a more drastic restructuring. The first occurs in the special case of colinear sources (Section 2.4.1(ii)). When the relative source strengths reach a critical ratio, given by Eqs.(2.46) and (2.47) and Figure 2.8, the two colinear null points coalesce and form a neutral line which arcs out of the photospheric plane. The spine curves of the infinite

number of adjacent null points making up the null line now also form a magnetic surface, and in this instance the coronal field is separated into four distinct regions of magnetic connectivity.

The second exception (Section 2.4.2(ii)) arises when the non-colinear field configuration is symmetric (or almost symmetric) about one axis. In this instance the restructuring of a field with initially independent fan surfaces proceeds via the formation of two new nulls along the symmetry axis. Thus the field briefly contains four null points, three of which then coalesce to leave the field with again just two nulls. Both the new nulls formed in this evolution lie in the photospheric plane, however, and whilst the coronal field takes on an interesting structure during this transition the volume remains split into just three distinct connectivity regions.

For a field generated by four magnetic flux sources the range of possible configurations is great and we have considered only two particular cases in this work. We have seen, however, that the evolution of the field may be very different from that of the two and three-source fields. We find distinct separatrix fan surfaces intersecting each other in separator field lines and changing the connectivity of the coronal volume. This is in contrast to the three-source field evolution described above where the separatrix surfaces merely press together and do not intersect each other. We have also shown here how an internal emerging bipolar flux region can rapidly break through the overlying coronal field, with an optimal internal angle of approximately $\theta_2 = \pi/4$. Furthermore, we have seen how the evolution of the basic topological structures described here may be used to model in a simple way the break-up of a flux region which separates fluxes of like polarity.

Several features of these flux systems need to be studied further in future work. In general non-potential flux systems contain magnetic helicity, both internal (twist) helicity and mutual (braiding) helicity, which is conserved to a high degree of approximation during the magnetic reconnection process. It would be intersesting, therefore, to set up similar complex force-free equilibria and understand how they evolve whilst conserving their global helicity.

Another issue is the nature of three-dimensional reconnection. A general framework for such reconnection has been set up by Schindler et al (1988) and two particular types have been studied in detail. In the first there are no null points and the topology is simple,

with reconnection occurring in quasi-separatrix layers where the field line mapping has large gradients (Priest & Démoulin 1995). In the second case, three different ways of reconnection occurring at null points have been identified, namely spine reconnection, fan reconnection and separator reconnection, where the current concentration and field line slippage are focused along the spine, the fan and the separator, respectively (Priest & Titov 1995). However, the analysis of reconnection at null points has so far mainly focused on the relatively local behaviour near the null point, and we may ask what are the consequences for the global topological structures discussed here?

For two unbalanced sources or three balanced sources the amount of flux contained by each separatrix is constant, independent of the source positions. Thus magnetic reconnection would involve the change of connectivity of particular field lines but with no net transfer of flux across the separatrices. By comparison, for three unbalanced sources or four or more balanced sources, the types of topology are more diverse and the flux bounded by the separatrices can change as the sources move. It may be interesting to explore such processes in more detail in future.

Chapter 3

Basic Topological Elements of Coronal Magnetic Fields

3.1 Introduction

In the previous chapter we have studied the varying topologies of fields produced by combinations of 2, 3, and 4 point sources of magnetic flux, which we have used to model the concentrated regions of flux seen at the photospheric surface. The coronal volume above the planar surface is divided into regions of distinct magnetic connectivity by the fan surfaces associated with the null points produced by these fields, and these nulls all lie in the source plane. The concentrations of flux observed at the solar surface will naturally, however, have a finite area and thus their modelling by point sources located at the surface will not give realistic surface flux contours.

A more realistic photospheric flux contour map may be generated by moving the sources a small but finite distance below the plane. This approach has been used, with a good deal of success, by several authors in attempts to model observed photospheric flux contours (e.g. Démoulin et al 1992 and 1994, Mandrini et al 1991). As in the previous chapter, we are interested in establishing the field topology since it is topological differences in the field which are likely to be a key factor in determining the behaviour of the corona in response to plasma motions and instabilities (Berger 1991). With the introduction of sub-photospheric sources, the vertical component of the field no longer automatically vanishes on the photospheric plane, and this introduces a new class of field

lines which would appear to be of very general significance. This new class involves coronal field lines which tangentially graze the much denser photospheric surface before returning upwards into the corona. This usually occurs at segments of the polarity inversion line (IL), and the importance of these segments for a topological analysis of coronal magnetic fields was first recognised by Seehafer (1986).

We shall call such segments 'Bald Patches' (BP's) following the notation of Titov et al (1993). The field lines passing through a BP form a separatrix surface, which separates the coronal field into regions of differing magnetic connectivity (see Figure 3.1b). It has been shown that, in the vicinity of a BP, shearing motions of the footpoints of a magnetic field, anchored at the photosphere, will cause the necessary formation of a current sheet along the associated separatrix surface (Low 1992, Low & Wolfson 1988, Wolfson 1989, Vekstein & Priest 1992, Billinghurst et al 1993). Thus the separatrix surfaces associated with BP's are possible sites for magnetic reconnection and the release of stored magnetic energy in the corona, just as were the null point separatrix fan surfaces of the previous chapter. It seems worthwhile, therefore, to determine the conditions under which a gradual evolution of equilibrium magnetic configurations in the corona leads to the appearance of BP's. The first study of this kind was made by Titov et al (1993) where they derived a general local criterion for the existence of BP's in a given magnetic configuration. Also they found that a BP appears at the central location of both potential and force-free fields, generated by a centro-symmetric arrangement of four sub-photospheric magnetic sources, and it exists over a wide range of parameters. In this chapter we shall see that BP's exist for a wide range of conditions in even simpler configurations than those previously studied by Titov et al (1993).

We shall also deal in this chapter with the concept of a 'separator', as already described in Chapter 2.5.1. Over recent years several studies have been made by various authors into likely sites for coronal reconnection based on this concept (e.g. Baum & Bratentahl 1980, Gorbachev & Somov 1988, Lau & Finn 1990, Mandrini et al 1991). A separator is defined as a field line representing the intersection of two distinct separatrix surfaces and is assumed to be a favourable site for current sheet formation in response to changes of boundary conditions. The separatrix surfaces intersecting at the separator separate the corona into regions of differing field line connectivity, and this serves as a characteristic

property of the separator distinguishing it from the other field lines. When modelling the coronal field with a number of discrete sources of magnetic flux placed below the photospheric boundary, however, the connectivity of the field has been determined in previous works by the discrete magnetic sources at either end of a given field line. So, locating the separatrix surfaces and hence the separator has required the tracing of coronal field lines back to their sub-photospheric sources. This sub-photospheric extrapolation is, however, not strictly valid since the force-free assumptions made about the coronal field will no longer hold in the much denser photosphere. These circumstances indicate that such an approach to determining the separator and separatrix surfaces is not self-consistent.

We shall show in this chapter that there is no need to search for a jump in magnetic connectivity (as in, say, Démoulin et al 1992) in order to find which field line belongs to a separatrix surface. The effect of such a jump is purely local and in general is completely determined by the presence of magnetic nulls in the configuration and BP's on the polarity inversion line (IL).

3.2 Basic Elements of Separatrix Surfaces in Magnetic Configurations

Any magnetic field line for a given field $\mathbf{B}(\mathbf{r})$ can be represented by a solution of the following system of ordinary differential equations:

$$\frac{d\mathbf{r}}{ds} = \frac{\mathbf{B}(\mathbf{r})}{|\mathbf{B}(\mathbf{r})|}, \tag{3.1}$$

where s is a natural parameter or the length of this line and $\mathbf{r} = (x, y, z)$ is a radius vector. Let $\mathbf{r}_0$ be its initial value corresponding to $s = 0$, then, according to the well-known theorem about a continuous dependence on the initial conditions (see, e.g., Arnol'd 1992), each solution $\mathbf{r}(s, \mathbf{r}_0)$ of Eq.(3.1) has a continuous and smooth dependence on $\mathbf{r}_0$ if the right-hand side of Eq.(3.1) is a smooth function.

Consider now the implications of this theorem for a topological analysis of coronal magnetic configurations. Mostly we are interested in closed-field regions of a magnetic configuration where the field lines connect positive and negative polarity regions of the photospheric surface. The example of such a line is schematically shown in Figure 3.1a.

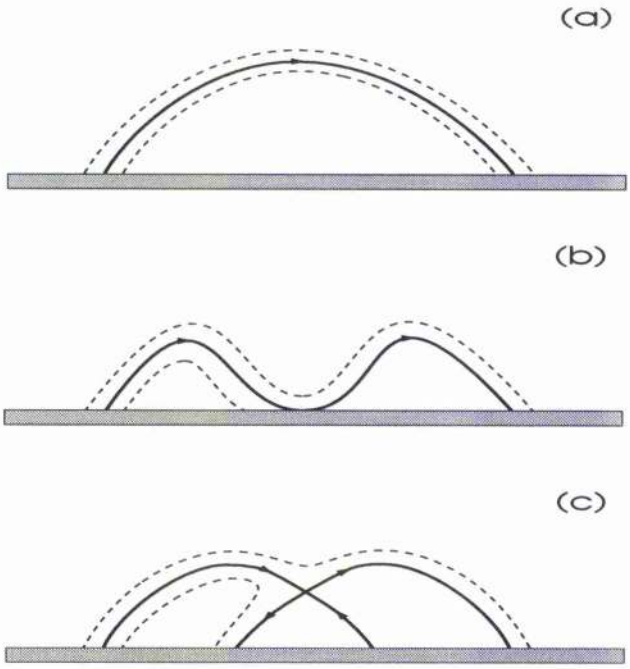

Figure 3.1: Three different magnetic topologies. (a) shows a field with no discontinuities in footpoint connectivity, whilst (b) and (c) illustrate the jumps in footpoint connectivity caused by a BP and a null point respectively.

The magnetic field differs from zero everywhere along the shown field line which lies *strictly* above the photosphere, so that the above theorem enables us to claim that the closer the footpoints of neighbouring field lines to the footpoint of the considered line at the positive polarity, the nearer the corresponding footpoints are at the negative polarity. Thus every 'normal' field line is surrounded by a bunch of the field lines characterized by continuous changes of the footpoint connectivity when passing from one line to another.

It is not the case, however, if the field lines touch the photosphere as in Figure 3.1b at some part of the IL (called a BP). There is a finite jump of footpoint connectivity in the neighbourhood of these lines, since the lower lines (with respect to the touching lines) are cut off earlier than the higher ones by the photospheric plane when moving along the lines towards the BP. It is obvious, however, that this feature does not contradict the above theorem, since the theorem refers only to the unbounded space.

The second opportunity for a discontinuous behaviour of footpoint connectivity is due to the possible presence of null points in the field, i.e. the points $\mathbf{r}_N$ such that $\mathbf{B}(\mathbf{r}_N) = 0$.

The right-hand side of Eq.(3.1) at these points becomes singular, so the above theorem is no longer applicable in the neighbourhood of the field line containing a null point. The field line at such a point bifurcates on several field lines, thereby causing a jump in the footpoint connectivity of the neighbouring field lines. This effect is illustrated on Figure 3.1c for a two-dimensional null point. A three-dimensional null point causes even more drastic effects, since the field line containing such a point bifurcates there on an infinite number of field lines.

Thus, we arrive at a very simple result: *the regions with different footpoint connectivity in coronal magnetic configurations are separated from each other by separatrix surfaces consisting of the field lines which 'thread' the BP's and the null points located above the photosphere*. For brevity we shall call such a set of separatrix surfaces 'the topological skeleton' (TS) of the configuration.

This result, in spite of its simplicity, has a number of important consequences. Firstly, to determine the TS of a given configuration, one needs only to find BP's, magnetic nulls and several field lines passing through them as will be done below. This is a much easier task than that undertaken in a series of papers (Mandrini et al. 1991, Démoulin et al 1992, Mandrini et al 1993) and based on a 'shooting method' in which a numerically integrated field line is considered to belong to the TS if it suddenly 'switches' from one sub-photospheric magnetic source to another.

Second, in many cases this 'shooting' method must lead to 'parasitic' separatrix surfaces because of the possible presence of sub-photospheric null points in the configuration, namely since the presence of magnetic nulls causes such a 'switching' of field lines. Also the separatrix surfaces due to the possible presence of BP's are overlooked by this method if one seeks only this 'switching'.

Finally, a self-consistent determination of a separator may be achieved only if one or two null points are located above or on the photospheric surface and belong to the separator, since only their presence gives a sense to this concept — in the absence of nulls and BP's there is nothing that could cause a jump in field line connectivity and thereby reveal the separator or its analogue. So any definition of a separator in the spirit of the above-mentioned works and which is connected with an extrapolation of the coronal field below the photospheric surface (to find such nulls and hence the separator) is not

satisfactory, because the force-free or potential approximation for the magnetic field is no longer applicable in the much denser photospheric plasma.

3.3 Source Model of Magnetic Configurations

Bald patches necessarily lie on a polarity inversion line (IL) since they are regions where the field is tangential to the photospheric boundary. For regions of the IL where coronal field lines touch the photosphere and return upwards into the corona we clearly require the field line concavity to be directed upwards, i.e. the normal component of the magnetic tension force evaluated at the IL must be positive. Thus

$$(\mathbf{B} \cdot \nabla) B_z \mid_{\mathrm{IL}} > 0, \tag{3.2}$$

where B_z is the field component normal to the photosphere. This result can be rewritten as

$$(\mathbf{B}_\mathrm{h} \cdot \nabla_\mathrm{h}) B_z \mid_{\mathrm{IL}} > 0, \tag{3.3}$$

where $_\mathrm{h}$ labels the horizontal components of both $\mathbf{B}$ and ∇. This result implies that the horizontal field at a BP is reversed, being directed from negative to positive polarity (Titov et al 1993), as was previously noted by Seehafer (1986) in his topological analysis of some numerically extrapolated active region magnetic fields. Thus, in order to find the location of a BP in a given magnetic configuration we simply need to apply Eq.(3.3) to points along the photospheric IL.

In general then, this is mainly a computational problem. Using observational magnetogram data, an extrapolation proceedure may be applied to generate a coronal magnetic field and BP regions may be found by applying Eq.(3.1). As mentioned in Chapter 1.3, the 180° ambiguity in the transverse field component of magnetogram data usually hampers such extrapolations. If, however, the transverse field direction is simply followed without sign and places where the transverse component becomes tangential to the IL are looked for (Low 1982), it is still possible to locate BP regions as they will occur between two such points (Titov et al 1993).

We shall continue here, as in the previous chapter, to model the field using a number of discrete magnetic sources and which are now located below the photospheric plane

$z = 0$. The field is given by

$$\mathbf{B} = \sum_{i=1}^{n} \mathbf{B}_i(\mathbf{r}_\mathrm{h} - \mathbf{r}_{\mathrm{h}i},\, z + d_i), \tag{3.4}$$

where n is the number of sources, $\mathbf{r}_{\mathrm{h}i} = (x_i, y_i)$ represents their positions in the horizontal (x, y)-plane placed at a depth d_i below the photosphere and the function $\mathbf{B}_i$ determines the magnetic field generated by the i-th source at the point $\mathbf{r} = (\mathbf{r}_\mathrm{h}, z)$. The form of this function will depend on which approximation, potential or constant-α force-free, is used for the field.

In any case, the equation

$$\sum_{i=1}^{n} B_{zi}(\mathbf{r}_\mathrm{h} - \mathbf{r}_{\mathrm{h}i},\, d_i) = 0 \tag{3.5}$$

determines implicitly the IL in such a configuration. The depths d_i are of the order of the spot sizes, which are often much less than the distances between the neighbouring spots, i.e.

$$d_i \ll |\mathbf{r}_{\mathrm{h}j} - \mathbf{r}_{\mathrm{h}i}|, \tag{3.6}$$

where $\mathbf{r}_{\mathrm{h}j}$ denotes the positions of the neighbouring spots in the horizontal plane. So in this case there is a wide range of $\mathbf{r}_\mathrm{h}$ for which d_i may be considered to be small and hence we can expand Eq.(3.5) by this small value to obtain the IL equation for a configuration with *quasi-coplanar sources*

$$\sum_{i=1}^{n} \delta_i \frac{\partial B_{zi}}{\partial z}(\mathbf{r}_\mathrm{h} - \mathbf{r}_{\mathrm{h}i}, 0) = 0. \tag{3.7}$$

Here we introduce the dimensionless parameter

$$\delta_i = \frac{d_i}{d_{\min}}, \qquad d_{\min} = \min_{i=\overline{1,n}} \{d_i\}, \tag{3.8}$$

which represents the relative weight with which the i-th source influences the IL shape determined approximately by Eq.(3.7).

If the sources have approximately the same size, i.e. $\delta_i \simeq 1$, $i = \overline{1,n}$, then Eq.(3.7) becomes equal simply to

$$\sum_{i=1}^{n} \frac{\partial B_{zi}}{\partial z}(\mathbf{r}_\mathrm{h} - \mathbf{r}_{\mathrm{h}i}, 0) = 0. \tag{3.9}$$

We shall call the photospheric line given by this equation the *discriminant line* (DL). It gives the limiting case of the IL when all of the charges lie in the photospheric plane. It will be shown below that this DL together with the IL, given by Eq.(3.7), separates in the photospheric plane the region of coronal nulls.

3.4 Nulls in a Quasi-Coplanar Source Model

If the magnetic sources are located near the photospheric plane $z = 0$, as was considered in the previous section, then one can expect that most of the magnetic null points are also in or near this plane. Recall now from Chapter 2.2 that the field in the vicinity of a null may be given to first order by Eq.(2.1), and we may determine the orthogonal eigenvectors of the matrix $\mathcal{B}$ (Eq.(2.2)) for sources lying in the photospheric plane, $z = 0$. These eigenvectors, given by Eq.(2.20), are the zeroth-order approximation relative to d_i and give two separatrix field lines lying in the photospheric plane together with the nulls whilst the third separatrix field line is perpedicular to this plane.

At the next order in d_i we have a displacement of nulls proportional to d_i. As follows from the discussion in section 3.2, it is important to know when these nulls will displace upwards into the corona. To consider this question, denote the position that we have for a null in the zeroth-order approximation by $\mathbf{r}_{\rm N} \equiv (\mathbf{r}_{\rm hN}, 0)$, and the corresponding displacement at first order by $\Delta\mathbf{r}_{\rm N} = (\Delta\mathbf{r}_{\rm hN}, \Delta z_{\rm N})$, so that

$$\mathbf{B}(\mathbf{r}_{\rm N}) \equiv \sum_{i=1}^{n} \mathbf{B}_i(\mathbf{r}_{\rm hN} - \mathbf{r}_{hi}, 0) = 0 \tag{3.10}$$

and

$$\sum_{i=1}^{n} \quad [(\Delta\mathbf{r}_{\rm hN} \cdot \nabla_{\rm hN})\mathbf{B}_i(\mathbf{r}_{\rm hN} - \mathbf{r}_{hi}, 0) + \tag{3.11}$$

$$\Delta z_{\rm N} \frac{\partial \mathbf{B}_i}{\partial z}(\mathbf{r}_{\rm hN} - \mathbf{r}_{hi}, 0) + d_i \frac{\partial \mathbf{B}_i}{\partial z}(\mathbf{r}_{\rm hN} - \mathbf{r}_{hi}, 0)\Big] = 0,$$

where $\nabla_{\rm hN}$ means differentiation with respect to $\mathbf{r}_{\rm hN}$. The first and the second equations here determine, respectively, $\mathbf{r}_{\rm hN}$ and $\Delta\mathbf{r}_{\rm N}$. Notice that

$$B_{zi}(\mathbf{r}_{\rm hN} - \mathbf{r}_{hi}, 0) \equiv 0\,, \tag{3.12}$$

since the left-hand side of Eq.(3.12) represents the z-component of the field generated by the i-th source in $(\mathbf{r}_{\rm hN}, 0)$, i.e. in the point of the same plane where this source is located. So in taking the z-component of Eq.(3.11), the first term vanishes for each i and we can easily find from there the desired result

$$\Delta z_N = -\frac{d_{\min} \sum_{i=1}^{n} \delta_i \frac{\partial B_{zi}}{\partial z}(\mathbf{r}_{\rm hN} - \mathbf{r}_{hi}, 0)}{\sum_{i=1}^{n} \frac{\partial B_{zi}}{\partial z}(\mathbf{r}_{\rm hN} - \mathbf{r}_{hi}, 0)}\,. \tag{3.13}$$

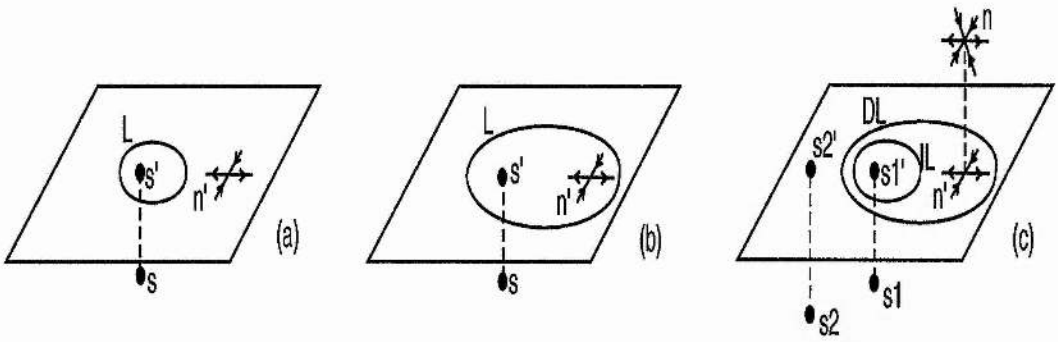

Figure 3.2: The projections s′ and n′ of the source, s, and null, n, respectively, when they are (a) separated and (b) not separated by the line L in the photospheric plane. (c) A coronal null, n, is always separated from all the sources (e.g. s1 and s2) by the inversion (IL) and discriminant (DL) lines.

This expression admits a very simple interpretation: the numerator and denominator here are, respectively, the z-component of the magnetic field at the first order in d_i and its gradient in zeroth-order, both determined at the photospheric plane. It is clearly seen from Eq.(3.13) that $\Delta z_{\rm N} > 0$ if these two values have opposite signs and $\Delta z_{\rm N} < 0$ provided the signs are identical.

The first case is the most interesting, since in this case the null turns out be situated in the corona and so becomes part of the TS of the coronal magnetic configuration. The sub-photospheric null together with the corresponding separatrix surfaces obtained in the second case may not be included in the TS, since the approximation used for the field fails below the photosphere and therefore the presence of such a null is probably an arterfact. Although knowledge of the movement of these nulls during an evolution of the studied configuration may be useful, especially if as a result of this movement the numerator or the denominator in Eq.(3.13) changes its sign. This may happen when the sub-photospheric null crosses the IL or the DL defined, respectively, by the formulae Eq.(3.7) and Eq.(3.9), which determine at the same time the lines of vanishing numerator and denominator in Eq.(3.13). Therefore such a movement leads to the appearance of the nulls above the photosphere, since it is accompanied by a change in sign of $\Delta z_{\rm N}$.

Let us now deduce the criterion for identifying coronal nulls near the photospheric

plane in the above model. We shall say that a null is separated from a source by the IL (DL) if it is not possible to connect the projections of the null and source onto the photospheric plane by a line in this plane without crossing the IL (DL) (see Figures 3.2a and 3.2b). It is clear then that for a given null point the signs of the numerator and denominator in Eq.(3.13) are given by the signs of the sources which are not separated from the null by the IL and DL, respectively. Thus, we obtain a very simple criterion for coronal nulls: *a null point, situated near the photospheric plane in a quasi-coplanar source model, is located above the photosphere if it is separated from all the sources by the inversion and discriminant lines* (see Figure 3.2c).

3.5 Potential Fields

We shall start in the simplest case by modelling the coronal field using a finite number of discrete potential magnetic sources, located below the photospheric plane $z = 0$. In this case the magnetic field at any location ($\mathbf{r}$) is given by

$$\mathbf{B} = \sum_{i=1}^{n} e_i \frac{\mathbf{r} - \mathbf{r}_i}{\mid \mathbf{r} - \mathbf{r}_i \mid^3}, \tag{3.14}$$

where $\mathbf{r}_i$ is the position of the magnetic source e_i and n is simply the number of sources .

3.5.1 Two Unequal Magnetic Sources

Consider first the simplest configuration of interest, given by just two sources of unequal strength and opposite polarity. This field may for example represent the localised field of a preceeding and following sunspot pair. Without loss of generality we may fix the first source (e_1) at $\mathbf{r}_1 = (0, 0, -d_1)$ and the second (e_2) at $\mathbf{r}_2 = (a, 0, -d_2)$. Let the ratio of the source strengths be $e_2/e_1 = -\epsilon$ (see Chapter 2.3). The vertical component of this field is now given by

$$B_z = \frac{e_1(z + d_1)}{[x^2 + y^2 + (z + d_1)^2]^{\frac{3}{2}}} + \frac{e_2(z + d_2)}{[(x - a)^2 + y^2 + (z + d_2)^2]^{\frac{3}{2}}}. \tag{3.15}$$

The polarity inversion line at the photosphere is simply found by setting $B_z = 0$ on $z = 0$ which gives a circle,

$$\left[x - \frac{a}{(1 - k)}\right]^2 + y^2 = \frac{a^2 k}{(1 - k)^2} - \frac{(\delta^2 - k)}{(1 - k)} d_1^2, \tag{3.16}$$

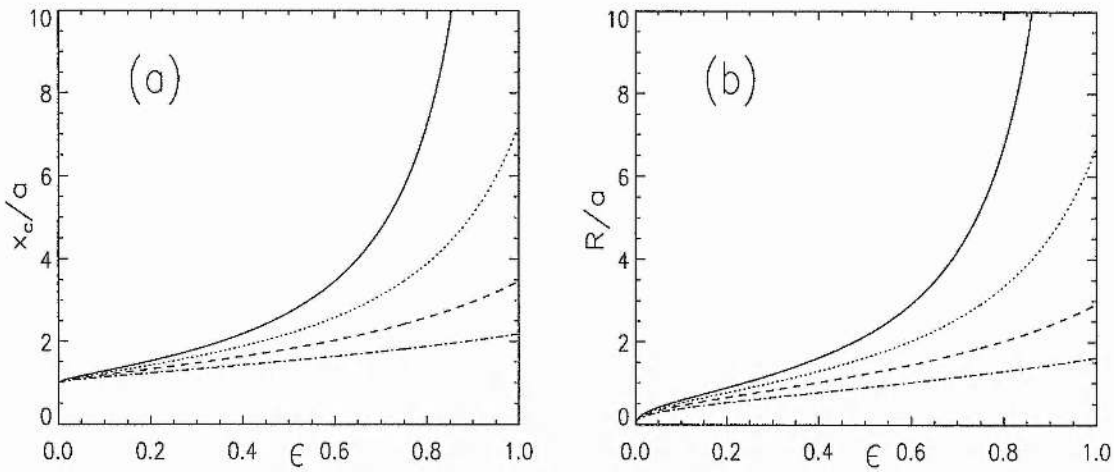

Figure 3.3: (a) The variation of the centre of the circular IL with source strength ratio for various values of the depth ratio δ. Values of $\delta = 1.0, 0.8, 0.6$, and 0.4 are represented by the solid, dotted, dashed, and the dot-dashed curves, respectively. (b) The change in IL radius with strength ratio for the same values of δ as in (a) but with a fixed lower depth of $d_1 = 0.1$.

where $k = |(e_2 d_2)/(e_1 d_1)|^{\frac{2}{3}} = (\epsilon\delta)^{\frac{2}{3}}$ and $\delta = d_2/d_1$. This circle is centred on $x_c = a/(1-k)$, $y_c = 0$ and has a radius given by

$$R = \left[\frac{ka^2}{(1-k)^2} - \frac{(\delta^2 - k)}{(1-k)} d_1^2\right]^{\frac{1}{2}}.$$

The variation of the centre, x_c, with the source strength ratio ϵ is shown in Figure 3.3a for differing values of the source depth ratio, δ. The four curves correspond to values of $\delta = 1.0, 0.8, 0.6$, and 0.4, respectively, thus representing in the case $\delta = 1$ the position of the centre of the IL when the two sources have the same depth, and in the remaining cases the effect of decreasing the depth, d_2, of the second source. Figure 3.3b shows the corresponding variation of the IL radius with strength ratio, ϵ, for the same values of the depth ratio, δ, as in 3.3a. These curves are plotted for a fixed initial depth of $d_1 = 0.1$. Thus it can be seen that as the depth d_2 decreases (from 0.1 to 0.04) the radius of the IL decreases. The discriminant line, DL, as defined previously in section 3.3 is simply given by the IL in the limiting case of both sources lying in the photospheric plane (i.e. $d_1 = d_2 = 0$). Since, as can be seen from Figures 3.3a and 3.3b, the position of the centre of the IL and its radius decrease as the sources are moved out of the same horizontal

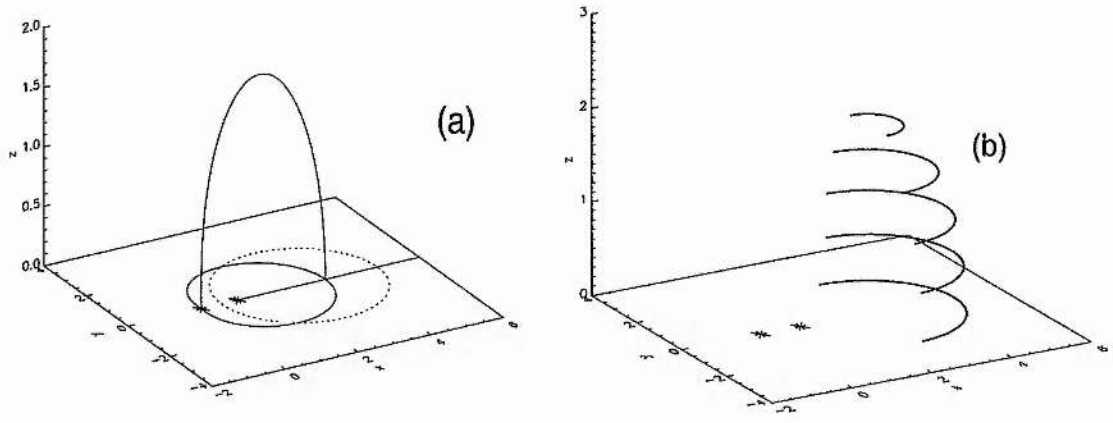

Figure 3.4: Topological features produced by two unequal sources of opposite polarity placed at equal depths. (a) The topological skeleton, with the two sources producing a null point in the photospheric source plane. The circular IL is shown as the dotted photospheric curve. (b) The variation in size of the BP (region of the IL satisfying Eq.(3.3)) with distance from the horizontal source plane.

plane (i.e. as δ decreases from 1) the IL will always be encircled by the DL in this simple two-source model.

Applying the BP criterion, Eq.(3.3), to Eq.(3.16) we find the existence of a BP covering a significant portion of this circular IL. In the special case of coplanar sources (i.e. $d_1 = d_2$) the BP covers exactly half of the IL, having end points at $(x_c, \pm R, 0)$. The BP's are found then to have a position and size that are on a scale comparable to the separation length scale, a, of the sources, and which depend on the source strength ratio, ϵ, the source depths, and the horizontal separation of the sources. Variations in source separation and source strength, however, effect both the size and shape of the BP in a similar manner, and thus for a topological study we may effectively fix the source separation, a, and simply look at the variation with strength ratio, ϵ. The main features of this simple two-source topology are demonstrated in Figures 3.4, 3.5, 3.6 and 3.7 .

The topological skeleton (TS) of the magnetic configuration is shown in Figure 3.4a, for a value of $\epsilon = 0.5$, in the limiting case when the sources both lie in the photospheric plane, $z = 0$. The two sources at $x = 0$ and $x = 1$ can be seen to produce a magnetic null point in the source plane, as an intersection of three separatrix field lines. This case is just that of the two-source field considered in Chapter 2.3 (c.f. Figure 2.4b).The

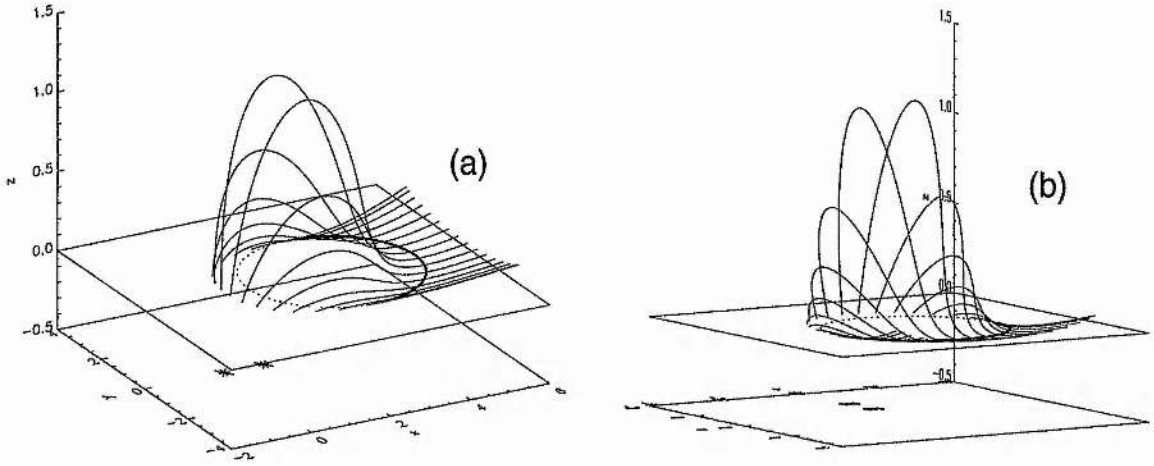

Figure 3.5: The coronal separatrix surface formed by field lines threading a BP, viewed from different angles in (a) and (b), produced by sources of strength ratio $\epsilon = 0.5$ at equal depth, $d_1 = d_2 = 0.5$.

IL (equal to the DL in this limiting case) is shown to encircle the weaker source and the null point. In this limiting case separatrix field lines threading the null point will form a separatrix surface and constitute the TS of the coronal field along with the null point itself. For cases where the sources are located at the same finite depth below the photospheric plane, the null point, which remains in the source plane, will not be present in the coronal field and the TS will then consist of field lines threading the corresponding BP which is found in the null's absence. Figure 3.4b shows the variation of the BP size with distance from the horizontal source plane. A selection of the field lines threading the BP and forming the separatrix surface in the coronal field are plotted in Figure 3.5, seen in differing projections in (a) and (b).

As is seen from Figure 3.4a, the IL initially encircles the horizontal positions of both the weaker source and the null point. However, we find from Figure 3.3 that as the source depths become unequal the IL shrinks in size and the BP covering part of the IL is found to shrink also. Whilst it will always encircle the horizontal position of the weaker source, as the depth d_2 is decreased with d_1 held fixed, there exists a critical value of the depth ratio, δ_c, for which the horizontal position of the null point is no longer enclosed by the IL. At this moment the size of the BP region shrinks to zero and the sign of the numerator in Eq.(3.13) changes. The sign of Δz_N thus changes and leads to the emergence of the

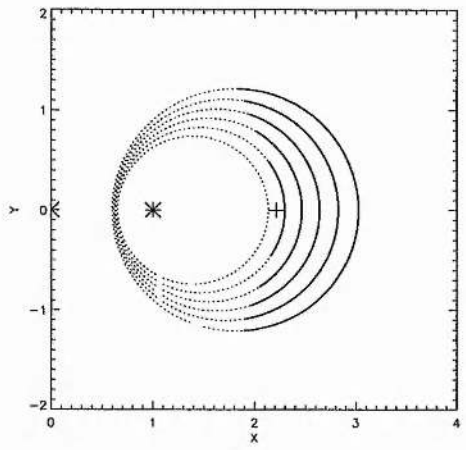

Figure 3.6: The shrinkage of the IL (dashed curves) and BP (solid curves) with decreasing depth d_2. The outer curve corresponds to equal source depths $d_1 = d_2$, with the curves decreasing as δ decreases from 1.0 to 0.5 in steps of 0.1. The IL crosses the horizontal position of the null (marked as a +) when $\delta = \delta_c$ signifying the emergence of the null point into the coronal field.

null point above the photospheric plane. This is demonstrated in Figure 3.6, which shows the IL, and corresponding BP, decreasing as the depth d_2 decreases for a fixed strength ratio. The horizontal position of the null is also shown.

As the coronal field evolves then, due to the rising of the weaker magnetic source, the BP is seen to shrink and eventually disappear with a coronal null point emerging in its place. The TS of the coronal field smoothly evolves from consisting of field lines threading the BP to field lines threading the newly emerged null. A selection of field lines making up the TS in each of these states is shown in Figures 3.7a and 3.7b. It is interesting to observe from Figures 3.5 and 3.7a that, as the BP shrinks, field lines threading it become more concentrated along the direction of the spine of the null point as it approaches the surface.

It should be noted that the BP's found in this simple arrangement lie outside the two magnetic flux sources. As the strength ratio, ϵ, tends to unity, which may be the case in a first approximate model of a simple active region, this BP migrates away from the source location. The field lines threading the BP and forming the coronal separatrix surface, however, remain rooted at the photosphere within the source region. Hence any effects of current build up along the separatrix surface may still occur *within the active region.* These external BP's may also provide locations for the formation of inverse

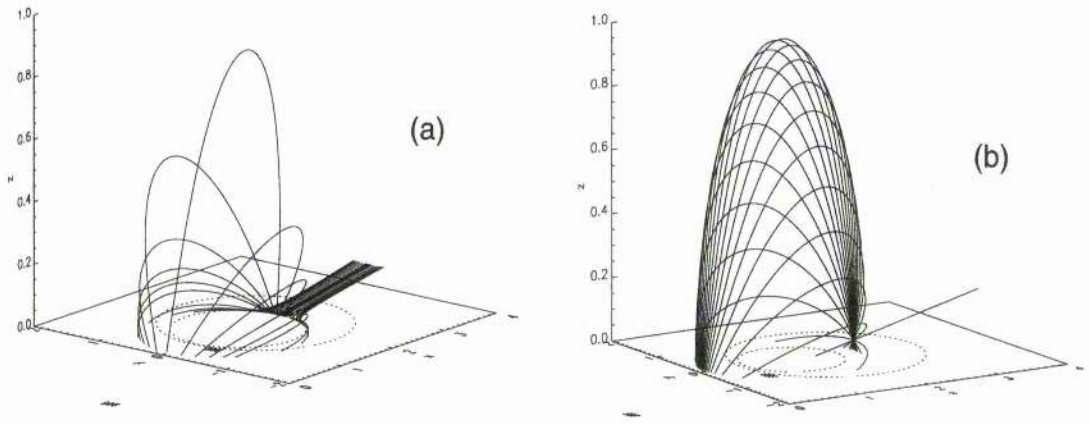

Figure 3.7: Evolution of the coronal field. Field lines forming the coronal separatrix surface are shown as the BP with $\delta = 0.6$, (a), is replaced by the null point with $\delta = 0.4$, (b).

polarity prominences witnessed around the edges of active regions (Leroy 1989).

3.5.2 Three Unequal Magnetic Sources

Let us now consider the addition of a third source of magnetic flux. We shall start, for simplicity, by assuming a symmetrical arrangement with sources e_2 and e_3 being of equal strength and polarity, and equidistant from the opposite polarity source (e_1) which we shall keep fixed at $\mathbf{r}_1 = (0, 0, -d_1)$, see Figure 3.8. This is similar to the arrangement studied in Chapter 2.4.2.

The equation of the photospheric IL in this case is given by

$$\frac{d_1}{[x^2 + y^2 + d_1^2]^{\frac{3}{2}}} = \frac{\epsilon d_2}{[(x-a)^2 + y^2 + d_2^2]^{\frac{3}{2}}} + \frac{\epsilon d_3}{[(x - a\cos\theta)^2 + (y + a\sin\theta)^2 + d_3^2]^{\frac{3}{2}}}. \quad (3.17)$$

The shape of this IL and the corresponding BP, which may be found by applying Eq.(3.3), are effectively determined by the source depths and strengths, as in the two-source case.

If the source depths are equal ($d_1 = d_2 = d_3$) then the variation of the IL and BP shape and size with distance from the source plane may be plotted, as in Figure 3.9a, for a given constant value of ϵ. Similar shaped IL's and BP's are produced if ϵ is varied for a fixed source depth. It is found then that if the depth of the sources is sufficiently great or the ratio of the weaker sources to the dominant source is sufficiently small, the

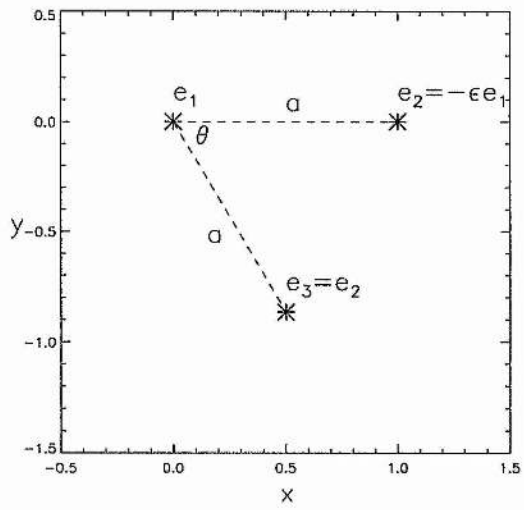

Figure 3.8: Symmetric planar arrangement of three sources with the two like-polarity sources equidistant from the opposite polarity source at the origin.

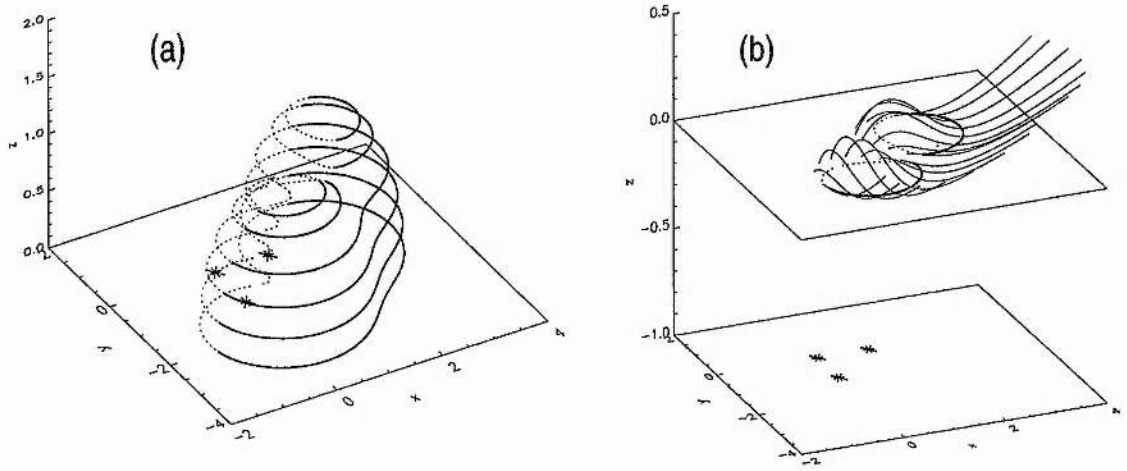

Figure 3.9: 'Bald Patches' produced by the coplanar, symmetrical three source arrangement of Figure 3.8 with $\theta = \pi/2$. (a) shows the variation of the IL and corresponding BP with distance from the source plane, whilst (b) shows field lines forming the coronal TS in the case where $d = 1.0$ and $\epsilon = 0.25$

IL will consist of two distinct closed curves each giving rise to a separate BP. As the depths or angle of separation, θ, of the symmetric sources decreases, or the strength ratio ϵ increases, the separate sections of the IL merge (along with their respective BP's) to form a single structure.

In all of these cases of coplanar sources, any nulls produced in the magnetic field will lie in the source plane and hence below the photospheric surface. Thus in these cases the TS of the coronal field will be formed purely by field lines threading the BP. An example of such a TS is shown in Figure 3.9b, which traces the coronal separatrix surface formed by field lines threading two distinct BP regions.

The evolution of the coronal TS in response to the rising of one or more of the sub-photospheric sources may now also be studied. For example, if the sources e_1 and e_3 are fixed at a depth $d_1 = d_3 = 0.1$ and the depth of source e_2 is gradually decreased, whilst maintaining the same horizontal position, we may follow the resulting shrinkage of the photospheric IL and corresponding BP. This is shown in Figure 3.10 with the outer curve representing the DL and the subsequent curves plotting the IL, and corresponding BP, as d_2 is decreased in steps of 0.01. The horizontal positions of the two magnetic null points are also shown. As in the two-source case already studied, the photospheric BP is found to shrink away in the vicinity of the rising sub-photospheric null point and the moment at which the IL crosses the null position marks the emergence of this null into the coronal field. The TS of the coronal field evolves continuously from purely BP threading field lines to a combination of BP and null point field lines. Figures 3.11a and 3.11b show this evolution of the coronal separatrix surface by tracing a selection of field lines forming this surface in configurations just prior to, and just after, null point emergence, respectively.

Only symmetrical source strengths and arrangements have been mentioned thus far but the same general scenario is found in non-symmetric cases. For coplanar, sub-photospheric sources the topological skeleton of the coronal field consists of BP's and the field lines threading them. As the plane of the sources become non-horizontal, null points may be found to emerge into the coronal field whenever the photospheric IL crosses the horizontal position of that null. The separatrix surfaces of the coronal field evolve smoothly through this emergence.

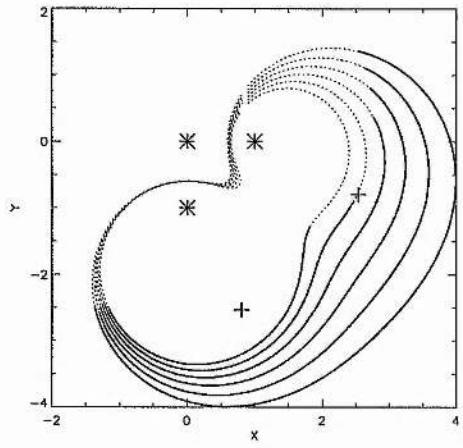

Figure 3.10: The shrinkage of the IL and BP due to a three quasi-coplanar as d_2 decreases from 0.1 to 0.05.

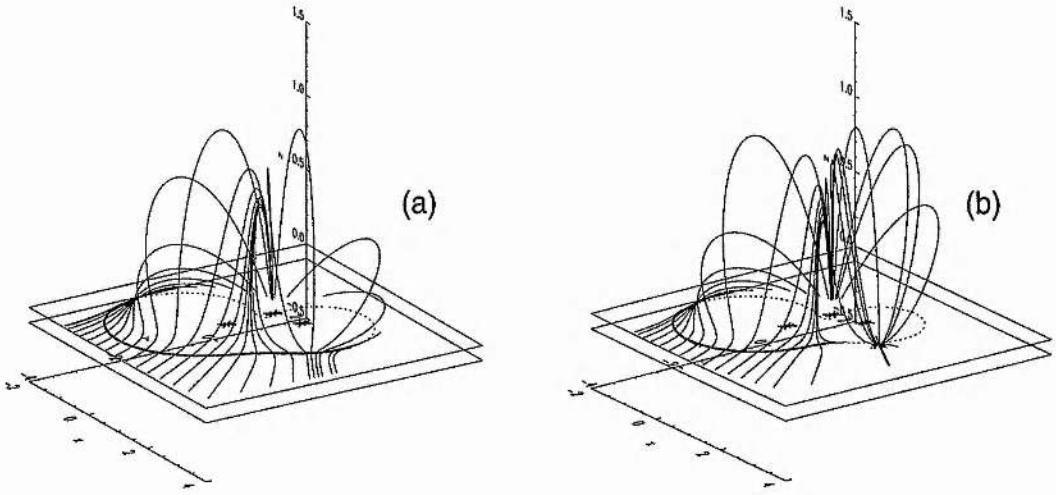

Figure 3.11: Coronal features due to three quasi-coplanar sources. A selection of field lines forming the coronal separatrix surface are traced in (a) and (b) for values of $\epsilon = 0.3$, $\theta = \pi/2$, $a = 1$, $d_1 = d_3 = 0.1$ and with $d_2 = 0.065$ and 0.05 in (a) and (b), respectively. The separatrix surface in (a) is due entirely to the BP, part of which shrinks as the null emerges in (b).

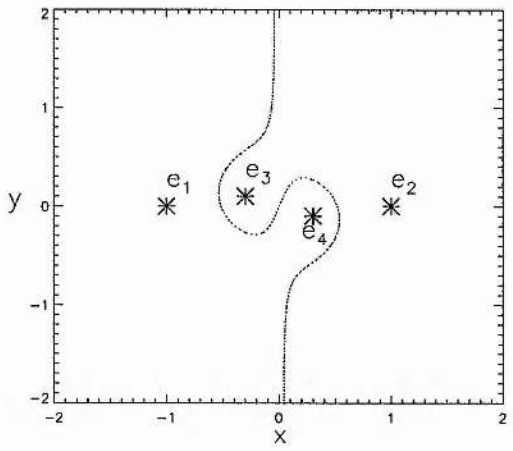

Figure 3.12: Planar arrangement of four centro-symmetric magnetic sources representing a main bipole (sources e_1 and e_2) and a parasitic bipole (sources e_3 and e_4). The 'S' shaped IL is also shown.

3.5.3 Four Magnetic Sources

The topological structure of a magnetic field generated by four sub-photospheric flux sources is not studied here in general terms. We consider only the special case of a centro-symmetric source arrangement, as previously used by Titov et al (1993), representing a main bipole and a parasitic bipole (Figure 3.12), and as considered in Chapter 2.5.1. Using a similar source arrangement, Gorbachev & Somov (1988) studied the emergence of a separator above the photospheric surface, and in Chapter 2.5.1 we have found this separator to rise rapidly as the internal bipole strength is increased (Figure 2.17). They demonstrated that field lines passing close to this separator intersect the photospheric plane in two ribbon-like regions. These ribbon-like regions it is claimed may be related to the H_α ribbons witnessed in large solar flares, with the energy release assumed to take place in the region of the separator. The separator studied in this work, however, is entirely due to the presence of null points in the magnetic field lying below the photosphere, and thus the separatrix surfaces intersecting to form this separator do not form a part of the coronal TS.

Titov et al (1993) showed that, prior to the emergence of this separator, a BP exists at the central location of a centro-symmetric source arrangement. In general, BP's may exist in many different regions of this particular four-source field, depending on the usual parameters of source separation, strength and depth. We will not study these BP's here,

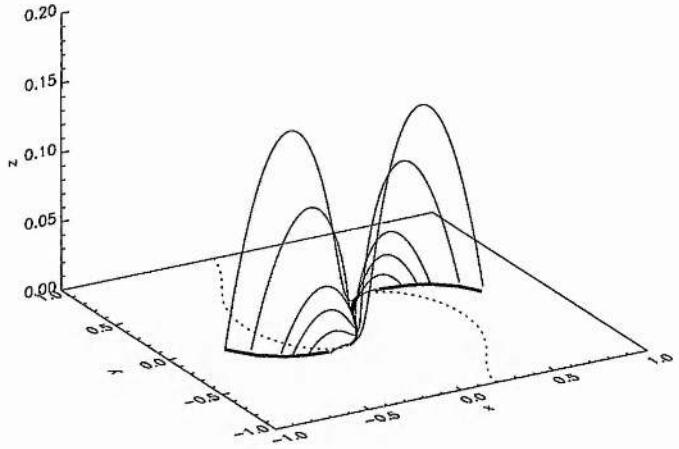

Figure 3.13: Plot showing a selection of field lines passing through the BP at the centre of a centro-symmetric four source arrangement. The thick curves in the photospheric plane $z = 0$ are the ribbon-like photospheric footpoint regions of these BP field lines.

but instead we restrict our attention solely to the BP of Titov et al (1993), located on the central region of the IL, between sources e_3 and e_4 (Figure 3.12). The field lines threading this central BP, and thus forming the separatrix surfaces of the coronal field, have been traced. It is found that, as for the field lines close to the separator of Gorbachev & Somov (1988), the photospheric end points of these BP field lines also form two ribbon-like regions, as shown in Figure 3.13. Thus the ribbon-like regions of Gorbachev & Somov (1988) are not just a feature of magnetic configurations containing a separator but are also common to BP configurations. The observed H_α features of large solar flares, therefore, may possibly be associated with coronal energy release in the presence of either BP's or separators.

Some very interesting new features may be discovered by studying further the evolution of the coronal field due to this simple coplanar source arrangement as the strength of the internal bipole (e_3 and e_4) is varied. Initially, a single BP is present at the central location, as has already been described, but, as the internal bipole increases in strength, this central BP is found to split in two at the centre. The two separate sections of the original single BP gradually move apart and shrink, eventually disappearing altogether as the parasitic strength continues to increase. It is this splitting of the central BP which is of particular interest.

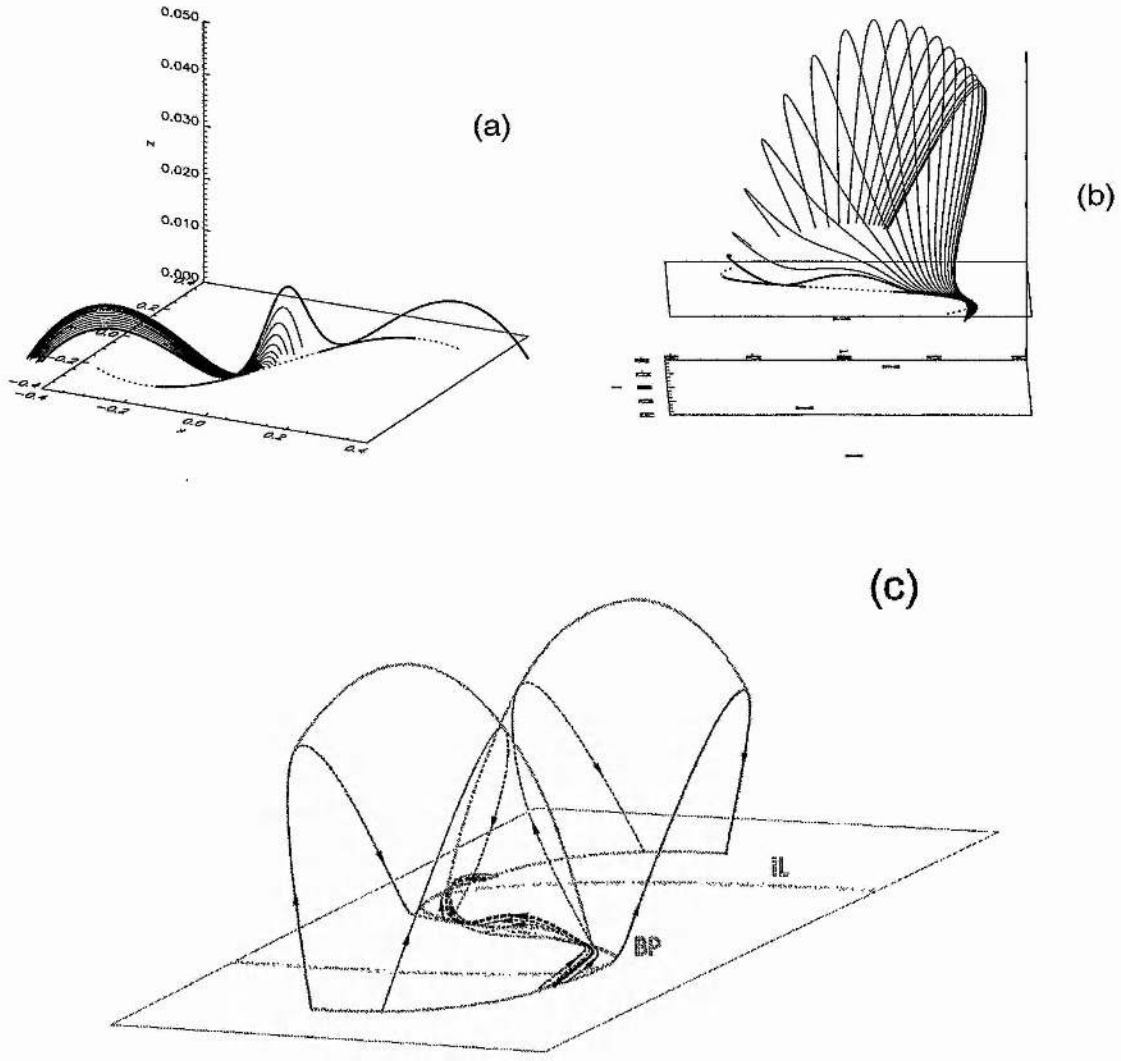

Figure 3.14: A separator field line in the absence of magnetic null points. (a) and (b) show a selection of field lines threading the inner and outer ends, respectively, of one BP section. The separator is shown as the bold, limiting field line in each case. (c) plots a general view of the overall 3D field topology, indicating the shape of the coronal separatrix surfaces and with the separator again represented by the darker field line.

Both of the distinct BP sections naturally give rise to a separatrix surface in the coronal field defined by the field lines threading that BP. Figures 3.14a and 3.14b show the field lines forming one of these surfaces. Those threading the more central end of the BP are seen in Figure 3.14a to re-cross the IL in the central region and return to the photosphere close by. Meanwhile, those field lines threading the outer end of the BP form the larger portion of the separatrix surface and return to the photosphere at a more distant location, as shown in Figure 3.14b.

As can also be seen from Figures 3.14a and 3.14b, there is a limiting field line threading the BP, represented by the thick curve, which simultaneously threads the other BP section as well. This field line then takes on a very significant role. Since it passes through both of the distinct BP regions it must belong to the distinct separatrix surface formed by each of those two regions. Hence it represents the intersection of the two separatrix surfaces and is therefore, by definition, a separator. Figure 3.14c gives a general 3D view of this field topology, tracing a selection of field lines threading both BP sections. The separator is shown as the thicker curve crossing the central portion of the IL at relatively low level. The lighter curves, without directional arrows, are not field lines but give an outline of the shape of the separatrix surfaces (as can also be seen from the field lines of Figure 3.14b).

A schematic plan view is given in Figure 3.15a in order to demonstrate more clearly the field line topology around this separator field line. Five field lines are shown threading each BP region (shown by the thick black curves), two inner field lines (dashed) and two outer (solid). The separator is shown as the thicker, solid field line treading both BP sections. Also shown in Figures 3.15b and 3.15c are the two differing intersections of the separatrix surfaces. In the central region between the two BP sections the surfaces formed by field lines threading the two sections intersect in an X-type formation, Figure 3.15b, whilst in the outer regions (beyond the point at which the separator threads the BP) the surfaces intersect in a T-type formation, as can be seen in Figure 3.15c.

As the internal bipole continues to increase in strength, the BP regions shrink and move apart, while the separator rises in height at its centre and its points of contact with the IL migrate towards the outer end of each BP. At the same time there is a gradual reduction in size of the separatrix surfaces of the coronal field starting at the outer portions

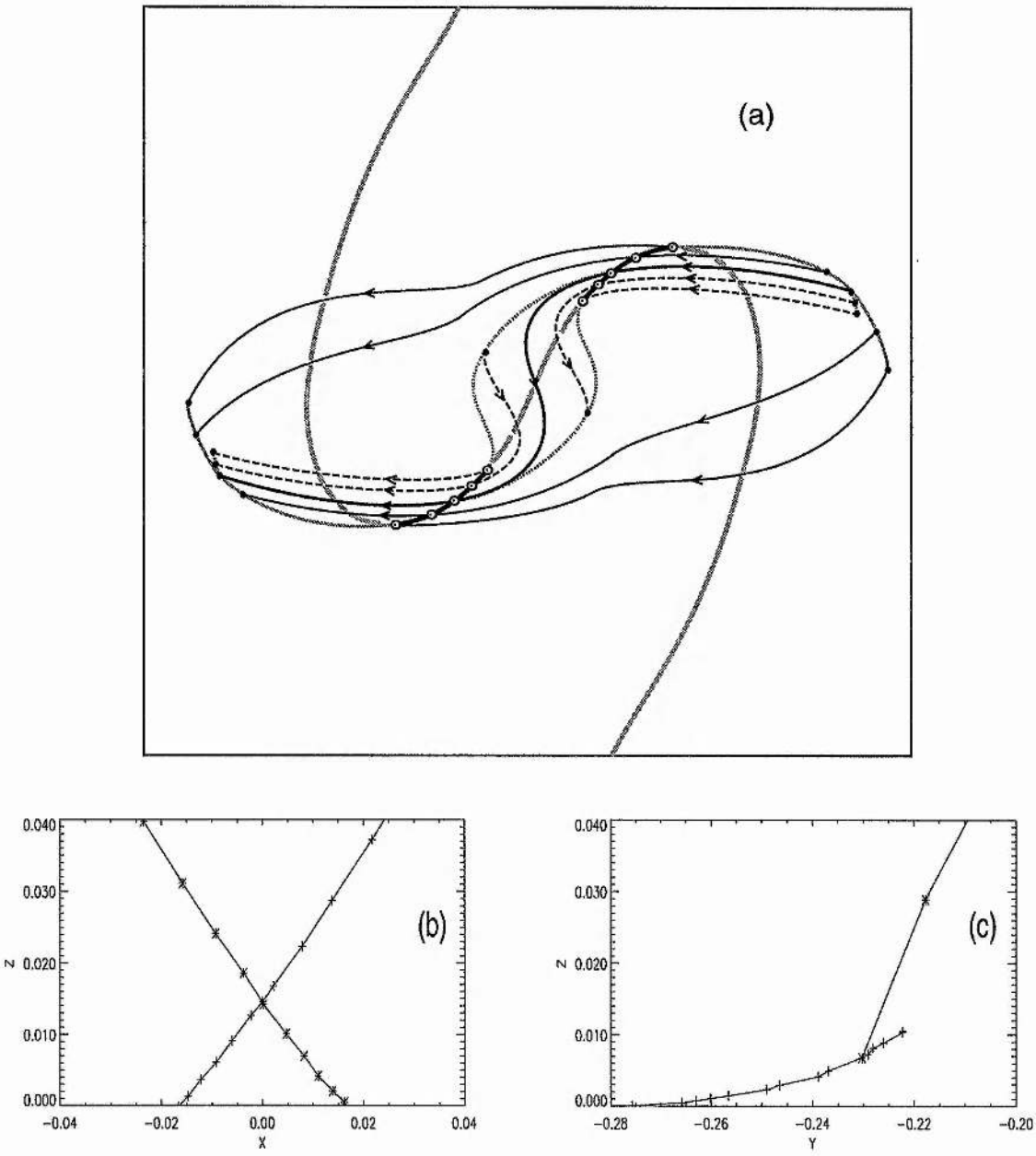

Figure 3.15: (a) A schematic plan view of the field line topology in the vicinity of the separator field line. (b) and (c) show the trace of separatrix field lines crossing the planes $y = 0$ and $x = -0.2$, respectively, demonstrating the X-type and T-type intersections of the separatrix surfaces in the inner and outer regions.

of the BP's. Upon reaching the ends of the shrinking BP's the separator finally disappears as the coronal separatrix surfaces shrink further and no longer intersect one another. The BP's and their separatrix surfaces eventually disappear, leaving a 'loop-like' coronal field crossing the IL in the normal direction from positive to negative polarity at all points.

This splitting of the original central BP, and the formation and rise of the separator field line, is analogous to the emergence of the separator of Gorbachev & Somov (1988); yet the method is self-consistent and requires no assumptions or knowledge of the magnetic field structure below the photospheric plane. Moreover, these separators are qualitatively different in the following three respects: first, the BP separator found here, contrary to the common understanding of separators, does not require for its determination the presence of any null points in the magnetic field, since it is a consequence purely of the presence of BP's; second, the central part of our separator is located along the IL and has points of contact with it, while previous separators have an arc-shaped form and cross the IL in a transverse direction, with footpoints relatively far from the IL; third, the new separator appears much earlier than the previous ones when the configuration evolves due to the internal bipole increasing in strength.

It should be emphasized, however, that the above topological reconstruction of the configuration may serve only as a rough sketch of its real evolution, since we have not taken into account the strong interaction between the evolving magnetic field and highly conductive plasma of the solar atmosphere. In reality, such an interaction must cause, first, the generation of a force-free component in the magnetic field and, second, current sheet formation along the separator and possibly at the separatrix surfaces both before and during the resulting topological reconstruction, as for the evolution of similar 2D magnetic configurations.

Starting from this point of view and considering the above configuration as a basic one for a two-ribbon flare, we can suggest the following possible scenario. The growth of the internal bipole in the initial stage causes an 'S'-shaped bending of the IL, appearance of the BP and the corresponding formation of a dip in the configuration above this BP. It could lead in turn to the formation of a prominence at the dip – the location of such a prominence in our model is in good agreement with observations. A further growth of the internal bipole splits the BP (Figures 3.14 and 3.15a) and such a splitting can be

identified with the emergence of new magnetic flux from below the photosphere. This new flux pushes the prominence upward, and interacts with the overlying field, giving rise to a current sheet – in our model (Figures 3.14 and 3.15) such a sheet is formed on the separator and possibly at the separatrix surfaces. The points of contact of the separator with the IL here correspond to the feet of prominence.

Since the current sheet is metastable, it subsequently goes unstable and gives rise to fast magnetic reconnection and release of the stored magnetic energy. Some of the material of the prominence is then taken up by the reconnecting current sheet and transformed into hot plasma of a flaring loop system. If the internal bipolar flux becomes sufficiently strong it may 'break through' the flux of the external bipole, causing the prominence to erupt. This effect was firstly recognised by Syrovatskii (1982) for four colinear photospheric magnetic sources, and we have shown in Chapter 2.5.1 that this effect exists with almost any orientation of the emerging internal bipole. Indeed, the break-through of the internal flux seems most efficient for an internal bipole angle of approximately 45°. Our model then naturally explains the observed correlation between the onset of solar flares and the eruption of prominences.

It is also worth noting that we have only studied here one particular source arrangement. However, a study of the parameter range (angle of internal bipole, source strengths and separations) for which BP's are present at the centre of symmetry is given by Titov et al (1993). For any such centro-symmetric source arrangement the upper limit on the internal bipole strength, e_+, as given in Titov et al (1993) will correspond to the moment of BP splitting, and the general scenario as described above will proceed.

3.6 Non-Potential Fields

So far in this work we have considered only potential fields. Whilst in many applications the potential model gives a good first approximation to observed features, large amounts of shear are sometimes seen in the coronal magnetic field. This shear is associated with the distribution of electric currents in the coronal plasma and allows the storage of large amounts of free energy. It may therefore be more realistic to model the coronal field using a sheared magnetic field rather than a potential one which has no free energy.

3.6.1 Linear Force-Free Fields

Force-free fields, of which the potential field is just a special case, may be used in order to model the desired shearing of a magnetic configuration. The force-free equation is in general, however, very hard to solve due to its non-linearity. This non-linearity also means that particular solutions, even if they can be found, cannot be superimposed to generate more general solutions. A great simplification arises if the force-free equation becomes linear; this is achieved by imposing a constant value of the α which appears in the force-free equation

$$\nabla \times \mathbf{B} = \alpha \mathbf{B}. \tag{3.18}$$

If this constant-α assumption is made, the linear force-free field generated by a single magnetic source may be described using a Green's function. The horizontal and vertical field components are given by

$$\begin{aligned} \mathbf{B}_{\mathrm{h}}(\mathbf{u}_i, z) &= e_i \left[\frac{\alpha}{u_i^2} \sin(\alpha(z+d_i)) - \frac{\alpha(z+d_i)^2}{R_i^2 u_i^2} \sin(\alpha R_i) + \frac{1}{R_i^3} \cos(\alpha R_i) \right] \mathbf{u}_i \\ &+ e_i \alpha \left[\cos(\alpha(z+d_i)) - \frac{(z+d_i)}{R_i} \cos(\alpha R_i) \right] \frac{\hat{\mathbf{z}} \times \hat{\mathbf{u}}_i}{u_i^2}, \end{aligned} \tag{3.19}$$

$$\mathbf{B}_z(\mathbf{u}_i, z) = \frac{e_i}{R_i^3}(z+d_i)[\cos(\alpha R_i) + \alpha R_i \sin(\alpha R_i)], \tag{3.20}$$

$$\begin{aligned} R_i^2 &= u_i^2 + (z+d_i)^2, \qquad u_i = \mid \mathbf{u}_i \mid = \mid \mathbf{r}_{\mathrm{h}} - \mathbf{r}_{\mathrm{h}i} \mid, \\ \mathbf{r}_{\mathrm{h}} &= (x, y), \qquad \mathbf{r}_{\mathrm{h}i} = (x_i, y_i) \end{aligned}$$

for a source e_i at position $\mathbf{r}_i = (x_i, y_i, -d_i)$ (Démoulin & Priest 1992, Aly 1992).

Using this more complicated field expression we may now, as in the previous section, simply apply the BP existence criterion, Eq.(3.3), to points on the photospheric IL of a field generated by a discrete number of sub-photospheric magnetic sources. Doing this we find essentially the same topological features as for the potential fields already studied. The simplest case of just two unequal sources is shown in Figure 3.16, which plots the topological skeleton of the magnetic field in the limiting case when the source depths are zero, and for a value of $\alpha = 0.1$.

Comparison of Figure 3.16 and Figure 3.4a, which both have the same source strengths and locations, shows that the introduction of shear does not affect the overall topology. A

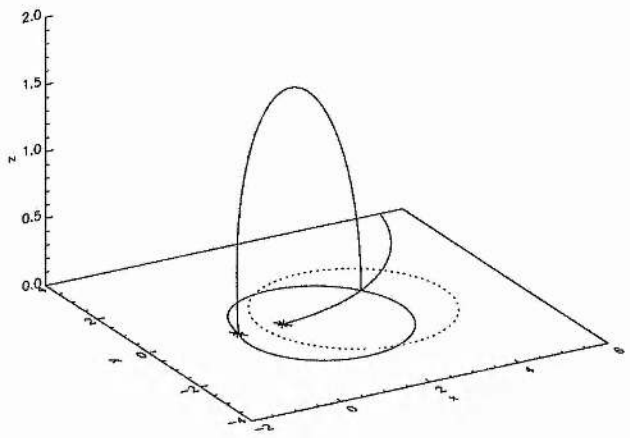

Figure 3.16: Simple linear force-free field due to two sources, at $x = 0$ and $x = 1$, of opposite polarity and with a strength ratio $\epsilon = 0.5$. The essential topological elements remain the same as for the potential field of Figure 3.4a and a large portion of the IL is still found to satisfy Eq.(3.3) and hence produce a BP.

magnetic null point is still seen to lie in the source plane with the IL enclosing this null and the weaker source. A BP can still be found on a large region of the IL, with its size and position, although slightly distorted from the potential case, still on a scale comparable to several source separation length scales. Similar results are also found for three sources. The essential topological features of the coronal magnetic field (i.e. the presence of BP's at the photosphere and the related separatrix surfaces) are, in general, unchanged by the introduction of shear in these linear force-free fields generated by sub-photospheric sources.

For the centro-symmetric, four source arrangement the same scenario of a splitting central BP with the formation of a separator field line may be found in this linear force-free case as for the potential case. Moreover, as shown by Titov et al (1993), the range of parameters, in particular the range of angles between the internal and the main bipoles, for which BP's can be found is increased by the shearing of the field. The condition for BP splitting and hence separator formation is again given by the value of e_+ as defined in Titov et al (1993). Thus the presence of these well-defined separator field lines may be found even for a relatively *small* 'S'-bending of the IL in this linear force-free field.

In studying the above sheared fields attention has to be paid to an inherent problem encountered with linear force-free fields. The field becomes periodic at large distances and

with increasing α. This behaviour is unphysical and thus we are restricted to studying the field close to the sources and to small values of α and hence only small amounts of shear.

3.6.2 A Non-Equilibrium Field

Observations of coronal active regions generally show that whilst large amounts of shear are present, the shearing of the field is localised. For example, Mandrini et al (1995) find that for the particular active region they study the shear is strongly localised around the photospheric IL with the distortion from the potential field decreasing with distance from these regions. The magnetic field given by

$$\mathbf{B} = \frac{e_i}{R_i^3}\left[\mathbf{R}_i + \frac{\alpha}{(z+d_i+R_i)}(\hat{\mathbf{z}} \times (\mathbf{r}_\mathrm{h} - \mathbf{r}_{\mathrm{h}i}))\right] \tag{3.21}$$

$$\begin{aligned} R_i &= |\,\mathbf{R}_i\,| = [\,|\,\mathbf{r}_\mathrm{h} - \mathbf{r}_{\mathrm{h}i}\,|^2 + (z+d_i)^2]^{\frac{1}{2}}, \\ \mathbf{r}_\mathrm{h} &= (x,y), \qquad \mathbf{r}_{\mathrm{h}i} = (x_i, y_i) \end{aligned}$$

has properties similar to those described. For a magnetic source e_i positioned at $\mathbf{r}_i = (x_i, y_i, -d_i)$ the field given by Eq.(3.21) is strongly sheared in the vicinity of the source and behaves like a potential field at large distances. Whilst this field is not in equilibrium, i.e. it is not force-free, it has many of the properties of observed coronal fields and a field similar in nature to this is successfully used by Mandrini et al (1995) to model active region fields with strong localised shearing.

The BP criterion, Eq.(3.3), is general for all magnetic fields. Thus it may be applied to non-equilibrium fields as well as potential and force-free fields. Consider the non-equilibrium field generated by several sources of magnetic flux described by Eq.(3.21). Applying Eq.(3.3) we again find the existence of BP's for a wide range of parameters in even the simplest cases. This result is not elaborated on here as it is as expected. For the simple cases given in Section 3.5, BP's occur at several scale lengths distance from the sources, and here the field of Eq.(3.21) is approximately potential.

3.7 Summary and Discussion

Coronal active regions consist of many concentrated regions of opposite polarity which we may model as simple magnetic sources. These concentrations of magnetic flux are all interlinked by field lines giving rise to a complex magnetic topology. In any localised region however, the main features of the field topology are likely to be determined by just a few dominant magnetic sources, with the more distant sources being less significant. Thus in the course of this chapter we have looked primarily at coronal fields generated by just a small number of magnetic sources.

Using the existence criterion of Titov et al (1993), Eq.(3.3), we have looked for regions of the photospheric inversion line (IL) which are tangentially touched by the coronal field. We find that these regions (named 'Bald Patches', BP's) are present for a large range of source strength ratios, separations, and sub-photospheric depths, in fields generated by as few as two or three magnetic sources. Thus any two adjacent, unequal flux concentrations of opposite polarity may potentially give rise to a BP. These BP's have a size which is on the order of the source separation length scale and are located exterior to the sources producing them.

We have described in Section 3.2 how BP's and coronal null points are the elemental topological features which, along with the separatrix field lines threading them, determine the topological skeleton (TS) of the coronal field, if the photosphere is taken as a natural boundary. For these simplified models of the coronal field using discrete sub-photospheric flux sources, however, Démoulin et al (1994) have found that null points only appear above the photospheric plane for very specific source arrangements. BP's, on the other hand, have been shown here to exist for a wide range of parameters. From studying the evolution of coronal fields due to two and three discrete sources we find that, in general, BP's are *precursors* to the emergence of magnetic null points into the coronal field. Indeed, we have also derived a criterion, Eq.(3.13), which indicates the existence of a coronal null point for quasi-coplanar source arrangements.

Following 2D studies, it is possible that BP's may be sites for coronal current sheet formation, and hence magnetic reconnection and energy release, as a result of photospheric compressive motions, if the magnetic field is assumed anchored at the photosphere (e.g. Low 1987, Sneyd 1993). To this end we have also studied the particular case of a centro-

symmetric arrangement of four coplanar magnetic sources, representing a main and a parasitic bipole. A configuration of this type has been studied by several authors in the past, using both magnetic sources (e.g. Baum & Bratentahl 1980, Gorbachev & Somov 1988, Titov et al 1993), and magnetic dipoles (e.g. Lau 1993). For this sub-photospheric, coplanar arrangement, no magnetic null point lies above the photosphere and hence the TS of the coronal field is defined purely by the field lines threading any BP's present. In studying this configuration we find, as previously by Titov et al (1993), a BP in the central region of the field. On evolution of the field due to an increase in strength of the parasitic bipole, this BP is found to split in two. This splitting of the BP gives rise to a *separator field line* which is well-defined, without requiring the presence of any null points in the coronal field. The separator field line may possibly be regarded as a favourable site for energy storage and release in response to photospheric footpoint motions, and field lines passing close to this separator, or threading the distinct BP regions, have been shown to return to the photosphere in two ribbon-like regions. They may possibly be related to the H_α-ribbons witnessed in large solar flares. This is similar to a result found by Gorbachev & Somov (1988) who also studied field lines passing close to a separator, but which was defined in terms of sub-photospheric nulls and thus has no topological significance in the coronal field. This newly found separator, defined without the presence of null points, may also possibly be related to the finding of Démoulin et al (1994), who find that there is no direct correlation between flaring regions of the coronal field and the presence of null points.

Karpen et al (1990, 1991) have argued that the anchoring of field lines at the photosphere is unphysical when concerned with BP regions. Realistically, the photosphere has a finite thickness and those field lines close to the BP may not penetrate sufficiently deeply into this photosphere for anchorage to be plausible. Using a finite photospheric thickness they found numerically that, whilst current structures are found along the BP field lines, the scale lengths are not sufficiently small for dissipation to become significant. More recently, however, Billinghurst et al (1993) have demonstrated that in special cases where the magnetic field strength decays sufficiently rapidly near the photospheric plane, these current structures may be sufficiently fine for dissipative effects to occur.

The arguments of Karpen et al (1990, 1991) do not, however, rule out the topological

importance of BP's. Even if they are not always relevant as locations for coronal sheet formation, the dipped nature of the field lines naturally marks BP's as possible sites for prominence formation. As we have also seen, the presence of BP's is closely linked with the possible emergence of null points into the coronal field.

Chapter 4

Current Sheet Configurations in Potential and Force-Free Fields

4.1 Introduction

In Chapter 1.4 we have discussed how the release of magnetic energy, stored in complicated field structures in the form of currents, plays an integral part in many coronal phenomena. To this end, current sheets play a very important role, acting as sites for this conversion and release of magnetic energy. The most likely sites for the formation of coronal current sheets would appear to be at the separatrix surfaces, where field lines of differing connectivity and differing orientation may become pressed together due to photospheric motions. We have seen in Chapter 3 how we may locate these separatrix surfaces in a model coronal field.

With current sheets being so central to the reconnection process, an analytical expression describing the structure of the magnetic field in the vicinity of such a sheet may prove useful, particularly for comparison with numerical simulations of ideal MHD phenomena. The study of three-dimensional magnetic reconnection, however, is still in its infancy and thus the nature of the magnetic field in a fully 3D current sheet is yet to be discovered. Any models, therefore, of the tangential discontinuities in the magnetic field which represent current sheets start by assuming a quasi-three-dimensional field, i.e. a three-dimensional field which is invariant in one coordinate. With this assumption being made, the simplest and most elegant means of expressing such fields is through the use

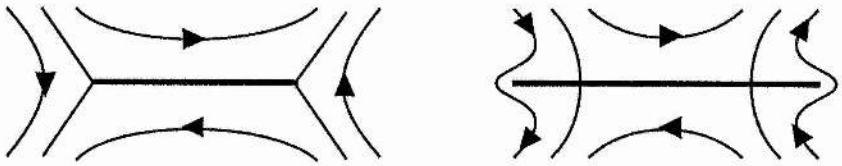

Figure 4.1: Sketches of the field configurations for the current sheets of (a) Green and (b) Syrovatskii.

of complex variable notation (Priest 1982).

Although Priest et al (1993) have recently developed a technique for modelling the dynamic time-dependent formation of current sheets, the two current sheet expressions which are the most widely known are those due to Green (1965) and Syrovatskii (1971). Green's expression,

$$B_y + iB_x = \sqrt{Z^2 - a^2}, \tag{4.1}$$

gives the configuration of a simple potential field containing a neutral current sheet with Y-type neutral points at the ends (Figure 4.1a). This type of sheet can be seen to be a special case of Syrovatskii's more general two-dimensional potential field,

$$B_y + iB_x = \frac{Z^2 - l^2}{\sqrt{Z^2 - a^2}}, \tag{4.2}$$

which, as shown in Figure 4.1b, incorporates a sheet with singular end points.

The Green and Syrovatskii solutions of Eq.(4.1) and Eq.(4.2) may just be written down by inspection, and this raises the question of whether other current sheet solutions may exist. Furthermore, these well-known solutions are potential (i.e. the field is purely two-dimensional), but what happens when a current sheet is embedded in a force-free field? In this chapter we will develop a more general technique for setting up the configurations of a constant-current, force-free field containing a straight current sheet, and in so doing generalise the analytical solutions of Green and Syrovatskii.

Related treatments have been given by Ridgeway, Amari and Priest (1992), who set up constant-current force-free fields for massive current sheets above a photospheric bound-

ary, and by Low(1993) who describes force-free fields with singular current-density surfaces.

4.2 Force-Free Fields

Due to the low plasma pressure of the solar corona in comparison with the magnetic pressure (i.e. low plasma β), the force-free field approximation may often be made, especially in active regions. Consider a $2\frac{1}{2}$-dimensional magnetic field with no dependance on the z-coordinate

$$B_x = \frac{\partial A}{\partial y}, \quad B_y = -\frac{\partial A}{\partial x}, \quad B_z(x,y), \tag{4.3}$$

where the magnetic field has been written in terms of the magnetic potential vector $A(x,y)\hat{\mathbf{z}}$ so as to satisfy automatically the condition $\nabla \cdot \mathbf{B} = 0$. The force-free condition $\mathbf{J} \times \mathbf{B} = 0$ together with Ampère's law, $\mathbf{J} = 1/\mu(\nabla \times \mathbf{B})$, gives the Grad-Shafranov equation

$$\nabla^2 A + \frac{1}{2}\frac{\mathrm{d}B_z^2}{\mathrm{d}A} = 0 \tag{4.4}$$

for the flux function (A), along with the condition that B_z is a function of A alone, $B_z = B_z(A)$. Solving this equation for A will now give different classes of force-free fields, depending on the functional form of $B_z(A)$ imposed (Priest 1982).

If complex variable notation is used, current sheets, which are essentially discontinuities in the magnetic field, may be simply modelled as cuts in the complex ($Z = x + iy$) plane. So the problem of finding force-free fields containing a current sheet involves solving the Grad-Shafranov equation, Eq.(4.4), in the region surrounding a cut in the complex plane, from $Z = -a$ to $Z = a$, say. A current sheet (or tangential discontinuity) in a force-free field is in "mechanical" equilibrium if the normal field component vanishes

$$B_n = 0,$$

on the sheet (so that there is no magnetic tension force along the sheet), and if the jump in magnetic pressure across the sheet vanishes

$$[B_t^2] = 0,$$

where B_t is the tangential field component at the sheet, so that the sheet is in lateral equilibrium under a balance of the magnetic pressure (e.g. see Aly & Amari 1989). These

two conditions lead to the magnetic potential A being a constant along the sheet. Thus a suitable boundary condition for this problem would be to impose the constant value $A(x,y)=0$, say, on the cut.

In the Z-plane this boundary condition is hard to impose due to the nature of the finite length cut on which it is to be imposed. This difficulty may be avoided, however, if the technique of conformal mappings is used. The mapping

$$Z = w(\tilde{Z}) = \frac{1}{2}(\tilde{Z} + \frac{a^2}{\tilde{Z}}), \tag{4.5}$$

which is a modified Joukowski transformation, conformally maps the complex Z-plane into the complex $\tilde{Z}$-plane. Under this map, the cut from $Z=-a$ to $Z=a$ is mapped onto a circle of radius $\tilde{r}=a$, centred at the origin of the $\tilde{Z}$-plane. The rest of space in the Z-plane transforms to region outside this circle in the $\tilde{Z}$-plane.

The Laplacian operator ∇^2 is, however, not invariant under this mapping and its transformation is given by

$$\nabla^2 A(x,y) = \frac{\nabla^2 A(\tilde{x},\tilde{y})}{\mid w' \mid^2}, \tag{4.6}$$

where, from Eq.(4.5),

$$\begin{aligned} \mid w' \mid^2 &= \frac{1}{4}\left(1 - \frac{a^2}{(\tilde{Z})^2} - \frac{a^2}{(\tilde{Z}^*)^2} + \frac{a^4}{\mid \tilde{Z} \mid^4}\right) \\ &= \frac{1}{4}\left(1 - \frac{2a^2 cos(2\tilde{\theta})}{\tilde{r}^2} + \frac{a^4}{\tilde{r}^4}\right). \end{aligned} \tag{4.7}$$

Here $\tilde{Z} = \tilde{r}e^{i\tilde{\theta}} = \tilde{x} + i\tilde{y}$ and $\tilde{Z}^*$ represents the complex conjugate of $\tilde{Z}$ (Bajer 1990).

The Grad-Shafranov equation, Eq.(4.4), which we are wanting to solve, has now become

$$\nabla^2 A(\tilde{r},\tilde{\theta}) = -\frac{1}{8}\frac{\mathrm{d}B_z^2}{\mathrm{d}A}\left(1 - \frac{2a^2 cos(2\tilde{\theta})}{\tilde{r}^2} + \frac{a^4}{\tilde{r}^4}\right) \tag{4.8}$$

in the $\tilde{Z}$-plane, and the problematic boundary condition at the cut now takes the easier form $A(\tilde{r},\tilde{\theta})=0$ for $\tilde{r}=a$, i.e. $A(a,\tilde{\theta})=0$. The penalty, however, for this easier form of the boundary condition is that in general the resulting equation to be solved in the $\tilde{Z}$-plane, Eq.(4.8), is much more complicated than the original Eq.(4.4).

A functional form for $B_z(A)$ now needs to be imposed before Eq.(4.8) can be solved. Analytical solutions to the original equation, Eq.(4.4), have been found by previous authors, using separable techniques, for various functional forms of $B_z(A)$ (e.g. Low 1977,

Priest & Milne 1980). Due, however, to the transformation of the Laplacian operator, Eqs.(4.6) and (4.7), the choice of forms for $B_z(A)$ which will readily admit separable solutions is now restricted, as far as we can see, solely to the constant-current force-free field given by

$$B_z(A) \sim (A + A_0)^{\frac{1}{2}}, \tag{4.9}$$

where A_0 is a constant introduced to ensure the positivity of B_z^2, as will be discussed further in Section 4.4.2. Thus, setting $B_z^2(A) = 2B_0\alpha(A + A_0)$ for some constant α, where B_0 is a constant introduced to denote the background field strength at unit distance, Eq.(4.8) reduces to

$$\nabla^2 A(\tilde{r}, \tilde{\theta}) = -\frac{B_0\alpha}{4}\left(1 - \frac{2a^2 cos(2\tilde{\theta})}{\tilde{r}^2} + \frac{a^4}{\tilde{r}^4}\right), \tag{4.10}$$

for which $\alpha = 0$ gives the particular case of a potential field.

4.3 General Solution and Boundary Conditions

For Eq.(4.10), the complementary function (A_c) satisfies $\nabla^2 A_c(\tilde{r}, \tilde{\theta}) = 0$, and this can be solved separably to give a general solution of the form

$$A_c(\tilde{r}, \tilde{\theta}) = \sum_{n=1}^{\infty}(\alpha_{1_n}\cos(n\tilde{\theta}) + \alpha_{2_n}\sin(n\tilde{\theta}))(\alpha_{3_n}\tilde{r}^n + \alpha_{4_n}\tilde{r}^{-n}) + \alpha_0 \ln\tilde{r} + \alpha_5 \tag{4.11}$$

where α_0, α_{i_n}, and α_5 are constants. The infinite sum of solutions with integral n is taken since we require the solution to be continuous in $\tilde{\theta}$ (i.e. $A(\tilde{r}, 0) = A(\tilde{r}, 2\pi)$).

A particular integral (A_{pi}) satisfying Eq.(4.10) may also be found in the form

$$A_{pi}(\tilde{r}, \tilde{\theta}) = -\frac{B_0\alpha}{16}\left(\tilde{r}^2 + 2a^2\cos(2\tilde{\theta}) + \frac{a^4}{\tilde{r}^2}\right). \tag{4.12}$$

Combining these two parts we find the most general solution of Eq.(4.11) is given by

$$\begin{aligned} A(\tilde{r}, \tilde{\theta}) \quad &= \sum_{n=1}^{\infty}(\alpha_{1_n}\cos(n\tilde{\theta}) + \alpha_{2_n}\sin(n\tilde{\theta}))(\alpha_{3_n}\tilde{r}^n + \alpha_{4_n}\tilde{r}^{-n}) \\ &+\alpha_0 \ln\tilde{r} - \frac{B_0\alpha}{16}\left(\tilde{r}^2 + 2a^2\cos(2\tilde{\theta}) + \frac{a^4}{\tilde{r}^2}\right) + \alpha_5. \end{aligned} \tag{4.13}$$

As already noted, the boundary condition at the current sheet is now, due to the mapping into the $\tilde{Z}$-plane, in the simple form $A(a, \tilde{\theta}) = 0$. The general solution can be

made to satisfy this condition by imposing the conditions

$$\begin{aligned}
\alpha_5 &= \frac{B_0 \alpha a^2}{8} - \alpha_0 \ln a \\
\alpha_{4_n} &= -\alpha_{3_n} a^{2n} \text{ for } n \neq 2 \\
\alpha_{4_2} &= a^4 \left(\frac{\alpha}{8} - \alpha_{3_2} \right), \ \alpha_{1_2} = B_0, \ \alpha_{2_2} = 0.
\end{aligned}$$

A second boundary condition arises by specifying the behaviour of the field at large distances from the sheet. We shall demand that the effect of the sheet becomes negligible as $Z \rightarrow \infty$. Consider the potential case given by $\alpha = 0$ in Eq.(4.10), and impose that at large distances the field behaves like that of the lowest-order neutral point, i.e an X-type neutral point. Thus, in complex notation we require

$$\mathbf{B} = B_y + iB_x = -\frac{\mathrm{d}F}{\mathrm{d}Z} = B_0 Z \tag{4.14}$$

and hence

$$F(x,y) \sim -B_0 \frac{Z^2}{2} \tag{4.15}$$

where $F(x,y)$ is the complex potential of which $A(x,y)$ is the real part. So we have $A \rightarrow Re\left(-\frac{1}{2} B_0 Z^2\right)$ as $Z \rightarrow \infty$, with B_0, as before, denoting the strength of the background field . Under the conformal transformation this becomes

$$A(\tilde{r}, \tilde{\theta}) = Re\left(-\frac{B_0 \tilde{Z}^2}{8} \right) = -\frac{B_0 \tilde{r}^2 \cos(2\tilde{\theta})}{8} \text{ as } \tilde{r} \rightarrow \infty, \tag{4.16}$$

and this behaviour is achieved by setting

$$\begin{aligned}
\alpha_{3_2} &= -1/8 \\
\alpha_{3_n} &= 0 \text{ for all } n \geq 3
\end{aligned}$$

in Eq.(4.13).

The general solution for $A(\tilde{r}, \tilde{\theta})$, together with the appropriate boundary conditions, can now be written as the real part of the complex potential given by

$$\begin{aligned}
F(\tilde{r}, \tilde{\theta}) = B_0 \Bigg[& a^2 b \ln\left(\frac{\tilde{Z}}{a}\right) + a(c - id)\tilde{Z} - a^3 (c + id)\tilde{Z}^{-1} - \frac{1}{8}\left(\tilde{Z}^2 - \frac{a^4}{\tilde{Z}^2}\right) \\
& - \frac{\alpha}{16}\left(|\tilde{Z}|^2 + \frac{2a^2 \tilde{Z}^2}{|\tilde{Z}|^2} + \frac{a^4}{|\tilde{Z}|^2} - 2a^2 - \frac{2a^4}{\tilde{Z}^2} \right) \Bigg]
\end{aligned} \tag{4.17}$$

where a is the specified half-length of the cut (current sheet), and b, c, and d are dimensionless, real constants.

At large $\tilde{Z}$ we see from Eq.(4.17) that

$$F(\tilde{r},\tilde{\theta}) \sim -\tilde{Z}^2 - \frac{1}{2}\alpha \mid \tilde{Z} \mid^2,$$

and thus for the potential $A(\tilde{r},\tilde{\theta})$ we have

$$A(\tilde{r},\tilde{\theta}) \sim -\tilde{x}^2(1+\frac{\alpha}{2}) + \tilde{y}^2(1-\frac{\alpha}{2}). \tag{4.18}$$

In the potential case ($\alpha = 0$), the field at large distances behaves like that of an X-type neutral point, as imposed by the second boundary condition. As α is varied from zero this X-point field becomes stretched until eventually, for $\mid \alpha \mid > 2$, the field at large distances takes the form of a distorted O-type neutral point.

This complex potential, Eq.(4.17) in the $\tilde{Z}$-plane, may now transformed back to the complex Z-plane using the inverse map to Eq.(4.5), namely,

$$\tilde{Z} = w^{-1}(Z) = Z + (Z^2 - a^2)^{\frac{1}{2}}. \tag{4.19}$$

The resulting complex potential in the Z-plane is finally found to be

$$\begin{aligned} F(x,y) &= B_0 \left[a^2 b \ln \left(\frac{re^{i\theta} + R^{\frac{1}{2}} e^{i\frac{\phi}{2}}}{a} \right) + 2acR^{\frac{1}{2}} e^{i\frac{\phi}{2}} - 2adire^{i\theta} - \frac{1}{2} rR^{\frac{1}{2}} e^{i(\theta+\frac{\phi}{2})} \right. \\ &- \left. \frac{\alpha}{16} \left(\Psi + \frac{a^4}{\Psi} - 2a^2 + \frac{2a^2(re^{i\theta} + R^{\frac{1}{2}} e^{i\frac{\phi}{2}})^2}{\Psi} - 2(re^{i\theta} - R^{\frac{1}{2}} e^{i\frac{\phi}{2}})^2 \right) \right] \end{aligned} \tag{4.20}$$

where

$$\begin{aligned} r &= (x^2+y^2)^{\frac{1}{2}} \\ R &= [(x^2-y^2-a^2)^2 + 4x^2y^2]^{\frac{1}{2}} \\ \theta &= \arctan(\frac{y}{x}) \\ \phi &= \arctan(\frac{2xy}{x^2-y^2-a^2}) \\ \Psi &= r^2 + 2rR^{\frac{1}{2}} \cos(\theta - \frac{\phi}{2}) + R. \end{aligned}$$

4.4 Field Configurations

Using the fact that the magnetic potential $A(x,y)$ is constant along lines of magnetic force, the magnetic configurations of these force-free solutions can be drawn by ploting contours of the real part of Eq.(4.20).

4.4.1 Potential Fields

Firstly we shall consider the potential fields given by setting $\alpha = 0$. In this case the complex potential of the field may be written explicitly as a function of the complex variable $Z(x,y)$ alone, namely,

$$F(Z) = B_0 \left[a^2 b \ln \left(\frac{Z + \sqrt{Z^2 - a^2}}{a} \right) + 2ac\sqrt{Z^2 - a^2} - 2adiZ - \frac{1}{2} Z\sqrt{Z^2 - a^2} \right]. \quad (4.21)$$

This may be differentiated with respect to Z to give an expression for the magnetic field components

$$\begin{aligned} B_y + iB_x &= -\frac{\mathrm{d}F}{\mathrm{d}Z} \\ &= -B_0 \left[\frac{ba^2 + 2acZ - Z^2 + \frac{1}{2}a^2}{\sqrt{Z^2 - a^2}} + 2adi \right]. \end{aligned} \quad (4.22)$$

If we now look at the special case given by $c = 0, d = 0$, Eq.(4.22) reduces to simply

$$B_y + iB_x = B_0 \left(\frac{Z^2 - a^2(b + \frac{1}{2})}{\sqrt{Z^2 - a^2}} \right), \quad (4.23)$$

which is equivalent to the solution of Syrovatskii (1971), giving a current sheet with a reversal of the current towards the edges and singular end points, (see Figure 4.1b). In the special case $b = \frac{1}{2}$, this reduces still further to give

$$B_y + iB_x = B_0\sqrt{Z^2 - a^2}, \quad (4.24)$$

which is now the original solution of Green (1965), giving a sheet with neutral end points. These two cases are shown in Figures 4.2d and 4.2e, respectively.

Varying the value of the constant b in Eq.(4.23) simply moves the position of the null points, as can be seen from Figure 4.2. Figure 4.2a shows the potential field configuration given by $b = -1.0$. This is seen to produce two null points in the surrounding field, along the imaginary y-axis normal to the sheet. As b increases these null points converge,

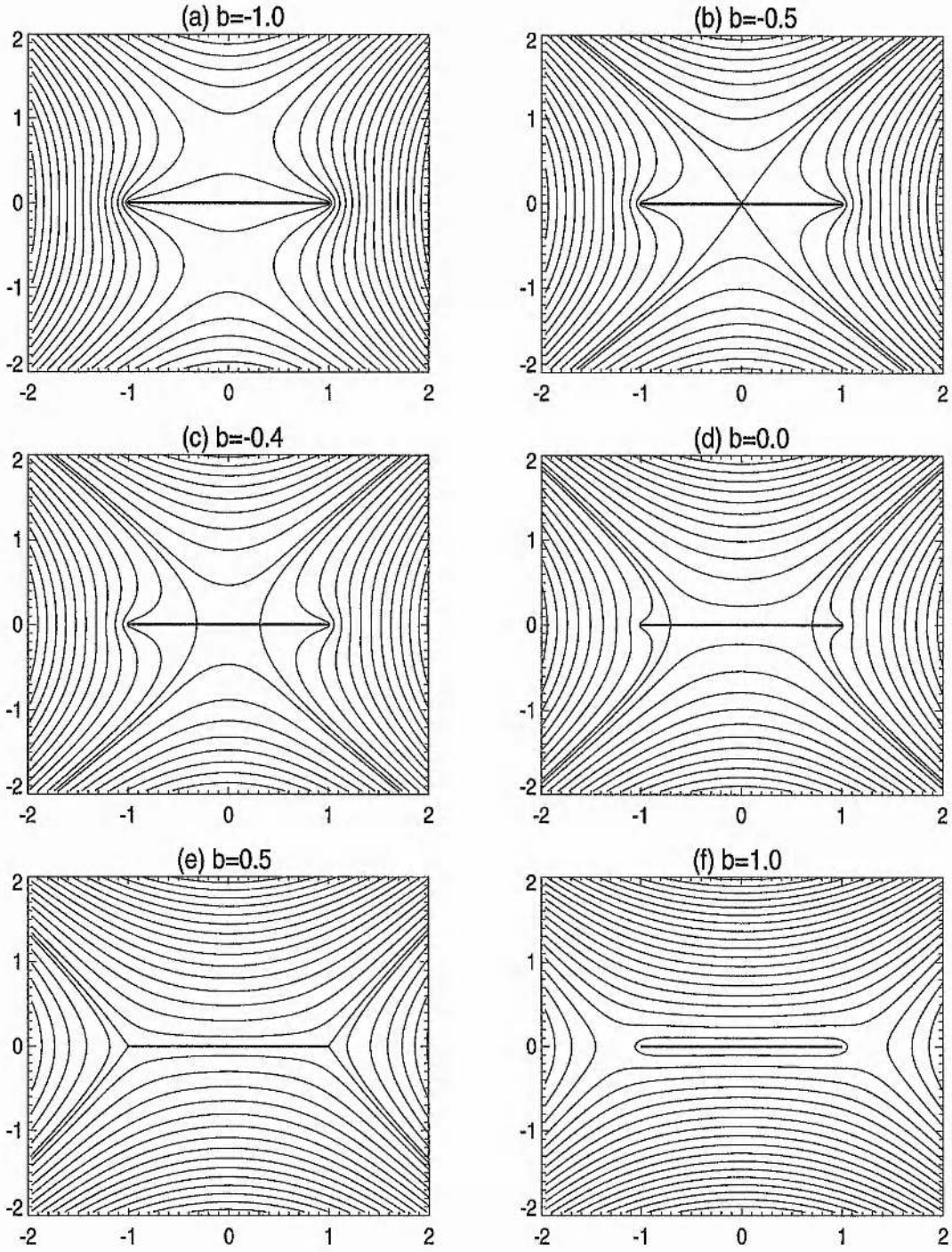

Figure 4.2: Potential magnetic fields for different values of the constant b, with $c = d = 0$. As b increases from -1.0 to 1.0, Figures 4.2a to 4.2f, the null points converge on the centre of the sheet for $b = -0.5$, and then diverge symmetrically along it. (d) is a solution of the form of Syrovatskii, whilst (e) is Green's solution.

meeting at $Z = 0$ for $b = -0.5$ (Figure 4.2b). Further increases in b now cause a divergence of the null points along the sheet, reaching the ends for $b = 0.5$, which gives Green's solution. Values of b greater than this create neutral points in the surrounding field, now along the length of the sheet on the x-axis (Figure 4.2f).

The contribution made to the field configuration by a non-zero value for the constant d is best seen from Eq.(4.22). Clearly any non-zero value for d will simply add a constant component to the magnetic field in the x-direction, parallel to the sheet. By differentiating Eq.(4.20) with respect to y, and taking the real part, the horizontal magnetic field component, B_x, can be found. The addition of a constant component to this horizontal field can easily be shown to destroy the magnetic pressure balance above and below the sheet, and therefore its equilibrium. Hence it is only realistic to consider cases of zero d, i.e. $d = 0$, and this will be assumed for the remainder of this work.

Suppose the constant c is now varied from zero. This has the effect of producing an asymmetry of the null points about the centre of the sheet. From Eq.(4.22), the null points of the field can be seen to occur at the roots of the numerator on the right hand side. These roots lie at the points

$$Z = ac \pm a\sqrt{c^2 + b + \frac{1}{2}}.$$

Thus there are two null points which converge to the one point $Z = ac$ for $c^2 = -(b + \frac{1}{2})$. Changing the value of c therefore changes the centre of convergence of the null points, along with the value of b for which this convergence occurs. Figures 4.3a and 4.3b show the configurations of a potential field where $c = -0.5$, with $b = -0.75$ and $b = -0.5$, respectively. The asymmetry of the null points about the centre of the sheet can lead to sheets as in Figure 4.3b with one singular end and one neutral end. Figures 4.3c and 4.3d take the value $c = -1.0$, so that the centre of convergence is at one end of the sheet, with the values $b = -1.5$ and $b = -1.2$, respectively.

In many of the solutions found, both potential and force-free, the field behaves as

$$\mathbf{B} \sim K(Z - a)^{-\frac{1}{2}}$$

for some constant K say, near an end ($Z = a$) of the sheet. Clearly our solutions fail at these singularities, where diffusive effects become important and slow-mode shocks are possibly generated (e.g. Petschek 1964, Priest 1985, Strachan & Priest 1994). The failure

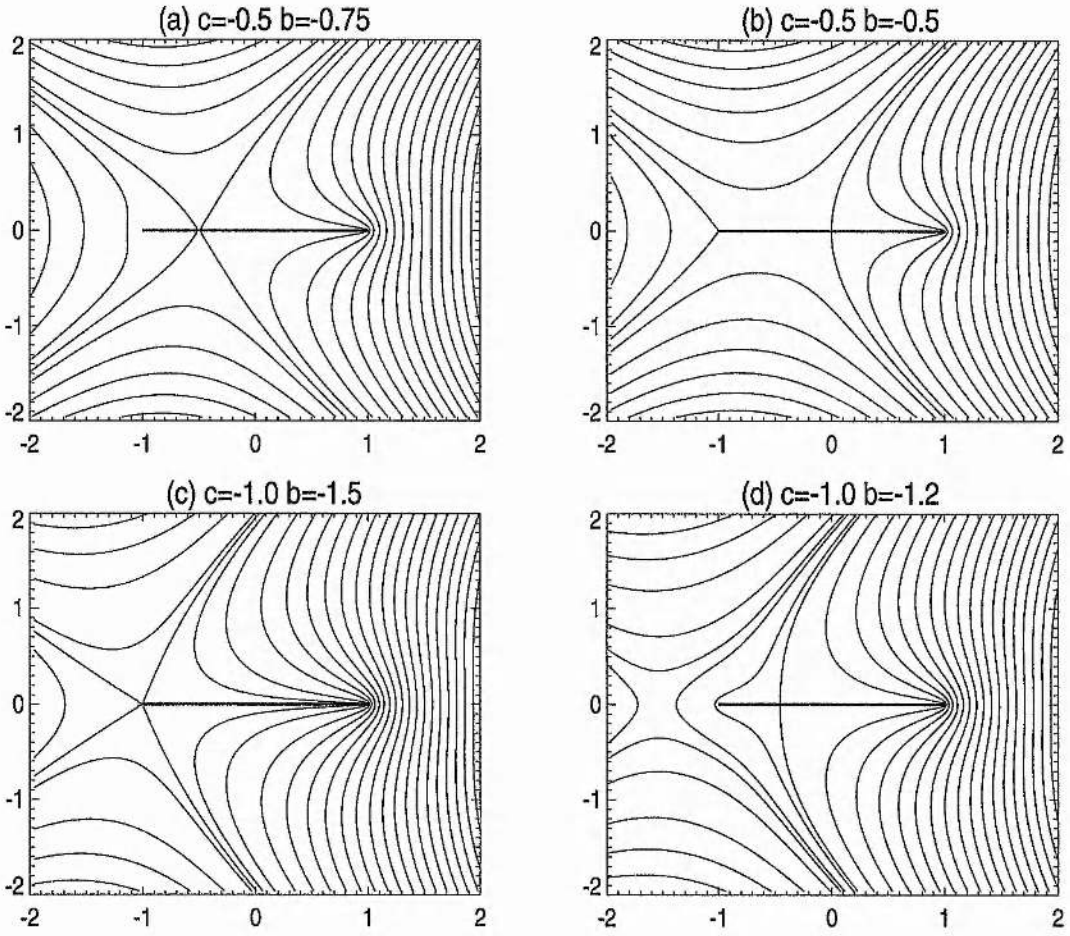

Figure 4.3: Asymmetrical potential magnetic fields given by non-zero values of the constant c. (a) and (b) have $c = -0.5$, whilst (c) and (d) take the value $c = -1.0$. In each case plots are given for two different values of b, for one of which the two null points combine at the point $Z = ac$.

is evidenced by the fact that the net magnetic force on the end of the sheet is non-zero (essentially due to the unbalanced inwards magnetic tension force) and so the end is not in equilibrium. The force on the end of the sheet is given by

$$\begin{aligned} F_y + iF_x &= \frac{1}{2\mu}\oint B^2 \mathrm{d}Z \\ &= \frac{\pi K^2 i}{\mu} \end{aligned}$$

(see Batchelor 1967, Aly & Amari 1989).

4.4.2 Force-Free Fields

All the configurations so far demonstrated have been potential. Suppose now that the constant α is varied from zero, making the fields force-free. It has already been noted that when no current sheet is present, the X-point of the potential field becomes stretched out as $\mid \alpha \mid$ increases, with the field lines closing over for $\mid \alpha \mid > 2$ giving an elongated O-point field. The same scenario is true when a current sheet of finite length is present. Figures 4.4a to 4.4f show a sequence of force-free configurations for increasing values of the constant α. Starting with $\alpha = -3.0$ in Figure 4.4a, where the field lines are closed over horizontally, the field can be seen to open up and become stretched out vertically, eventually closing over again, this time vertically, in Figure 4.4f where $\alpha = 3.0$.

The force-free field configurations shown in Figure 4.4 all have the constant values $b = c = 0$, and the null points (the positions where the separatrix field lines intersect the sheet) can be seen to remain fixed. Varying the values of these constants has exactly the same effect as in the potential case, with b changing the position of the null points and c shifting the centre of symmetry away from the origin.

In the case of force-free fields, where $\alpha \neq 0$, the question of the validity of the solutions needs to be raised. No problem arises in the potential case ($\alpha = 0$) where

$$B_z(A) = (2B_0\alpha)^{\frac{1}{2}}(A + A_0)^{\frac{1}{2}},$$

is always zero. However, for non-zero α we must ensure that $2B_0\alpha(A + A_0)$ be positive for meaningful solutions to exist. The particular boundary condition chosen at the sheet, namely $A = 0$, leads to a change in the sign of A as we cross a separatrix of the field, and hence both positive and negative values of A exist. Depending on the sign of α therefore,

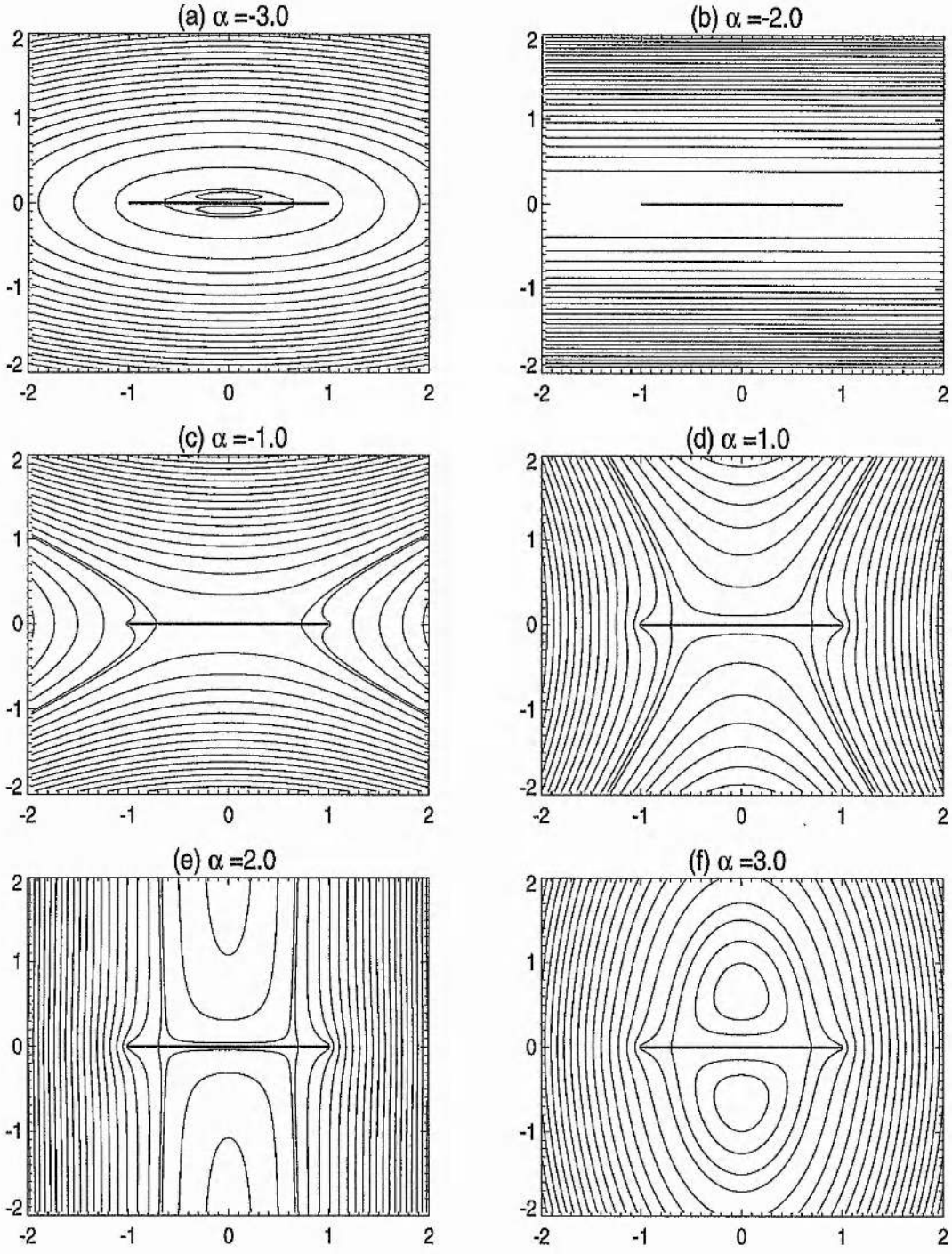

Figure 4.4: Constant-current force-free field configurations for a range of values of α, with $b = c = 0$ held fixed. As α varies, the stretching and closing of the field lines for $|\alpha| > 2$ is demonstrated. Figures (b) and (e) show the critical values of $\alpha = -2.0$ and $\alpha = 2.0$, respectively.

the value of the additional constant A_0 may be chosen so as to ensure the positivity of $B_z^2(A)$ in the considered domain, provided that domain is finite. Changing the value of the constant A_0 has the effect of increasing B_z^2 and therefore the shear of the magnetic field surrounding the current sheet, but this will not alter the projection of the field lines in the xy-plane. Clearly the larger the domain of validity that is required the greater the size of the constant A_0, and the larger the amount of shear, that must be incorporated.

The new features demonstrated in the solutions include the presence of an asymmetry along the length of the sheet, giving both potential and force-free fields with asymmetric current distributions. In particular, for force-free fields, the embedding of the current sheet inside a closed field line configuration and the presence of magnetic islands close to the surfaces of the sheet are interesting features of these constant-current solutions.

4.4.3 Current Distribution

By differentiating Eq.(4.20) with respect to y, and evaluating it at $y = 0$, an expression for the magnetic field, B_x, along the sheet may be found. Thus the current at any point in the sheet may be calculated as

$$\begin{aligned} J &= -\frac{2B_x(y=0)}{\mu} \\ &= -\frac{2B_0}{\mu}\left[\frac{a^2b + 2acx - x^2(1+\frac{\alpha}{2}) + \frac{a^2}{2}}{\sqrt{a^2-x^2}}\right]. \end{aligned} \tag{4.25}$$

For each of the potential magnetic field configurations demonstrated in Figures 4.2 and 4.3, and the force-free fields of Figure 4.4, the corresponding current distribution along the sheet is demonstrated in Figures 4.5, 4.6 and 4.7. The asymmetry produced by a non-zero value of the constant c can be very clearly seen from the current distributions in Figures 4.6a to 4.6d.

The total current in the sheet may also now be calculated by integrating Eq.(4.25) along the length of the sheet

$$J_T = -\frac{2B_0}{\mu}\left[a^2\pi(b - \frac{\alpha}{4})\right]. \tag{4.26}$$

For the potential cases considered in section 4.4.1, with the constant α zero, Eq.(4.26) shows that with b negative the total current in the sheet is positive. With $b = 0$, as in

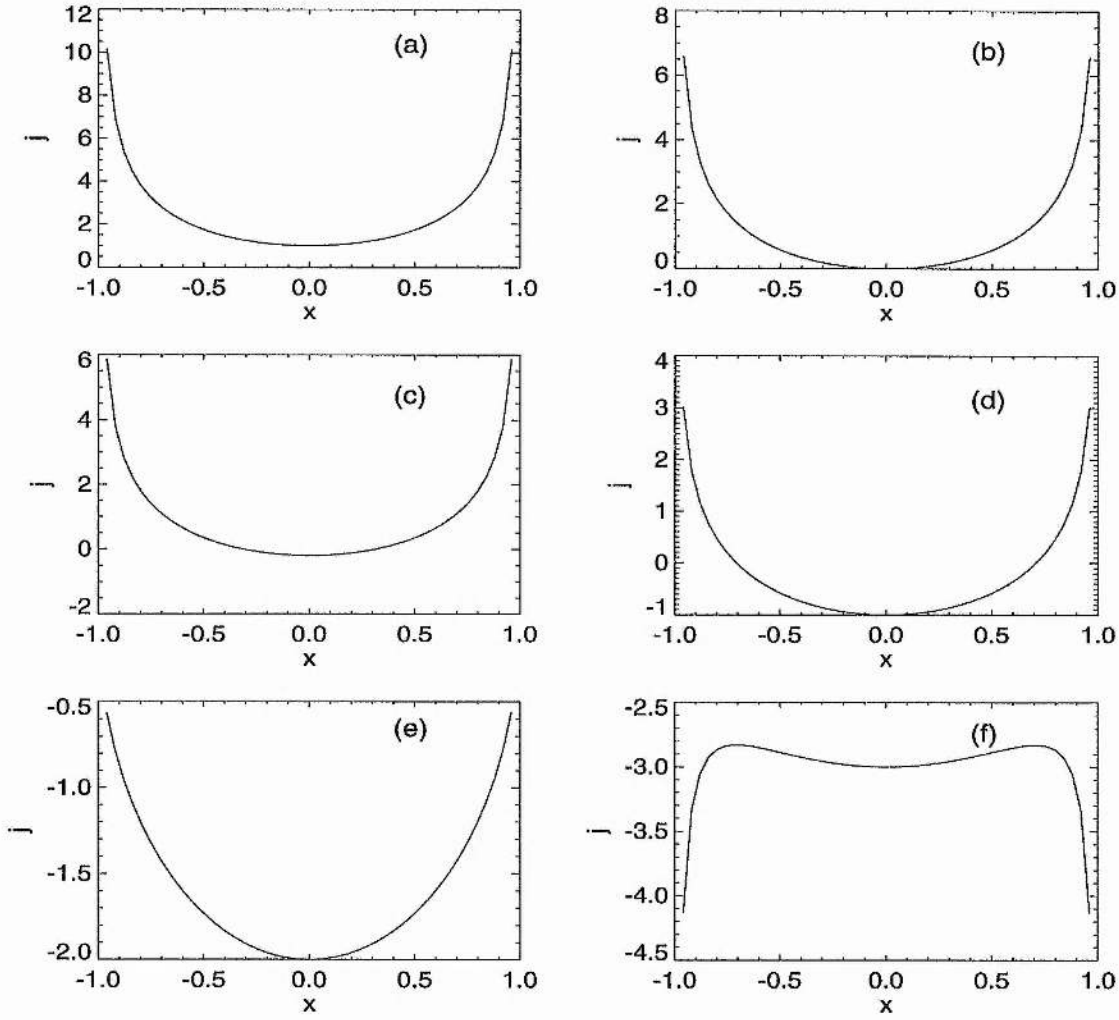

Figure 4.5: Current distribution along a sheet of half-length $a = 1.0$ for the symmetric potential fields given in Figure 4.2.

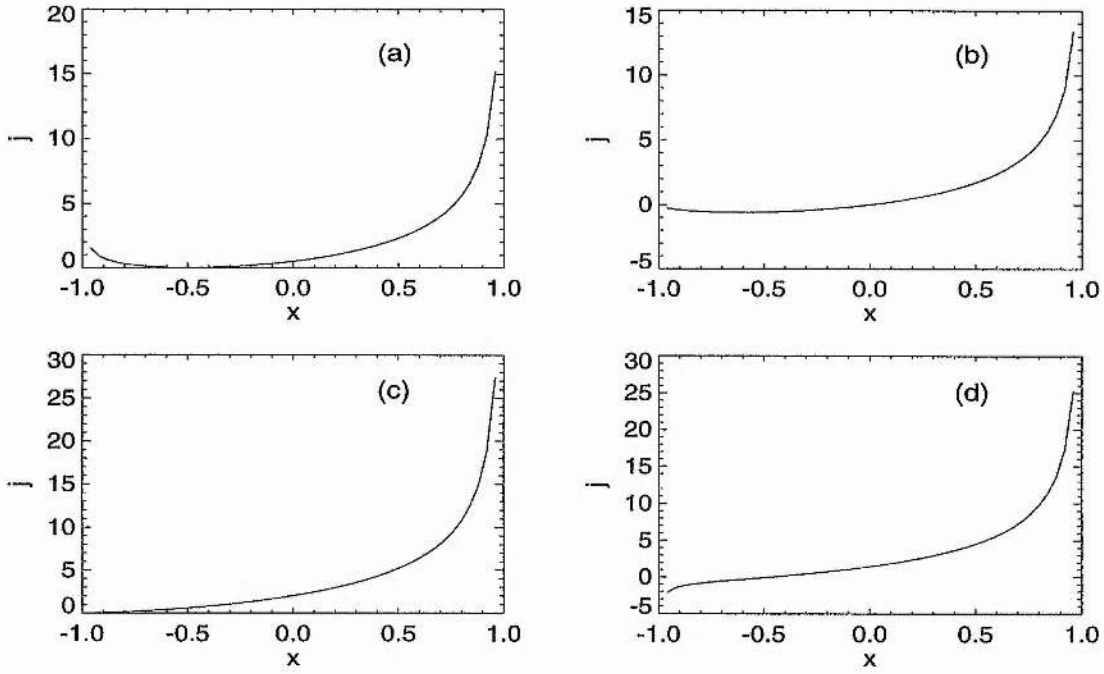

Figure 4.6: Current distribution along a sheet of half-length $a = 1.0$ for the asymmetric potential fields of Figure 4.3.

Figure 4.2d, the reversed currents match the forward current and the sheet has an overall zero current. Positive values of b give the sheet a negative total current.

The effect of varying α from zero on the total current in the sheet can also be seen from Eq.(4.26), with negative values adding current in the reverse direction, and positive values increasing the size of the forward current.

4.5 Summary and Discussion

Previously, two particular solutions for the field of a current sheet in a potential field have been discovered, by Green (1965) and Syrovatskii (1971). However, these solutions were essentially just spotted and written down by inspection and they left open the possibility of other solutions. Indeed, for many years the Syrovatskii solution was overlooked because of the singularities at the ends of the sheet.

In this paper, we have developed a general technique for finding such current sheet fields, of which the Green and Syrovatskii solutions are special cases. We have also extended the analysis to include current sheets in force-free fields, in particular presenting

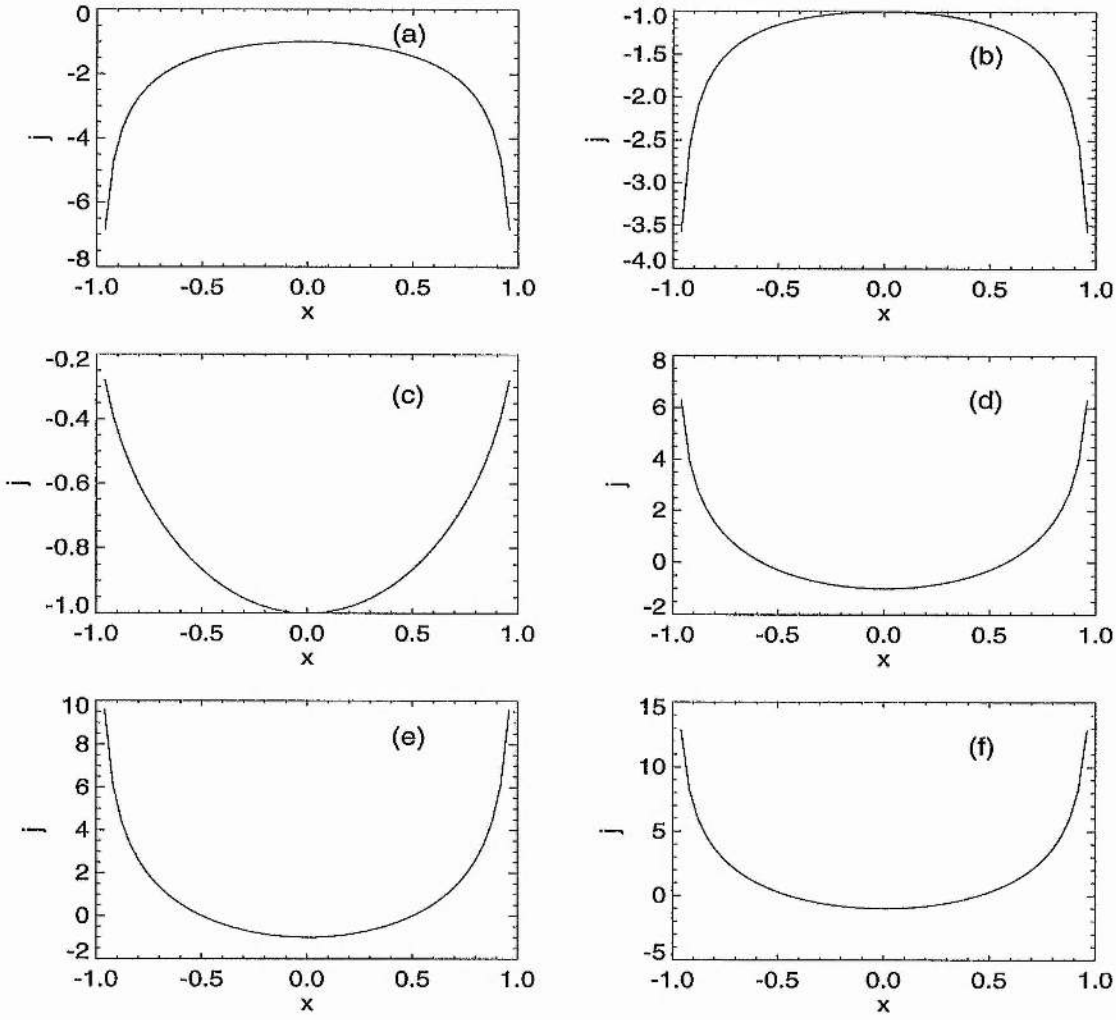

Figure 4.7: Current distribution along the sheets contained in the force-free fields of Figure 4.4.

a general analytical expression, Eq.(4.20), for the complex potential of a constant-current force-free magnetic field in the region surrounding a straight current sheet. Due to the use of a conformal mapping, and the change of the Laplacian operator under such a mapping, the constant-current case is the only form of force-free field for which an analytical solution may be easily found using separable techniques. A linear force-free field may also be treated, but not separably (Bajer 1990): such solutions suffer from the usual disadvantage of becoming periodic at large distances, and so they need to be truncated before periodicity sets in. Similarly, the solutions presented here suffer from the common constant-current field problem of having a divergence of the field at large distances. This, however, could possibly be overcome by matching the field onto that of a surrounding potential field which is well-behaved at large distances (Low 1993, Schönfelder & Hood 1995).

The solutions presented here apply equally well to magnetostatic fields in which B_z^2 in Eqs. 4.4 and 4.9 is simply replaced by $2\mu P(A)$. It is worth mentioning that in the case of force-free solutions, when applying them to coronal arcades one may wish to impose the constraints of footpoint displacements, as stressed by Priest (1981). In contrast, applications to magnetostatic fields in incompressible fluids involve the constraint of conserving flux tube areas (Linardatos 1993).

It should also be noted that in this derivation of current sheet configurations, interest has been restricted solely to the static field configurations that are possible. No attempt has been made to describe the method of formation of the sheet. Some previous work by authors on the properties and configurations of fields containing current sheets has also considered the formation of the sheet, representing most simply the evolution of the field as a series of quasi-static states in an ideal plasma (e.g. Syrovatskii 1971, Priest & Raadu 1975, Tur & Priest 1976, Aly & Amari 1989). The 'freezing-in' of the field in this ideal plasma approximation leads to the conclusion that no new neutral points may appear in the field surrounding the sheet, which places restrictions on the range of allowable values for the constants b, c and α. Furthermore, Priest et al (1993) have recently developed a technique for studying the dynamic non-linear, time-dependent formation of a current sheet, and so it would be interesting to apply such a technique to some of the new solutions discovered here.

Chapter 5

Summary and Discussion

The magnetic field has long been suspected of playing a major role in many of the characteristic features of the solar atmosphere. This may range from being a means of supporting against gravity the cool, dense plasma associated with prominences, to the provision of energy to the coronal plasma as a source of heating. In the introduction of this thesis we have discussed a few of the main issues relating to the coronal magnetic field: it's origins beneath the solar surface, the difficulties in measuring and extrapolating the coronal field directly, and finally, the differing mechanisms by which dynamic photospheric energy may be transferred to the coronal plasma via the magnetic field.

We have seen that the photospheric magnetic flux is concentrated into topologically discrete regions, with these regions being swept together at the supergranule boundaries. Wherever these topologically distinct magnetic fields press together as they expand into the low-density atmospheric plasma we may expect tangential discontinuities to arise. The process of magnetic reconnection, by which stored magnetic energy may be rapidly released, may naturally be expected to occur at such regions where the field changes over short length scales. For this reason we are interested in locating the boundaries between regions of differing magnetic connectivity and hence determining the topology of the field, since it is the topological structure of a particular field which is likely to be a key factor in determining the response of that field to plasma motions and instabilities (Berger 1991).

We have started in Chapter 2 by modelling the coronal magnetic field using simple point sources of magnetic flux placed on the planar photospheric boundary to represent the observed discrete concentrations. We have studied the fields generated by two, three

and four potential sources in order to build up a picture of the how the various separatrix surfaces evolve and interact for these simple fields. Any separatrix surfaces present in the fields are entirely due to the presence of magnetic null points lying in the source plane, and correspond to the fan surfaces of these null points (Priest & Titov 1995). Thus the toplogical skeleton of the field is simply made up of the null points, their spine curves, and their separatrix fan surfaces.

We find that with just two unbalanced sources the coronal field is simply split into two regions of distinct connectivity by just one separatrix surface. For fields generated by three sources there exist, in general, two null points and their respective separatrix fan surfaces now separate the volume into three topologically distinct regions. The two fan surfaces may be either nested or independent and the field evolves smoothly from one state to the other as the sources move or grow, with the separatrix surfaces, despite becoming pressed together, never intersecting. There are two special cases, however, where the field evolution and restructuring is more complex, involving the coalescence (or bifurcation) of nulls and the birth of either a null line (Chapter 2.4.1(ii)) or the formation and eventual destruction of new nulls (Chapter 2.4.2(ii)).

Fields generated by four, balanced flux sources may be very different from those of two and three sources. The separatrix surfaces will now, in general, intersect one another at a separator field line. This separator field line lies then at the mutual intersection of four topologically distinct regions and is regarded as a favoured site for the occurrence of reconnection processes. We have shown in Chapter 2.5.1 how, with the emergence of a new bipolar region in the midst of an existing bipolar field, a separator is formed and may rapidly rise as the emerging flux grows and erupts through the overlying field. In particular we have shown that this rapid separator rise and the break-through of the internal flux may occur for almost any internal bipolar angle and is not just restricted to the special anti-parallel case studied by Syrovatskii (1982). Indeed there appears to be an optimum internal bipolar angle of approximately 45° for which the break-through is most rapid. We have also demonstrated how observational features such as the break-up of a flux concentration which separates two opposite polarity regions may be simply modelled using just four sources, and the energy release seen at such locations related to the topological reconstruction of the field (Chapter 2.5.2).

In Chapter 3 we have continued our study into the evolution of coronal separatrix surfaces but now with the discrete flux sources displaced a small but finite distance below the photospheric surface. The restriction that all the sources lie in same horizontal plane is also relaxed and these two features now allow the generation of more realistic photospheric flux contour maps. The small vertical displacement of the sources has two important consequences. Firstly, it introduces the possibility of coronal field lines which tangentially graze the photospheric surface before returning upwards into the corona. These field lines will form separatrix surfaces and hence contribute to the topological skeleton of the field. Secondly, only those null points located above the photospheric plane are now of relevance to the determination of the coronal topology. The force-free assumption breaks down in the photosphere and any extrapolation of field lines below the surface, therefore, is not strictly valid. Thus, photospheric nulls and the field lines emanating from them cannot be considered as contributing to the toplogical skeleton.

To this end we have derived in Chapter 3.4 a simple criterion for determining whether null points in a quasi-coplanar source configuration will appear above the photospheric boundary and hence contribute to the global topology. We find that regions of the photospheric inversion line (IL) where field lines tangentially touch the boundary from above (named 'Bald Patches', BP's) exist for a wide range of parameters in even the simplest of fields due to just two unbalanced sources. The topological structure of the field, which is determined uniquely by those field lines which thread the BP's and coronal nulls, is found to evolve smoothly through the disappearance of BP's and the emergence of nulls. Indeed, the presence of BP's is often seen to be a precursor to the emergence of coronal null points.

One further very interesting result of Chapter 3.5.3 comes from the study of a centrosymmetric internal bipole emergence, as in Chapter 2.5.1. We find the presence of a separator field line representing the mutual intersection of two BP separatrix surfaces. This separator field line is well-defined and does not require the presence of null points in the coronal field. Furthermore, this separator runs almost parallel to the IL as is seen to be the case for field lines threading coronal prominences.

Over recent years, several authors have modelled observed photospheric fields using a number of sub-photospheric flux concentrations (e.g. Mandrini et al 1991, Démoulin et al

1994). In these works, however, the topology has been determined by tracing field lines back to their sub-photospheric sources in order to locate a 'switching' of endpoints from one soure to another. This method is not only time consuming but is also not strictly valid due to the sub-photospheric extrapolation. Furthermore, the 'switching' of field line endpoints is entirely due to the presence of sub-photospheric null points. In the future, therfore, it would be interesting to repeat such coronal field models and determine the topology instead using the simpler, self-consistent approach of merely locating all BP regions and coronal nulls and then tracing just those field lines threading these fundamental structures. Indeed, the presence of BP separatrix surfaces is overlooked by the previously used 'switching' algorithm.

In Chapter 4 we haved moved on to consider the local structure of the field in the region surronding a linear current sheet. Using complex notation and the method of conformal mappings we have derived a general analytical expression describing the structure of both potential and constant-current force-free fields containing a current sheet. The previously well known solutions arise as special cases of our more general expression. Our solutions include the possibilities of asymmetric current distribution along the sheet and the presence of magnetic islands close to the sheet surfaces in the force-free case.

Solutions such as those derived in Chapter 4 are for quasi three-dimensional fields. Our understanding of magnetic reconnection in fully three-dimensional systems is still limited and much work is needed before we can gain a full understanding of the process. In particular, magnetic reconnection in fields both with and without null points needs to studied in order that we may understand better how energy release may occur at the separatrix surfaces found in Chapters 2 and 3. It would also be interesting to study how the structure of a particular null point may affect the reconnection process. For example, we have seen in Chaptesrs 2.4.2(ii) and 2.5.2 how the local structure of the nulls may change from having radial fan field lines to becoming more and more improper, with the fan field lines closing up along a preferred direction (see Parnell et al 1995). Is the process of magnetic reconnection any different for these different local structures? Furthermore, a greater understanding of general three-dimensional reconnection is needed before models of fully three-dimensional current sheets may be constructed.

References

Aly, J. J. 1992, Solar Phys. 138, 133

Aly, J.J., Amari, T. 1989, Astronomy & Astrophysics, 221, 287

Arnol'd, V.I. 1992, Ordinary Differential Equations, Springer textbook

Athay, R.G. 1976, The Solar Chromosphere & Corona: Quiet Sun, D.Reidel, Dordrecht, Holland

Athay, R.G., White, O.R. 1977, Proc. OSO8 Workshop, Nov. 1977, University of Colorado

Baum, P., Bratentahl, A. 1980, Solar Phys. 67, 425

Bajer, C. 1990, Phd thesis, Cambridge University

Batchelor, G.K. 1967, An Introduction to Fluid Dynamics, Cambridge University Press

Berger, M.A. 1991, in Advances in solar system MHD (ed.s E.R.Priest & A.W.Hood) Cambridge, p241-256

Billinghurst, M.N., Craig, I.J.D., Sneyd, A.D. 1993, A&A 279, 589

Biskamp, D. 1986, Phys. Fluids 29, 1520

Browning, P.K. 1991, Plasma Phys. & Controlled Fusion, 33 No.6, 539

Bungey, T.N., Priest, E.R. 1995, A&A 293, 215

Bungey, T.N., Titov, V.S., Priest, E.R. 1995, A&A in press.

Cargill, P.J. 1993, Solar Phys. 147, 263

Choudhuri, A.R. 1989, Solar Phys. 123, 217

Démoulin, P., Hénoux, J.C., Mandrini, C.H. 1992, Solar Phys. 139, 105

Démoulin, P., Hénoux, J.C., Mandrini, C.H. 1994, A&A 285, 1023

Démoulin, P., Priest, E.R. 1992, A&A 258, 535

Démoulin, P., van Driel-Gesztelyi, L., Schmieder, B., Hénoux, J.C., Csepura, G., Hagyard, M.J. 1993, A&A 271, 292

D'Silva, S., Choudhuri, A.R. 1991, Solar Phys. 136, 201

Fan, Y., Fisher, G.H., DeLuca, E.E. 1993, ApJ 405, 390

Galsgaard, K., Nordlund, A. 1995, JGR, submitted

Gary, G.A., Démoulin, P. 1995, ApJ 445, 982

Gilman, P.A., Morrow, C.A., DeLuca, E.E. 1989, ApJ 338, 528

Gorbachev, V.S., Somov, B.V. 1988, Solar Phys. 117, 77

Green, R.M. 1965, in Stellar and solar Magnetic Fields, ed. R.Lust, IAU Symp. 2 2 p.389

Heyvaerts, J., Priest, E.R. 1983, A&A 117, 220

Hollweg, J.V. 1979, Solar Phys. 62, 227

Karpen, J.T., Antiochos, S.K., DeVores R.C. 1990, ApJ 356, L67

Karpen, J.T., Antiochos, S.K., DeVores R.C. 1991, ApJ 382, 327

Lau, Y.T. 1993, Solar Phys. 148, 301

Lau, Y.T., Finn, J.M. 1990, ApJ 350, 672

Leroy, B. 1981, A&A 97, 245

Leroy, J.L. 1989, in: Priest E.R. (ed.) Dynamics and Structure of Quiescent Solar Prominences, Kluwer academic publishers, Dordrecht, p77

Linardatos, D. 1993, J. Fluid Mech., 246, 569

Low, B.C. 1977, ApJ, 212, 234

Low, B.C. 1982, Solar Phys. 77, 43

Low, B.C. 1987, ApJ 323, 358

Low, B.C. 1992, A&A 253, 311

Low, B.C. 1993, ApJ, 409, 798

Low, B.C., Wolfson, R. 1988, ApJ 324, 574

Low, B.C., Lou, Y.Q. 1990, ApJ 352, 343

Mandrini,C.H., Démoulin, P., Hénoux, J.C., Machado, M.E. 1991, A&A 250, 541

Mandrini, C.H., Rovira, M.G., Démoulin, P., Hénoux, J.C., Machado, M.E., Wilkinson, L.K. 1993, A&A, 272 609

Mandrini, C.H., Démoulin, P., Rovira, M.G., de la Beaujardiere, J.F., Hénoux, J.C. 1995, A&A, in press

McClymont, A.N., Mikic, Z. 1994, ApJ 422, 899

Moreno-Insertis, F. 1986, A&A 166, 291

Parker, E.N. 1958, ApJ 128, 664

Parker, E.N. 1972, ApJ 174, 499

Parker, E.N. 1988, ApJ 330, 474

Parnell, C.E., Smith, J., Neukirch, T., Priest, E.R. 1995, Phys. of Plasmas, submitted

Petschek, H.E. 1964, AAS-NASA Symp. on Solar Flares, NASA SP-50

Priest, E. R. 1981, Solar Flare MHD, Gordon and Breach, London.

Priest, E. R. 1982, Solar Magnetohydrodynamics, Kluwer, Dordrecht.

Priest, E.R. 1985, Rep. Prog. Phys., 48, 995

Priest, E.R., Démoulin, P. 1995, JGR submitted

Priest, E.R., Forbes, T.G. 1986, JGR 91, 5579

Priest, E.R., Lee, L.C. 1990, J. Plasma Phys. 44, 337

Priest, E.R., Milne, A.M. 1980, Solar Phys., 65, 315

Priest, E.R., Raadu, M.A. 1975, Solar Phys., 43, 177

Priest, E.R., Titov, V. S., Rickard, G. J. 1993, Phil. Trans. of the Royal Soc. 351 No.1695, p1

Priest, E.R., Titov, V.S. 1995, Phil. Trans. of the Royal Soc., in press

Ridgeway, C., Amari, T., Priest, E.R. 1992, ApJ, 385, 718

Roberts, B. 1985, Magnetohydrodynamic Waves, in E.R. Priest (ed.), Solar System Magnetic Fields, Reidel

Roumeliotis, G. 1995, ApJ submitted

Sakurai, T. 1981, Solar Phys. 69, 343

Schindler, K., Hesse, M., Birn, J., 1988, JGR 93, 5547

Schönfelder, A.O., Hood, A.W. 1995, Solar Phys. 157, 223

Seehafer, N. 1986, Solar Phys 105, 223

Sneyd, A.D. 1993, Geophys. Astrophys. Fluid Dynamics 70, 195

Strachan, N.R., Priest, E.R. 1994, Geophys. Astrophys. Fluid Dyn. 74, 245

Sweet, P.A. 1958, IAU Symp. 6, 123

Syrovatskii, S.I. 1971, Sov. Phys. JETP, 33, 933

Syrovatskii, S.I. 1982, Solar Phys. 76, 3

Titov, V.S., Priest, E.R., Démoulin, P. 1993, A&A 276, 564

Tur, T.J., Priest, E.R. 1976, Solar Phys., 48, 89

Van Ballegoijen, A.A. 1985, ApJ 298, 421

Van Ballegoijen, A.A. 1986, ApJ 311, 1001

Vekstein, G.E., Priest, E.R. 1992, ApJ 384, 333

Velli, M., Hood, A.W. 1989, Solar Phys 119, 107

Wolfson, R. 1989, ApJ 344, 471

Zhang, G. 1994, Solar Phys. 154, 41

Zirin, H. 1972, Solar Phys. 22, 34

Zweibel, E.G., Li, H.S. 1987, ApJ 312, 423